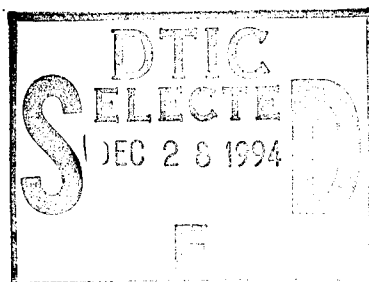




Division of Sponsored Research  
Office of Research  
University of South Florida  
140 Seventh Avenue South, MSL-136E  
St. Petersburg, Florida 33701-5001  
(813) 893-9150  
FAX (813) 893-9189

December 8, 1994



Defense Technical Information Center  
Building 5  
Cameron Station  
Alexandria, VA 22314


RE: FINAL REPORT FOR GRANT #N00014-89-J-1091  
P.I.: Kendall L. Carder

Dear Sir/Madame:

Enclosed please the final report for the above referenced grant entitled, "Development of an Average Cosine Meter" for your retention.

If I may be of any further assistance, please do not hesitate to contact me.

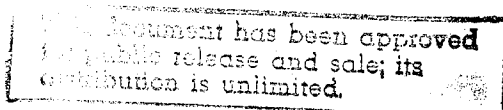
Sincerely,

  
Estella Bunch  
Grants Specialist

/eb

Enclosure

19941213 023



DTIC QUALITY INSPECTED 1

# FINAL REPORT to the OFFICE OF NAVAL RESEARCH

for activity from 01 October 1990 to 30 September 1994

**PRINCIPAL INVESTIGATOR:** Kendall L. Carder

# PROJECT TITLE

## Average Cosine Meter and High Spectral Resolution Measurements at the Marine Light Mixed Layer Site

ONR Contract #N00014-88-J-1091

[illegible]

University of South Florida  
Marine Science Department  
140 Seventh Avenue South  
St. Petersburg, FL 33701

INTERNET: [kcarder@monty.marine.usf.edu](mailto:kcarder@monty.marine.usf.edu)  
OMNET: K.CARDER  
VOICE: 813-893-9148  
FAX: 813-893-9189

## Introduction

The goals of this research have been to develop in situ optical instruments and computer models of the apparent and inherent optical properties of the submarine light field. The radiative transfer function in seawater is a complicated mix of signals caused by many components some of which are covariant. The approach taken in this research has been to measure by utilizing custom and commercial optical instrumentation as many of the components of light field at a single site rather than combine spotty information at many sites. A fundamental contribution to the program was our participation in the Marine Light Mixed Layer Experiment in the North Atlantic. This provided an opportunity to simultaneously measure the optical components of the light field in a multi-investigator environment. We supported this project with state-of-the-art high spectral resolution optical field instrumentation and computer modelling of the submarine light field. The apparent optical properties of the MLML site were measured with the Spectral Transmissometer and Radiometer (STAR) and the Average Cosine Meter (ACM).

## RESULTS

There were three major efforts this program. These included instrument development, modelling, and cruise support. The development of optical instruments and sampling technique are synergistic with the computer modelling. Advances in instrumentation provided more known quantities in the modelling effort which indicated the direction to pursue new instrumentation.

### Instrument efforts

There were effectively two instruments developed under this project. The proposed instrument was the Average Cosine Meter. The prototype was completed using what was at the time state-of-art components. It was deployed on a small floating reel and electromechanical release, this novel and inexpensive method eliminated shadowing from the ship. The ACM measured irradiance at 490nm using cosine and 4 $\pi$  collectors as well as detector dark current. The ACM was utilized in conjunction with the Spectral Transmissometer and Radiometer which provided hyperspectral downwelling irradiance and upwelling radiance. During the summer experiment at MLML site, the STAR was lost when the hydrowire on the USNS Bartlett failed due to age and fatigue. A new hyperspectral instrument was constructed from plans and spare parts that were already on hand to upgrade the STAR. The new instrument due to its reduced size and increased capabilities effectively replace both the ACM and the STAR. This instrument has been named the Submersible Upwelling and Downwelling Spectrometer SUDS. It is a hyperspectral upwelling radiometer and downwelling irradiator utilizing fiber optics, and shutter to a common holographic grating spectrometer and 512 element linear array detector. (Steward, et al. 1994)

### Modelling efforts

During this project, a Monte Carlo type model of the submarine spectral irradiance field was

produced (Reinersman et al. 1994). It uses measured or simulated incoming solar and sky irradiance and the inherent optical properties of the sea. It has been used to help validate Q-factors for a remote sensing reflectance model (Lee et al. 1994) that inverts high spectral resolution, remote sensing reflectance or irradiance reflectance. These reflectance data can be interpreted in terms of absorption that when divided by the average cosine provides a good estimate of the diffuse attenuation coefficient. Specifically, one can predict the spectral vector irradiance and spectral scalar irradiance fields with depth for variable chlorophyll-a environments. These fields specify the general availability of light for passive visual or other optical observations and the spectral quanta available for absorption by phytoplankton for photosynthesis.

### Cruise Support

Four persons participated in two cruises to the MLML site in the North Atlantic. The first cruise was aboard the R/V Endeavor from May 14-June 2, 1991 (Reykjavik, Iceland to Narragansett, Rhode Island). This was a process-oriented experiment with a number of investigators working on concurrent sampling. Some of the data collected on this experiment by our group included:

- a. Specific absorption
- b. Remote sensing reflection
- c. CDOM absorption
- d. CDOM absorption and fluorescence on concentrated extractions

The second cruise was the Mesoscale Mapping experiment aboard the USNS Bartlett August 11-31, 1991 Cork, Ireland to Newport, Rhode Island. Due to restriction in access, rough weather, and the transect nature of this work; fewer samples were collected. A similar suite of samples were collected to make seasonal comparisons with the spring processes cruise.

### RESULTS/IMPACT

The significance of the work performed under this funding is best described by summary of the peer-reviewed publications which have resulted. These publications have been included in the Appendix.

1. Aircraft flying below the clouds (e.g. Unmanned Air Vessels UAV's) will be able to derive accurate absorption coefficients for phytoplankton and gelbstoff and accurate chlorophyll a concentrations from hyperspectral remote sensing reflectance data. (Carder, et al. 1992)
2. The data derived above can be used to estimate primary productivity values some three times more accurately than using traditional methods. A mathematical simulation of the absorption coefficient of phytoplankton derived from hyperspectral remote sensing reflectance makes more accurate estimation of the primary productivity than techniques that use chlorophyll a concentration, irradiance, average chlorophyll specific absorption,

and quantum yield of carbon fixation. (Carder et al. accepted, Lee, et al. submitted)

3. Measurements of dissolved organic carbon DOC on transects to and from the MLML site contributed to a model of flux of dissolved organic matter DOM and dissolved nitrogen between the North Atlantic and the equator. Results of the modelling suggest how future optical measurements by remote sensing platforms will be important in discrimination of particulate and dissolved components of the organic carbon flux and verify the importance of continental margins and DOM in global biogeochemical cycles. (Walsh, Carder, and Muller-Karger, 1992)

### RELATIONSHIP TO OTHER PROJECTS

1. This project provided high latitude data helpful in validating Seawifs algorithms.
2. This project developed methods of deriving quantum yield data for primary production useful to John Marra and other coinvestigators that deployed moorings and drifting arrays equipped with primary productivity incubators and simple photosynthetically available radiation PAR meters.

### PUBLICATIONS

P - Lee, Z. P., K.L. Carder, S.K. Hawes, R.G. Steward, T.G. Peacock, and C.O. Davis. 1994a. A model for interpretation of hyperspectral remote sensing reflectance, Applied Optics, 5721-5732.

PI - Costello, D.K., K.L. Carder, and W. Hou. (submitted to a special issue of Deep-Sea Research). Aggregation of a diatom bloom in a mesocosm: bulk and individual-particle optical measurements.

PI - Costello, D.K., K.L. Carder and R.G. Steward. (in prep. for a submission to Deep-Sea Research). Design and performance of the Marine Aggregated Particle Profiling and Enumerating Rover (MAPPER).

PI - Costello, D.K. and K.L. Carder. (in prep. for submission to Journal of Geophysical Research). Underwater light attenuation by the 3-dimensional distribution of large marine particles in Monterey Bay.

R - Costello, D.K., W. Hou and K.L. Carder. 1994. Some effects of the sensitivity threshold and spatial resolution of a particle imaging system on the shape of the measured particle size distribution. In: Ocean Optics XII, Jules S. Jaffe, Editor, Proc. SPIE 2258, Bergen, Norway.

R - Costello, D.K. and K.L. Carder. 1994a. New instrumentation and platforms for subsurface optical measurements. In: Ocean Optics XII, Jules S. Jaffe, Editor, Proc. SPIE 2258, Bergen,

Norway.

R - Costello, D.K. and K.L. Carder. 1994b. Using unmanned vehicle systems for ground-truthing oceanographic satellite data. AUVS '94 - Intelligent Vehicle Systems and Technology, Proc. Asso. for Unmanned Vehicle Systems, Detroit, MI.

R - Costello, D.K., K.L. Carder, and R.G. Steward. 1994. Particle size spectra and optical properties. In: Mesocosm Experiment Data Report to the Office of Naval Research under the Accelerated Research Initiative, Significant Interactions Governing Marine Aggregation (SIGMA). 51 pp.

R - Costello, D.K., K.L. Carder, W. Hou and R.G. Steward. 1994. 3-dimensional particle size spectra, transmissometry and temperature profiles, and filter pad absorption data. In: Monterey Bay Field Experiment Data Report to the Office of Naval Research under the Accelerated Research Initiative, Significant Interactions Governing Marine Aggregation (SIGMA). 24 pp.

#### ONR SPONSORED PRESENTATIONS

C - Costello, D.K., K.L. Carder, R.G. Steward and A. Alldredge. 1994. The Distribution and Optical Properties of Large Marine Particles: Data From a Culture Tank and Field Experiments. EOS AGU/ASLO (75), 3, 35.

C - Hou, W., D.K. Costello, K.L. Carder and R.G. Steward. 1994. High-resolution Marine Particle data from MAPPER, a new, in situ optical ocean instrument. EOS AGU/ASLO (75), 3, 21.

C - Lee, Z. P., K. L. Carder, and T. G. Peacock, 1994b. Hyperspectral modeling of remote sensing reflectance: from the Florida Shelf to the Mississippi River. EOS AGU/ASLO (75) 3, 193.

C - Peacock, T. G., K. L. Carder, P. G. Coble, Z. P. Lee, and S. K. Hawes, 1994. Long-path Spectrometer for measuring gelbstoff absorption in clear waters. EOS AGU/ASLO (75) 3, 22.

C - Reinersman, P., F. Chen, and K. L. Carder, 1994. Monte Carlo Simulation of Atmospheric Point Spread Function With Application to Coastal Image Processing. EOS AGU/ASLO (75) 3, 136.

C - Steward, R. G., K. L. Carder, and T. G. Peacock. 1994. High resolution, in water optical spectrometry using the Submersible Upwelling and Downwelling Spectrometer (SUDS). EOS AGU/ASLO (75) 3, 102.

C - Young, L. R., K. L. Carder, and P. Hallock, 1994. Hyperspectral remotely sensed colored dissolved organic matter as a photoprotective agent against bleaching in corals and foraminifera. EOS AGU/ASLO (75) 3, 103.

## APPENDIX

The following publications or drafts have been included:

Carder, K.L., Z. Lee, T.G. Peacock, R.G. Steward, C.O. Davis, 1992. Aircraft algorithms for water absorption coefficients: rain or shine. Western AGU

Carder, K.L. Z. Lee, J. Marra, R.G. Steward, and M.J. Perry, (in press). Calculated quantum yield of photosynthesis of phytoplankton in the Marine Light-Mixed Layer (59°N/21°W), J. Geophys. Res. (Special Edition).

Lee, Z., K.L. Carder, S.K. Hawes, R.G. Steward, T.G. Peacock, C.O. Davis, 1994. Model for the interpretation of hyperspectral remote sensing reflectance. Applied Optics 33:24, 5721-5732.

Lee, Z., K.L. Carder, J. Marra, R.G. Steward, M.J. Perry, (in press). Estimating primary productivity from remote sensing reflectance: a new approach. J. Geophys. Res.

Walsh, J.J., K.L. Carder, F.E. Muller-Karger, 1992. Meridional fluxes of dissolved organic matter in the North Atlantic Ocean. J. Geophys. Res. 97-c10, 15625-15637.

# Aircraft Algorithms for Water Absorption

Coefficients: Rain or Shine

L Carder, Z Lee, T G Peacock, R G Steward (All  
at Department of Marine Science, University of  
South Florida, 140 7th Avenue S., St. Petersburg,  
FL 33701-5016; 813-893-9148  
; O Davis (Jet Propulsion Laboratory, Mail Stop  
300-323, 4800 Oak Grove Drive, Pasadena, CA 91109)

Algorithms for calculating the absorption and the  
diffuse attenuation coefficients of surface waters  
were derived for use in aircraft flying near the sea  
surface during sunny or overcast conditions. Cloud-  
fast areas are typical of many upwelling or high-  
latitude regions where autonomously piloted vehicles  
(APVs) may be needed to remotely measure water  
clarity and chlorophyll pigments to supplement ocean-  
color satellite data. Data from forty stations were  
used to develop algorithms for the absorption  
( $a(490)$ ) and diffuse attenuation ( $k_d(490)$ )  
coefficients at 490 nm that are based upon spectral  
ratios of remote-sensing reflectance  
( $R_{rs}(520)/R_{rs}(560)$ ). The algorithms provided  
estimates with correlation coefficients of 0.98 and  
accuracies better than  $\pm 10\%$ . A curvature algorithm  
is also presented that flags  $R_{rs}$  data which contain  
effects of bottom reflection. The diffuse  
attenuation coefficient is used to classify optical  
water types and to parameterize models that  
characterize the vertical structure of the  
chlorophyll field for various bio-optical domains.

1. 1992 Fall Meeting

2. Member #000575311

3. (a) K L Carder  
Dept. of Marine Science  
Univ. of South Florida  
140 Seventh Avenue South  
St. Petersburg, FL 33701  
(b) tel. 813-893-9148  
(c) fax. 813-893-9189

4. 0

5. (a) Marine Light Mixed Layer  
(special session) or  
008 Remote Sensing of Ocean  
Color  
(b) 4275, 4855  
(c) Ocean color algorithms

6.

7. 0%

8. Charge K.L. Carder  
AM EX AX 3787 020098 21 005  
Exp. 7/94

9. C

10.

11. No



**Aircraft Algorithms for Water Absorption Coefficients:  
Rain or Shine**

**K.L. Carder<sup>1</sup>, Z. Lee<sup>1</sup>, T.G. Peacock<sup>1</sup>, R.G. Steward<sup>1</sup>**

**Department of Marine Science, University of South Florida  
140 Seventh Avenue South, St. Petersburg, FL 33701**

**C.O. Davis<sup>2</sup>**

**Jet Propulsion Laboratory, California Institute of Technology  
4800 Oak Grove Blvd., Pasadena, CA 91109**

## 1. Introduction

In 1981, Austin and Petzold<sup>1</sup> developed an algorithm to estimate the diffuse attenuation coefficient  $K$  at 490nm using the in-water upwelling radiance ( $L_u$ ) ratio at 443 and 550nm:

$$K(490) = 0.0883 \left( \frac{L_u(443)}{L_u(550)} \right)^{-1.491} + 0.022 \quad (1)$$

The importance of this value is that it can be used to classify optical water types.  $L_u$  can be related directly to the water-leaving radiance ( $L_w$ ) and remote-sensing reflectance ( $R_{rs}$ , see below), so a similar expression may be written using  $R_{rs}$  spectral ratios.

By applying a similar algorithm to our West Florida Shelf (WFS) data and other stations (Table 1), we found the correlation between the absorption coefficient at 490nm ( $a(490)$ ) and the remote-sensing reflectance ratio of 443 to 550nm is less than for an algorithm using the ratio of 520 to 560nm (Fig.1). This may be explained in part by the influence of bottom reflectance and other components not covarying with chlorophyll for these "Morel Case-2"<sup>2</sup> waters.  $K(490)$  and  $a(490)$  are equivalent in near-surface waters (Eq. 6).

For studying regions that include shallow coastal and "Morel Case-2" waters, we present an algorithm for the calculation of  $a(490)$  based on the study of 39 stations, including blue-sky and over-cast sky

conditions. A curvature algorithm also is presented to "flag" remote sensing data in which bottom reflectance represents more than 20% of the total. We also studied the effect of the 20% bottom contribution on the calculation of pigment (Chl *a* + phaeo *a*) concentration using the "Morel Case-1" algorithm<sup>3</sup>.

Table 1

Data source	Date	Number of stations	Number of overcast stations
Lake Tahoe	Aug. 1990	1	0
TBX I	Mar. 1990	3	0
TBX II	May 1992	11	0
MLML I	May 1991	10	6
Monterey Bay	Apr. Sep. Oct. 1989	9	2
TT010	July 1992	5	5

TBX: Tampa Bay eXperiment (subtropical Gulf of Mexico)

MLML: Marine Light Mixed Layer (high lat. North Atlantic)

TT010: Thomas Thompson 010 (Pacific, San Diego to Hawaii)

## 2. Background and Results

### A. Absorption Algorithm.

Since we do not have total absorption measurements for most of the stations, we used the remote-sensing reflectance model of Lee *et al*<sup>4</sup> to obtain  $a(490)$ . We call this modeled value "*Mod.  $a(490)$* ". Figure 1 shows the relation between the reflectance ratio and *Mod.  $a(490)$* . Figure 2 compares the reflectance ratio to the sum of absorption components due to water molecules and particles ( $a_w + a_p$ ), which includes all in-water absorption except a small gelbstoff residual. We find, in both cases, a higher correlation when 520 to 560nm reflectance ratios are used.

Performing regression analysis on the  $R_{rs}(520)/R_{rs}(560)$  data in Figure 1 yields an algorithm for calculating  $a(490)$ ,

$$Calc.a(490) = 0.14 \left( \frac{R_{rs}(520)}{R_{rs}(560)} \right)^{-2.08} \quad (2)$$

with  $r^2 = 0.96$  and coefficient of variation of 12.5%.

In order to compare Eq. 2 to Eq. 1, we note that remote-sensing reflectance is defined by

$$R_{rs} = \frac{L_w}{E_d} \quad (3)$$

where  $L_w$  is the above surface water-leaving radiance, and  $E_d$  is the

above surface downwelling irradiance. Methods are detailed in Lee *et al.*<sup>4</sup>. Also, the relation between  $L_u$  and  $L_w$  is

$$L_w = \frac{t}{n^2} L_u \quad (4)$$

with  $t$  = transmittance of the air-sea interface, and  $n$  = the index of refraction of seawater. Applying Eqs. 3 and 4, Eq.1 can be rewritten

$$K(490) = 0.0883 \left( \frac{R_{rs}(443) * E_d(443)}{R_{rs}(550) * E_d(550)} \right)^{-1.491} + 0.022 \quad (5)$$

For oceanic waters, the back-scattering coefficient  $b_b$  is small, so  $a$  and  $K$  can be related by

$$a(490) = \mu * K(490) \quad (6)$$

where  $\mu$  is a path-length factor. We used an average value<sup>5</sup> of  $\mu \approx 1/1.5 = 0.67$ , and of  $E_d(443)/E_d(550) \approx 0.95$ , so Eq. 5 is recast as

$$Calc.a(490) = 0.064 \left( \frac{R_{rs}(443)}{R_{rs}(550)} \right)^{-1.491} + 0.015 \quad (7)$$

Figure 3 compares the results using Eq.2 and Eq.7 to estimate  $a(490)$ . If we apply appropriate corrections to the reflectance ratio in Eq.2 to simulate Case I waters (e.g. remove bottom reflectance, colored dissolved organic matter (CDOM) fluorescence, and water Raman

scattering<sup>4</sup>),  $r^2$  is 0.99 and the coefficient of variation is about 10%, and

$$a(490) = 0.136 \left( \frac{R_{rs}(520)}{R_{rs}(560)} \right)^{-2.29} \quad (8)$$

## B. Curvature vs. Bottom Reflectance

Based on the work of Gordon et al<sup>6</sup>, Morel & Prieur<sup>7</sup>, Carder and Steward<sup>8</sup> and Lee *et al*<sup>4</sup>, the remote-sensing reflectance for optically shallow water is expressed as

$$R_{rs} \doteq 0.176 \frac{b_{bw} + b_{bp}}{Q * a} [1 - e^{-3.1aH}] + 0.173 \rho e^{-2.6aH} \quad (9)$$

where  $b_{bw}$  and  $b_{bp}$  are back-scattering coefficients of water and particles respectively,  $a$  is the total absorption coefficient,  $Q$  is the ratio of sub-surface upwelling irradiance to upwelling radiance,  $\rho$  is the bottom albedo, and  $H$  is the bottom depth. This expression excludes the terms for CDOM fluorescence and water Raman scattering, since they play minor roles in this application. Eq.9 is then used to define two curvature numbers:

$$Cur.1 = \frac{R_{rs}(490)^2}{R_{rs}(440) * R_{rs}(560)} \quad (10)$$

$$Cur.2 = \frac{R_{rs}(560)^2}{R_{rs}(490) * R_{rs}(620)} \quad (11)$$

For SeaWiFS usage the 620nm band in *Cur.2* could be changed to

660nm, without altering the validity or usefulness of the expression, but we suggest the addition of a 620nm band to the satellite for the following two reasons: 1)  $L_w(620)$  has a higher signal:noise ratio and less influence from pigment absorption than  $L_w(660)$ , and 2) with this band, the remote-sensing reflectance curve can be modeled more closely to a high resolution curve (Figure 4).

Using Morel's model<sup>9</sup> to provide  $a$  and  $b_b$ , a  $Q$  value<sup>10</sup> of 4.9, and  $\rho = 0.15 * (\lambda/400)^2$  (a general assumption based on the measurement of bottom albedo at several WFS stations) in Eq. 9, we analyzed the change of the two curvature numbers with bottom depth and pigment concentration. Figures 5 and 6 are the results of this analysis. Figure 7 shows the change in  $Cur.1$  for optically deep water versus water with a 20% bottom reflectance contribution. The triangles in the figure are the  $Cur.1$  values of the optically shallow stations in the WFS data set.

The 20% bottom signal is defined for the 440, 490, 520, 560, 620 and 660nm wavelength bands. When the remote-sensing reflectance due to the bottom is 20% of the total signal for any of these bands, then we say there is a 20% bottom signal. Figure 8 illustrates, at low and high pigment concentrations, how the remote-sensing reflectance varies when a 20% bottom signal is present.

Figure 9 shows how the derived pigment concentration from the "Morel Case-1" algorithm varies when a 20% bottom reflectance contribution is included. In Figure 9, percent difference is calculated



through

$$\textit{Percentdiff.} = \frac{C' - C}{C} \times 100 \quad (12)$$

where

$$C = 1.92 \left( \frac{R(440)}{R(560)} \right)^{-1.80} \quad (13)$$

is the "Morel Case-1" algorithm<sup>3</sup>, and  $C$  is calculated with the same equation, but with a reflectance ratio that includes a 20% bottom reflectance contribution.

### 3. Summary

A. Bottom reflectance in optically shallow waters will cause significant error in the derived pigment concentration through its effect on the radiance or reflectance ratios.

B. For shallow coastal waters and "Morel Case-2" waters, an algorithm that uses a spectral ratio between 520 and 560nm seems a better choice to remotely derive total absorption at 490nm.

C. This remote-sensing algorithm (Equation 2) performs well in both clear-sky and overcast conditions.

D. Curvature analysis of the remotely sensed reflectance can provide a "flag" for bottom reflectance contributions of 20% or more of the total signal, to denote pixels likely to produce significant error in pigment concentration calculations.

E. A 20% bottom signal contributes more than 40% error for derived pigment concentrations larger than  $2 \text{ mg/m}^3$ . The error will be even greater for larger bottom signals.

## References:

1. Austin, R.W. and T.J. Petzold, 1981, "The determination of the diffuse attenuation coefficient of sea water using the coastal zone color scanner", in Oceanography from Space, edited by J.F.R. Gower, Plenum press, Marine Science 13, 239-256.
2. Gordon, H.R. and A. Morel, 1983, "Remote assessment of ocean color for interpretation of satellite visible imagery: A review. Springer.
3. Morel, A., 1980, "In-water and remote measurement of ocean color", Boundary Layer Meteorology, 18, 177-201.
4. Lee, Z., K.L. Carder, S.K. Hawes, R.G. Steward, T.G. Peacock, and C.O. Davis, 1992, " An interpretation of high spectral resolution remote sensing reflectance", Ocean Optics XI, Proc. SPIE. 1705: in press.
5. Marshall, B.R. and R.C. Smith, 1990, "Raman scattering and in-water ocean properties", Applied Optics, 29(1), 71-84.
6. Gordon, H.R., O.B. Brown and M.M. Jacobs, 1975, "Computed relationship between the inherent and apparent optical properties of a flat homogeneous ocean", Applied Optics, 14, 417-427.
7. Morel A. and L.Prieur, 1977, "Analysis of variations in ocean color", L&O, 22(4), 709-722.
8. Carder, K.L. and R.G. Steward, 1985, "A remote sensing reflectance model of a red tide dinoflagellate off West Florida", L&O, 30(2), 286-298.
9. Morel, A., 1988, "Optical modeling of the upper ocean in relation to its biogenous matter content (Case I waters), JGR, 93(C9), 10, 10,749-10768.

10. Kirk, J.T.O., 1986, Light and photosynthesis in aquatic ecosystems, Cambridge University Press.
11. Smith, R.C., and K.S. Baker, 1981, Optical properties of the clearest natural waters (200-800 nm), Appl. Opt., 20(2), pp.177-184.

**Figure 1:** Reflectance ratios (from data uncorrected for bottom reflectance contribution) plotted against modeled total absorption coefficient at 490nm (from Lee *et al*<sup>4</sup> model).

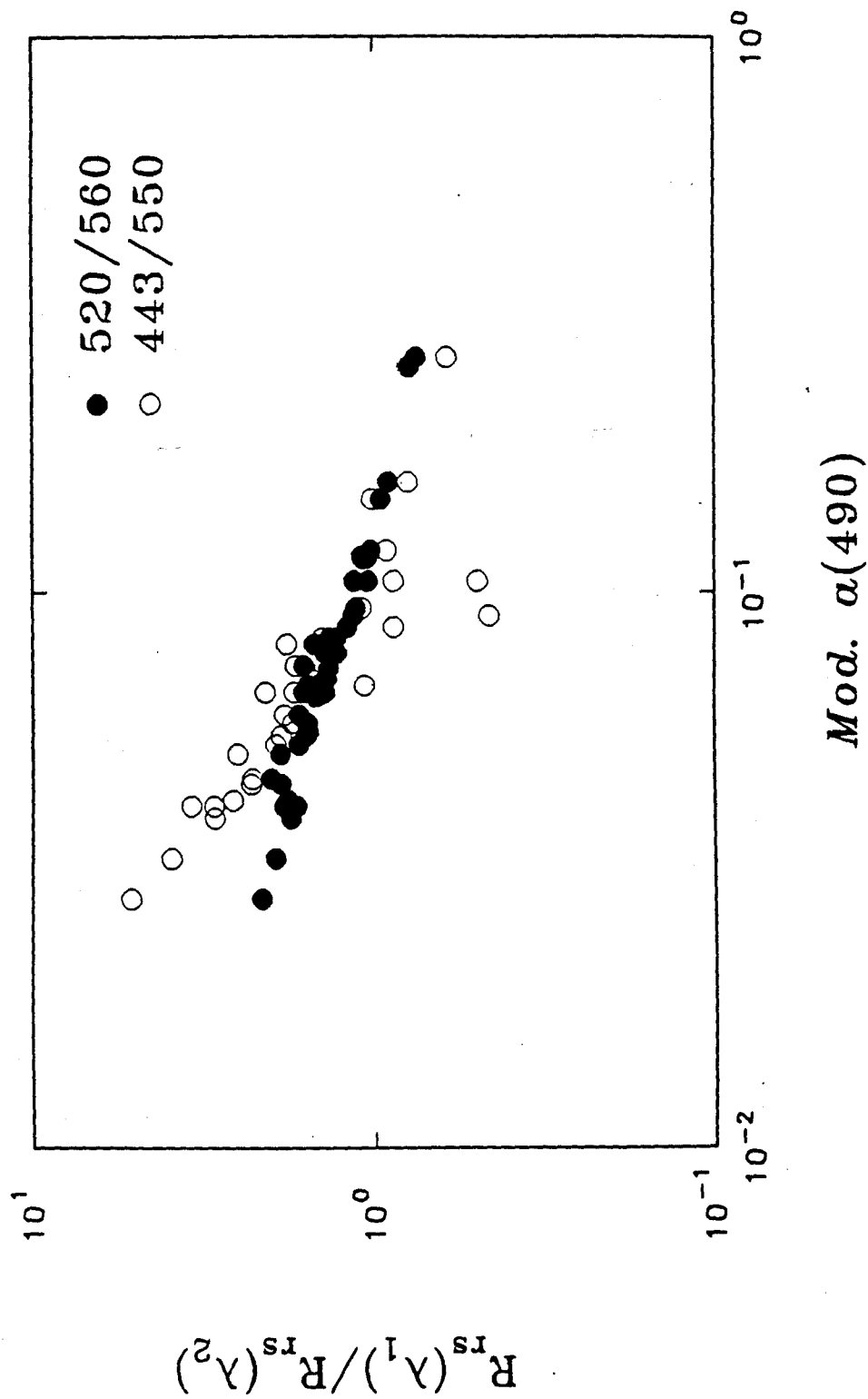


**Figure 2:** Reflectance ratios from Figure 1 plotted against the sum of water and particulate absorption at 490nm.  $a_w$  is from Smith and Baker<sup>11</sup>,  $a_p$  is measured.

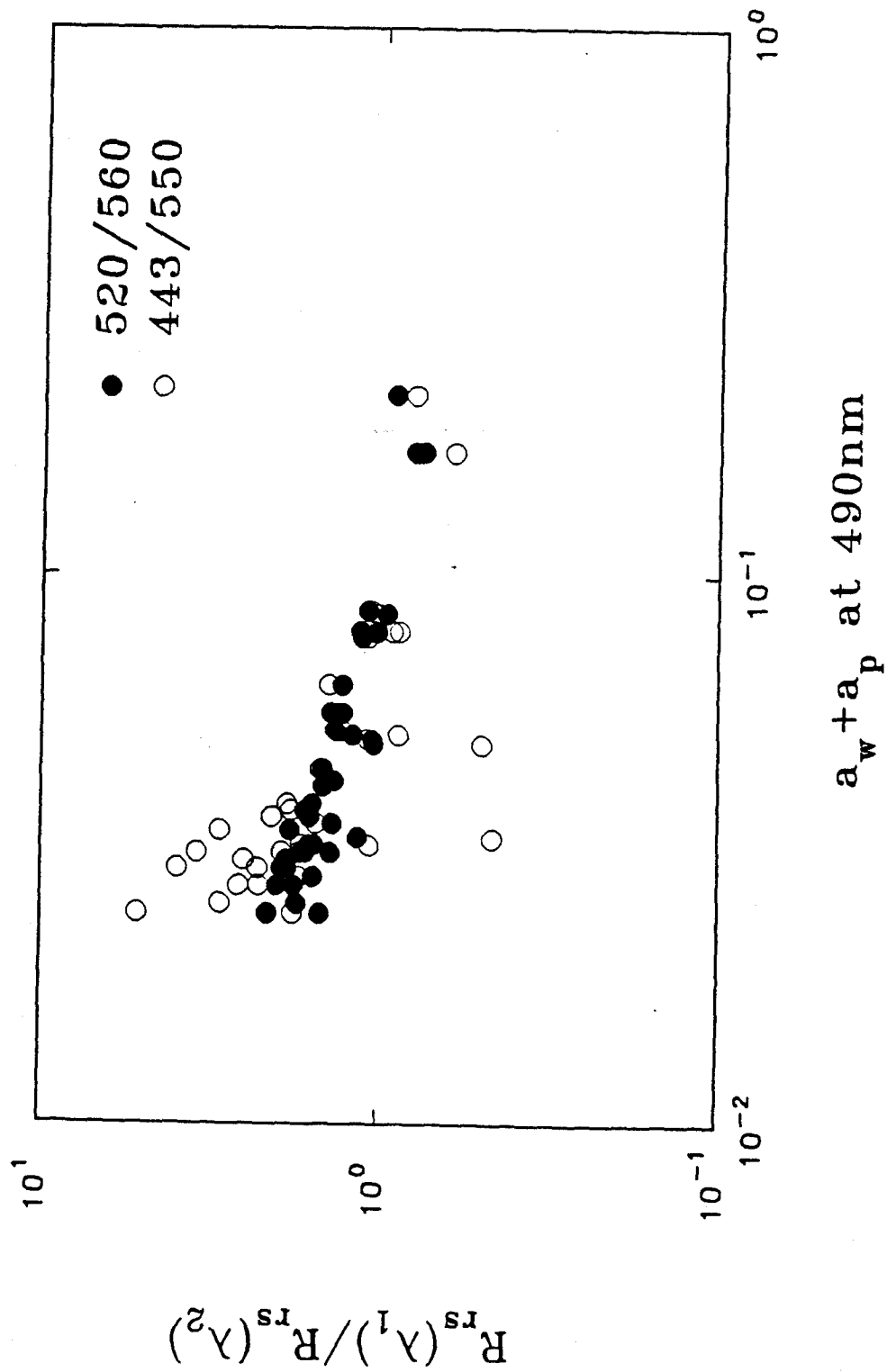


**Figure 3:** Calculated  $a(490)$  from Equations 2 and 7 plotted against modeled  $a(490)$  from Lee *et al*<sup>4</sup> model. Reflectance ratios used to calculate  $a(490)$  are those plotted in Figures 1 and 2.

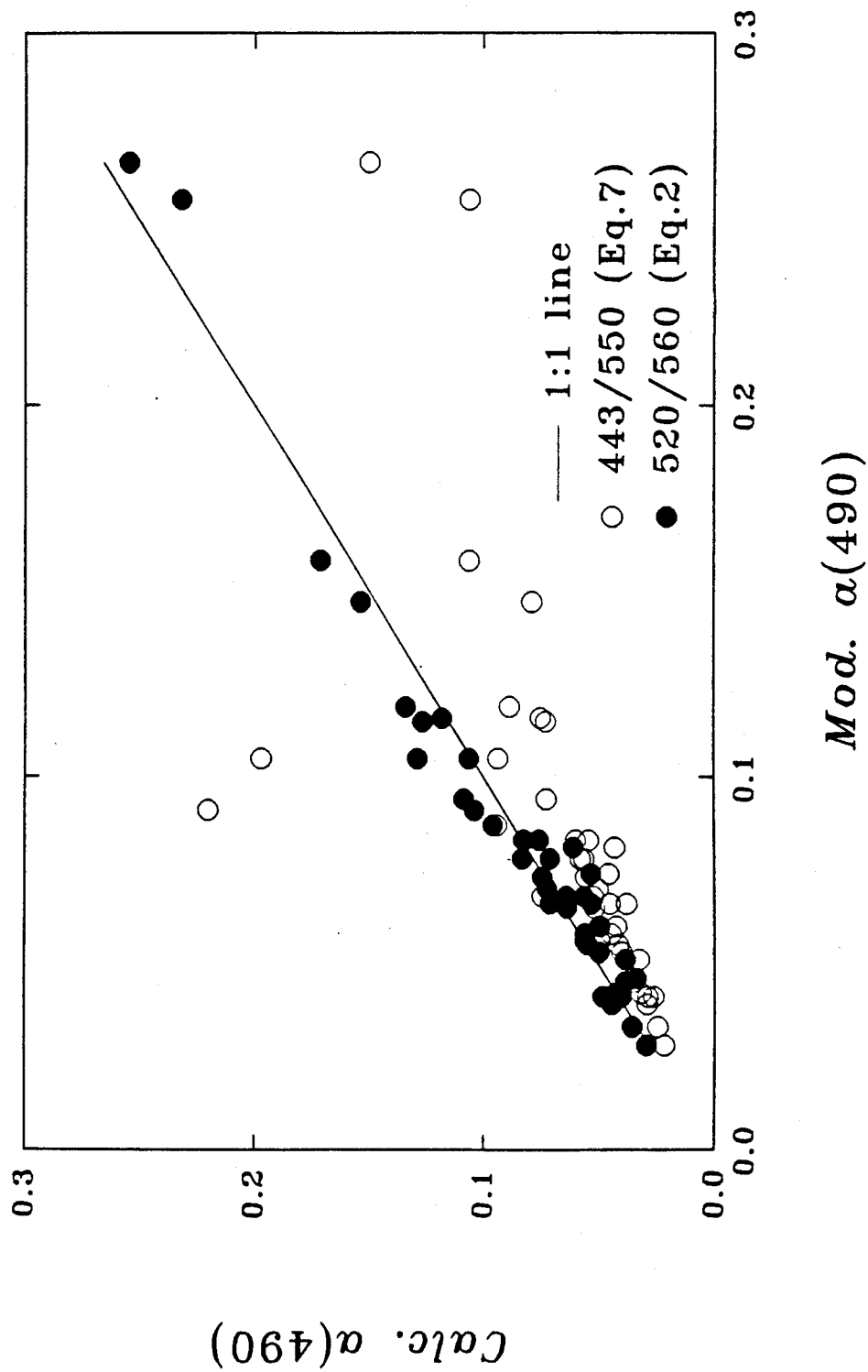


**Figure 4:** High resolution remote-sensing reflectance (solid line), and SeaWiFS spectral bands. The dotted lines are water column and bottom reflectance components. Depth is 7.5 m, and pigment concentration is  $1.23 \text{ mg m}^{-3}$ .

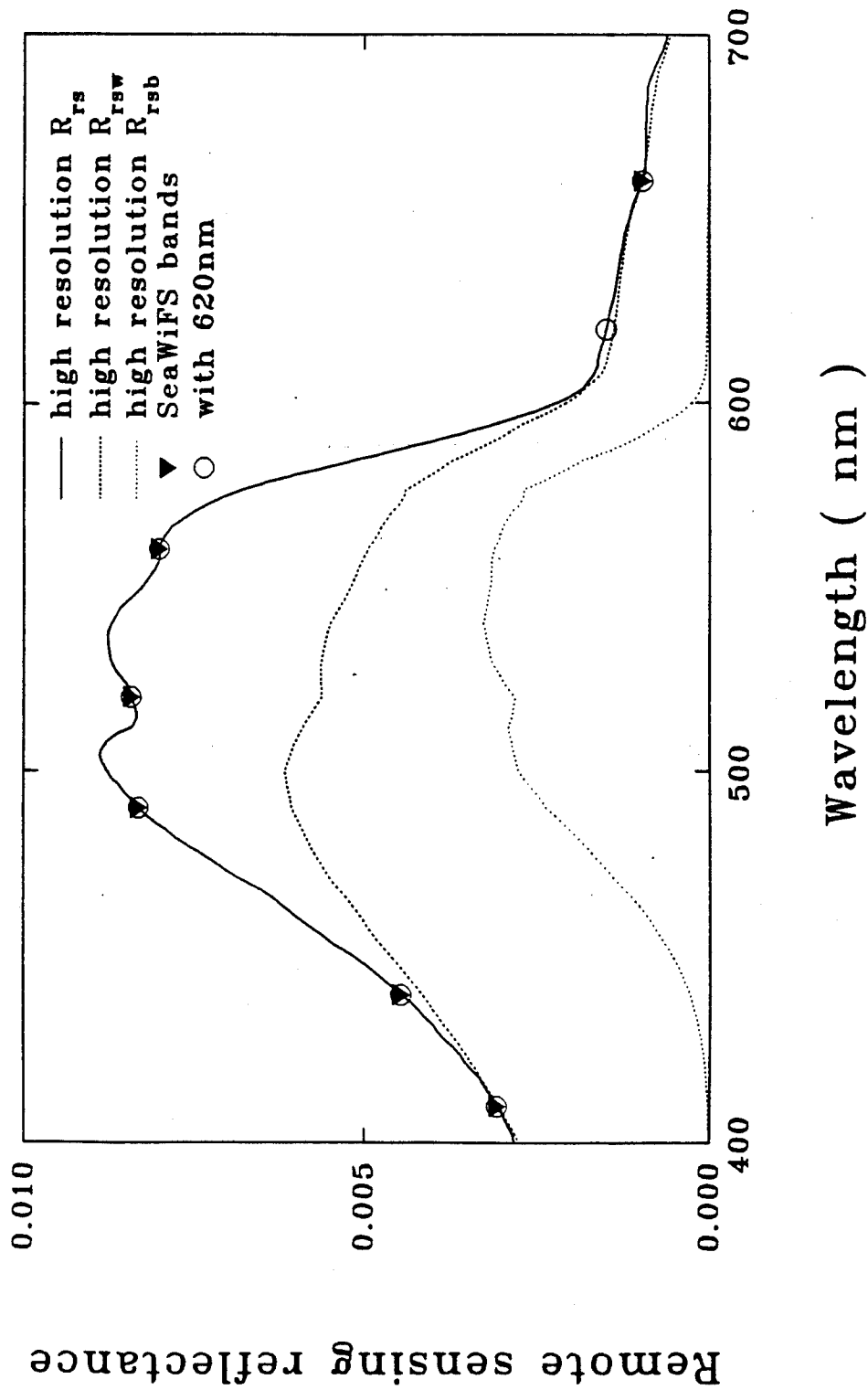




**Figure 5:** Surface plot of Equation 10. Total absorption  $a(490)$  and bottom depth effects are convoluted within the  $R_{rs}$  values, where  $a(490)$  varies with pigment concentration according to Morel<sup>9</sup>.

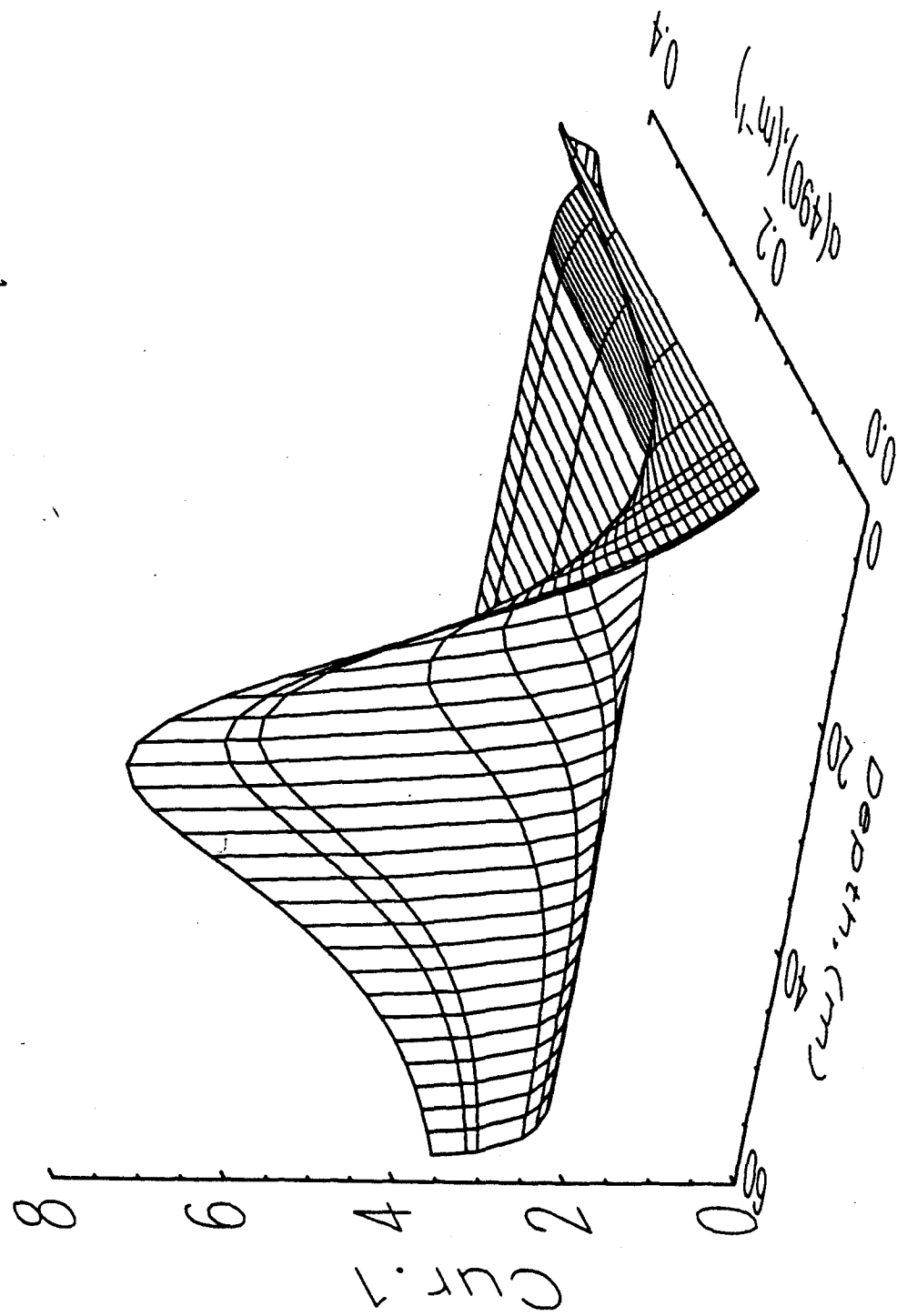


**Figure 6:** Surface plot of Equation 11. Note the reversal of the  $a(490)$  axis with respect to Figure 5.

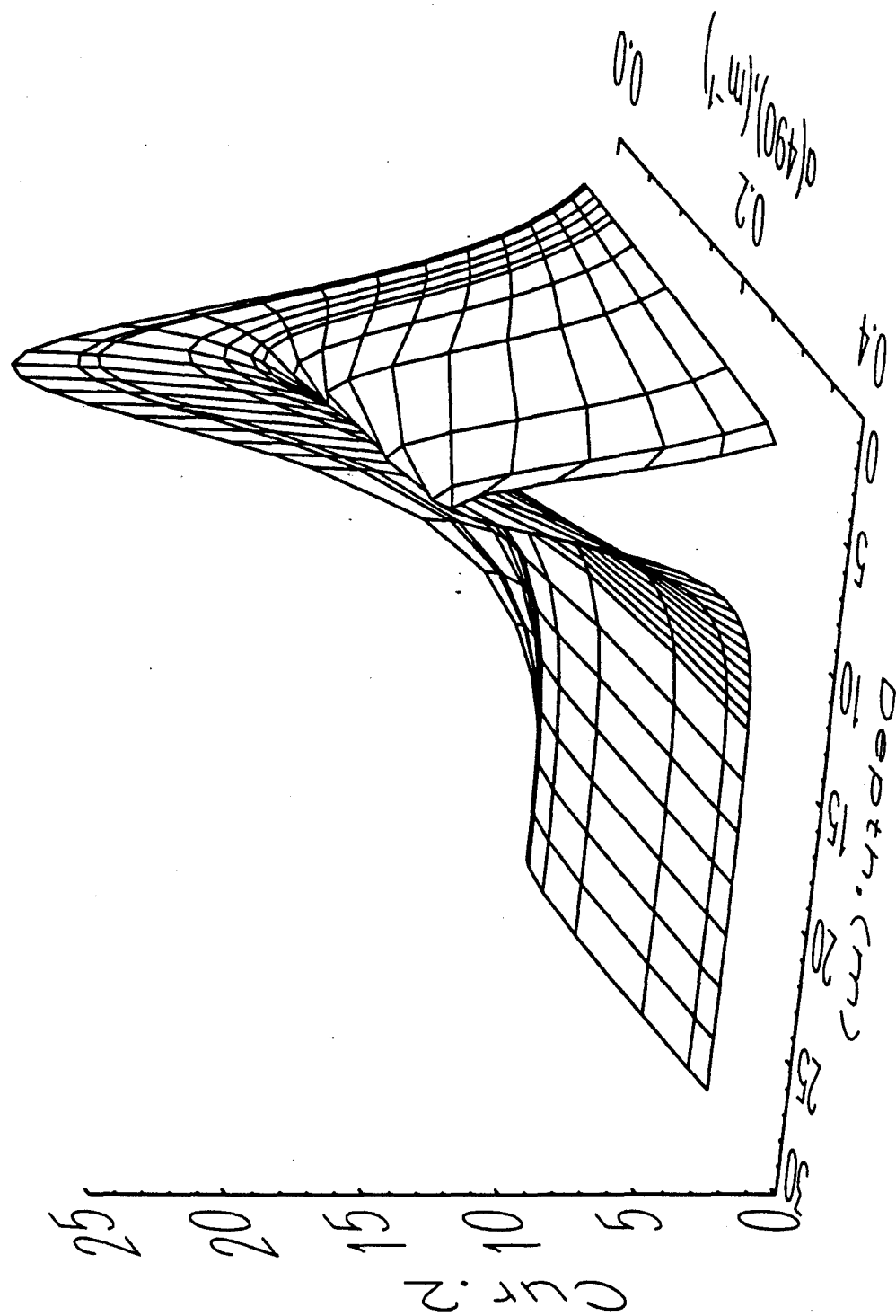
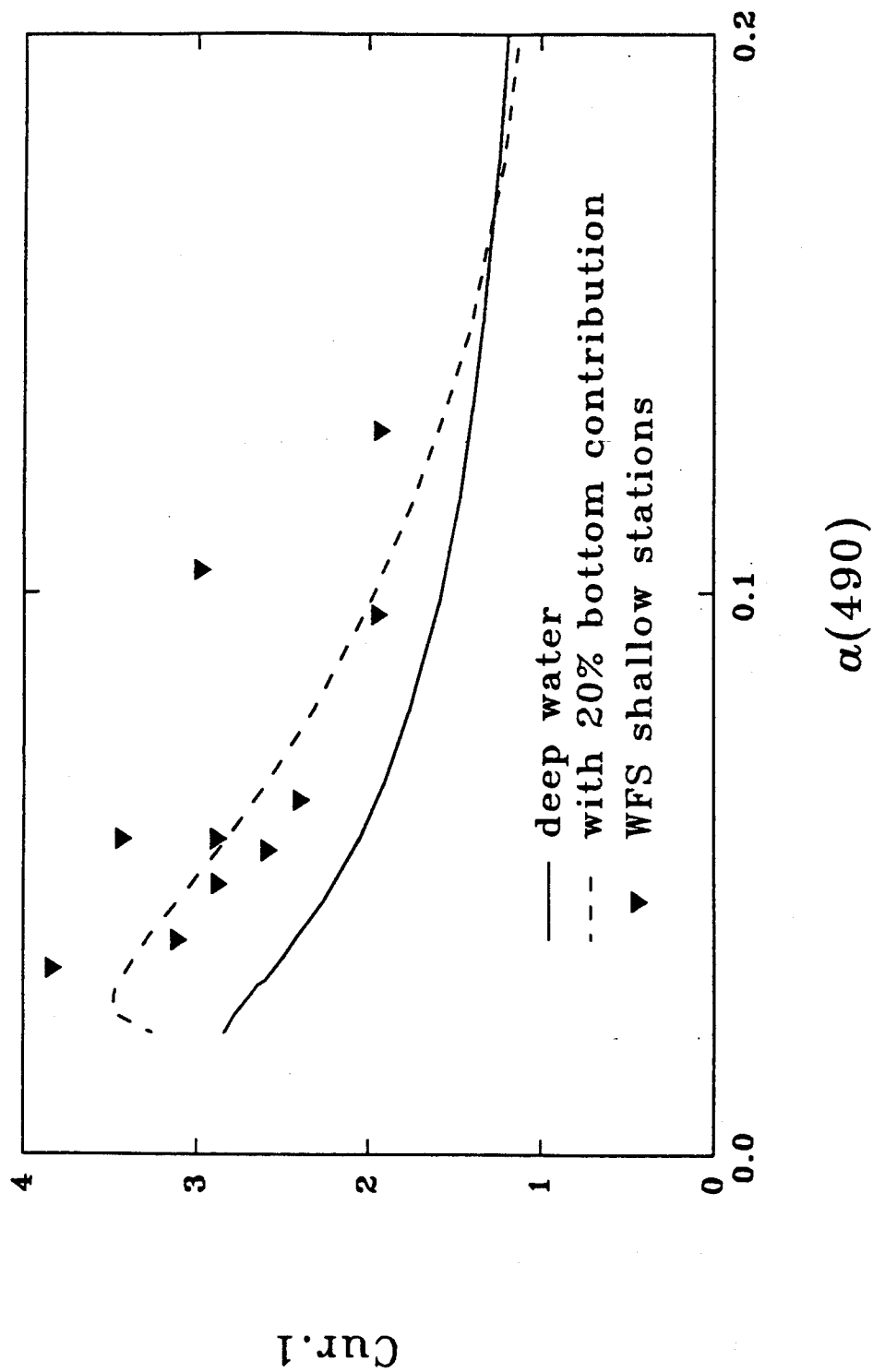
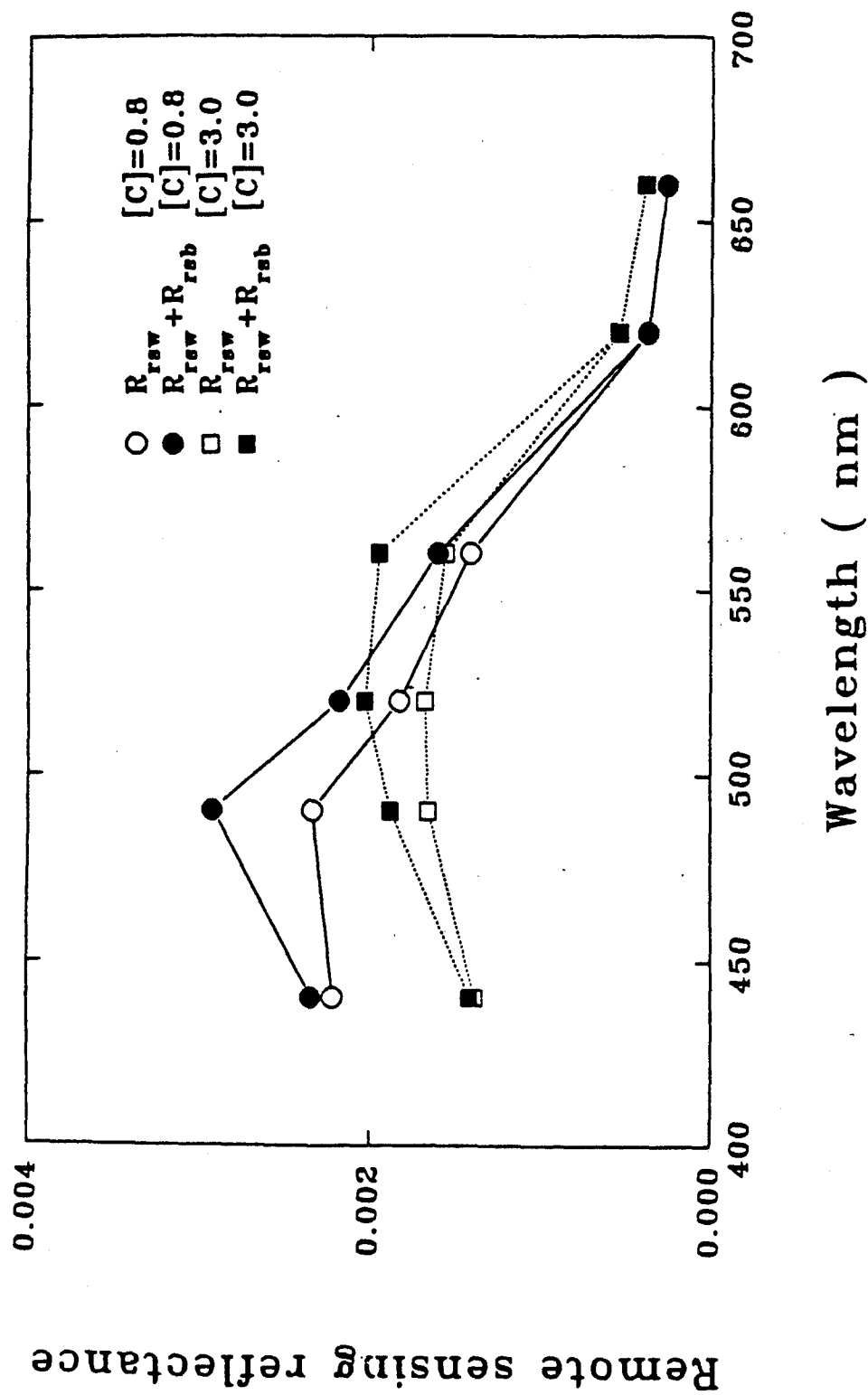


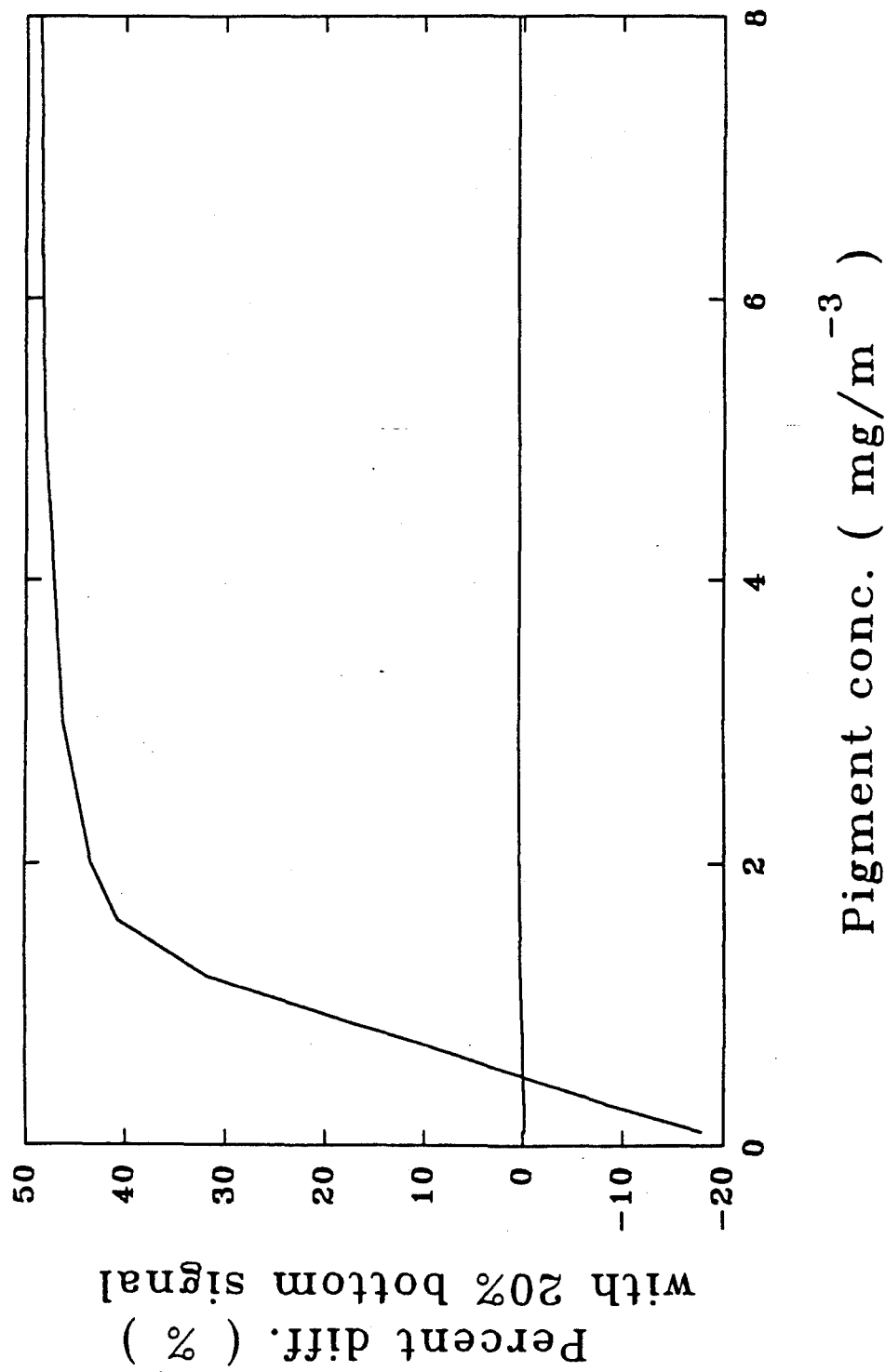
Figure 7: Effect of bottom reflectance on Equation 10, as a function of total absorption at 490nm.



**Figure 8:** Effect of bottom reflectance on remote-sensing reflectance. Subscripts  $r_{sw}$  and  $r_{sb}$  refer to the remote-sensing reflectance signal of the water column and bottom, respectively.  $[C]$  is the pigment concentration ( $\text{mg m}^{-3}$ ).



**Figure 9:** Percent difference in pigment concentration calculated from "Morel Case 1" algorithm, when a 20% bottom reflectance contribution is present and unaccounted for.



Calculated Quantum Yield of Photosynthesis of Phytoplankton  
in the Marine Light-Mixed Layers (59°N/21°W)

K.L. Carder<sup>1</sup>, Z.P. Lee<sup>1</sup>, J. Marra<sup>2</sup>, R.G. Steward<sup>1</sup>, and M.J. Perry<sup>3</sup>

<sup>1</sup>Department of Marine Science  
University of South Florida  
St. Petersburg, FL 33701

<sup>2</sup>Lamont-Doherty Earth Observatory of Columbia University  
Palisades, New York 10964

<sup>3</sup>School of Oceanography, WB-10  
University of Washington  
Seattle, WA 98195

running heading: *quantum yield of photosynthesis*

submitted to Journal of Geophysical Research (Special Edition)

## ABSTRACT

The quantum yield  $\phi$  of photosynthesis ( $\text{mol C (mol photons)}^{-1}$ ) at 6 depths for the waters of the Marine Light-Mixed Layer (ML-ML) cruise of May 1991 were calculated. As there were *PAR* (photosynthetically available radiation) but no spectral irradiance measurements for the primary production incubations, three ways are presented here for the calculation of the absorbed photons by phytoplankton (*AP*) for the purpose of calculating  $\phi$ . The first is based on a simple, non-spectral model; the second is based on a non-linear regression using measured *PAR* values with depth; and the third is derived through remote sensing measurements. We show that the results of  $\phi$  calculated using the non-linear regression method and those using remote sensing are in good agreement with each other, and are consistent with the reported values of other studies. In deep waters, however, the simple non-spectral model may cause quantum yield values much higher than theoretically possible.

## INTRODUCTION

Traditional methods for estimating the light absorbed by phytoplankton at depth in the ocean have often used nonspectral *PAR* (Photosynthetically available radiation) measurements or calculations, and spectrally averaged (without light-field weighting) phytoplankton specific-absorption coefficients. Two alternative, spectral methods are presented here for use with remotely sensed data: one for use with remote floating or moored arrays equipped with nonspectral *PAR* sensors, and one for use with satellite or aircraft-derived remote-sensing reflectance data. Both alternatives utilize spectrally dependent total absorption coefficients to model the depth dependent, spectral light field. These light fields are then spectrally integrated at depth for comparison to *PAR* measurements.

Primary production (*PP*) in the ocean is dependent on the absorption of incident photons by phytoplankton and on the efficiency with which phytoplankton use this absorbed energy. At depth  $z$  for a time period of  $T$ , *PP* is

$$PP(z) = \phi(z) \int_T \int_{\lambda} E_q(z, \lambda, t) [chl\ a(z)] a_{ph}^*(z, \lambda, t) d\lambda dt, \quad (1)$$

(Symbols are defined in Table 1. To be terse, the functionality of one quantity to another might not be explicitly expressed in the remaining text.) The symbol  $\phi$  in the right side of Eq. 1 describes the energy-conversion efficiency for photosynthesis and is defined as quantum yield of photosynthesis [Bannister, 1974; Tyler, 1975; Kiefer and Mitchell, 1983; Bannister and Weidemann, 1984; Dubinsky et al., 1984 and Cleveland et al., 1989]. The rest of the right side of Eq. 1,

$$AP(z) = \int_T \int_{\lambda} E_q(z, \lambda, t) [chl\ a(z)] a_{ph}^*(z, \lambda, t) d\lambda dt, \quad (2)$$

describes the absorbed photons by phytoplankton at that depth for the time period. Eqs. 1 and 2 are usually integrated over hours or a day, and over a wavelength range from 400 to 700 nm. So quantum yield  $\phi$ , a time average, is

In order to estimate primary production through optical properties, using either moored sensors [Marra et al., 1992] or remote measurements [Cullen, 1990; Platt et al., 1991; Balch et al., 1992], the magnitude and



$$\phi(z) = \frac{PP(z)}{AP(z)} \quad (3)$$

variability of the quantum yield of photosynthesis ( $\phi$ ) in the ocean must be known. Laboratory studies have been carried out [Kiefer and Mitchell, 1983; Langdon, 1988 and references cited], but there is a paucity of *in situ* estimates of  $\phi$ . Ship-board incubations have been used to simulate *in situ* studies, but most have used white light, which can cause errors as large as a factor of two [Laws *et al.*, 1990]. Also, in many cases, non-spectral models have been used to calculate the light absorbed by phytoplankton at depth for  $\phi$  estimations [Tyler, 1975; Bannister, 1979; Marra *et al.*, 1992]. However, due to the filtration effect of the overlaying water column, non-spectral models do not accurately describe the light absorbed by phytoplankton at depth [Morel, 1978; Kishino, 1986]. For more accurate *in situ*  $\phi$  measurements, the spectral interaction between the light at depth and the phytoplankton absorption needs to be considered.

Bannister and Weidemann [1984] and Kishino [1986] presented approaches to derive *in situ*  $\phi$ . However, these approaches require obtaining knowledge of the spectral character of  $E_d(\lambda, z)$ , which can be a rather expensive proposition: either i) a ship must remain near an incubation array to measure the spectral light field at each incubation depth, or ii) a spectral, scalar-irradiance meter must be attached to the floating array at each incubation depth.

Neither of these alternatives were feasible for the ML-ML study, although spectrally integrated *PAR* measurements (inexpensive) were made at four depths from a floating array. For the calculation of  $\phi$ , *AP* at the incubation depths (different from the depths of *PAR* measurements) were calculated by three simplified methods. The first is a typical non-spectral method [*e.g.* Marra *et al.*, 1992] to show how the results differ from spectral model results. The second is through use of a non-linear regression method for interpolating *PAR* values between and below *PAR* measurements. The third, based upon surface *PAR* and absorption coefficients derived from surface remote-sensing measurements, is applicable to ocean color data collected from spacecraft or aircraft. These methods were tested at four Marine Light-Mixed Layer stations, and the differences among the results are discussed and evaluated.

## MEASUREMENTS

Data of  $PAR(z)$ ,  $PP(z)$ ,  $a_{ph}(\lambda)$  (absorption coefficient of phytoplankton) and  $R_r(\lambda)$  (remote-sensing reflectance) were collected on an ML-ML cruise from May 17 to May 24, 1991 in the waters south of Iceland. The water depths where  $PAR$  and  $PP$  were measured were not the same (see subsections a and b below), although they were carried out on the same floating array for four days: May 17, 20, 22 and 24. The sampling site, conditions, wind, mixing, and nutrients are presented in Marra et al., Jones et al. and Plueddemann et al. [*all in this issue*].

a. Photosynthetically available radiation,  $PAR(z)$

$PAR(z)$  at four depths (0, 2, 12.5, and 25 m) were monitored and averaged for every 10 minute interval throughout the day with a Biospherical  $PAR$  sensor attached to each incubation array [*see Marra et al., this issue*].

b. Primary production,  $PP(z)$

Dawn-to-dusk (17 hours) incubations with four replicates were carried out *in situ* at each of six depths (5, 10, 15, 20, 30 and 40 m) chosen to span the euphotic zone. Primary production measurements were made using the  $^{14}C$  technique [*see Marra et al., this issue*].

c. Absorption coefficient of phytoplankton pigments,  $a_{ph}(\lambda)$

Measurements of  $a_{ph}(\lambda)$  for replicates of the incubation samples were obtained in the following manner. The method described by Mitchell & Kiefer [1988] was used to measure the particulate absorption coefficients, with a Lambertian diffuser added between the light source and the filter pad to minimize any dependence of the diffuse transmittance on the optical geometry of the light which is incident on the pad. This arrangement is very similar to that of Bricaud & Stramski [1990], who illuminated a pad in front of a diffusing window which was adjacent to an end-on photomultiplier tube. Our collector was a Spectron Engineering Spectroradiometer with  $10^\circ$  acceptance angle. We filtered about 300 ml water samples onto Whatman GF/F pads, the transmission spectra (380-780nm)

of these pads were ratioed against that of wetted blank pads to obtain the optical density of the particles, and this optical density was corrected for large particle scattering. The particulate absorption coefficient was calculated, using Eq. 2 from Bricaud & Stramski [1990] to correct for optical pathlength elongation due to scattering in the pad ("β factor"). After this measurement each sample was soaked in hot methanol [Kishino *et al.*, 1985; Roesler *et al.*, 1989] for about 15 minutes to remove pigments, and its transmission spectra was again measured and ratioed against a methanol wetted blank to obtain the detrital absorption coefficient ( $a_d(\lambda)$ ). The difference between the particle and detrital absorption coefficients provided the absorption coefficient for phytoplankton,  $a_{ph}(\lambda)$ .

Gelbstoff absorption coefficients for surface waters were reported in Walsh *et al.* [1992], who filtered seawater through 0.2 μm Gelman Supor-200 filters and measured the absorption on a Cary model-2200 spectrophotometer with a 10 cm cell. The approach followed that of Bricaud *et al.* [1981] where absorption at 370 nm was extrapolated to 440 nm as  $a_t(440) = a_t(370)e^{-0.014(440-370)}$  with an average semi-log, spectral slope of - 0.014 nm<sup>-1</sup>.

#### d. Remote sensing reflectance, $R_{rs}(\lambda)$

Hyperspectral remote-sensing reflectance  $R_{rs}(\lambda)$  (the ratio of water leaving radiance to the downwelling irradiance above the sea surface) was measured at noon for each station by the method developed by Carder and Steward [1985], using the Spectron Engineering Spectroradiometer. It has 253 channels and covers the wavelength range from 370 - 1100 nm. With this instrument the water-leaving radiance and downwelling sky radiance were directly measured, and downwelling irradiance was measured by viewing a standard diffuse reflector (Spectralon, ~8.5%). Sky radiance reflected from the sea surface was removed by the method of Carder and Steward [1985] when calculating  $R_{rs}(\lambda)$ .

### AP and φ CALCULATION

#### a. Simple, non-spectral model.

Due to the expense of obtaining the spectral light field  $E_d(\lambda)$  with depth, a simplified model for PP is

usually used [Tyler, 1975; Bannister, 1979; Morel, 1991; Marra et al., 1992],

$$PP(z) = \phi(z)[chl\ a(z)]\bar{a}_{ph}^*(z)PAR(z), \quad (4)$$

where  $\bar{a}_{ph}^*$  ( $m^2\ (mg\ chl\ a)^{-1}$ ) is the spectrally averaged chlorophyll-specific absorption coefficient:

$$\bar{a}_{ph}^* = \frac{\int_{400}^{700} a_{ph}(\lambda) d\lambda}{[chl\ a](700-400)}, \quad (5)$$

and

$$PAR(z) = \int_T \int_{400}^{700} E_q(\lambda, t, z) d\lambda dt. \quad (6)$$

For the calculation of  $PAR$  at incubation depths,  $K_{PAR}$  was calculated first according to

$$K_{PAR} = \frac{\ln[PAR(z_1)] - \ln[PAR(z_2)]}{z_2 - z_1}, \quad (7)$$

and then the  $K_{PAR}$  value between 2 and 12.5 m is used to calculate  $PAR(5)$  and  $PAR(10)$ , and the value between 12.5 and 25 m is used to calculate  $PAR(15)$ ,  $PAR(20)$ ,  $PAR(30)$  and  $PAR(40)$ .

Thus, from Eqs. 1 and 2, we have

$$\phi(z) = \frac{PP(z)}{[chl\ a(z)]\bar{a}_{ph}^*PAR(z)}. \quad (8)$$

Since  $PP$ ,  $[chl\ a]$  and  $\bar{a}_{ph}^*$  were measured, it is easy to calculate  $\phi$  this way. However, as has been pointed out by Morel [1978] and Kishino [1986], a simple average for  $\bar{a}_{ph}^*$  (Eq. 5) does not accurately describe the phytoplankton absorption at depth, and a light-field-weighted average needs to be applied to  $\bar{a}_{ph}^*$ . Thus, a better approximation that includes the character of light at depth is necessary. The following two sections describe two ways to model the spectral character of the light field at depth when only  $PAR(z)$ , or  $R_{\pi}(\lambda)$  and  $a_p(\lambda, z)$  are available.

#### b. Non-linear regression.

At depth  $z$ , daily  $PAR$  can be expressed as

$$PAR(z) \sim \int_{Day} \int_{\lambda} E_q(0, \lambda, t) e^{-\{K(\lambda)\}z} d\lambda dt, \quad (9)$$

where  $E_q(0, \lambda, t)$  is the sub-surface scalar irradiance at time  $t$  in units  $\text{mol quanta m}^{-2}\text{s}^{-1}\text{nm}^{-1}$ ,  $\{K\}$  is the vertically-averaged diffuse attenuation coefficient, and  $\{K\}$  is approximated by  $\{K\} = 1.08(a + b_b)/\mu_0$  [Kirk, 1984; Gordon, 1989]. In Eq. 9, since most of the stations were cloudy,  $E_q$  from the Sun and from the sky are combined. For clear sky situations, separation of these two may be necessary since the average cosine values for sun light and sky light are generally different [Platt *et al.*, 1991]. Since there were no time series of  $E_q(0, \lambda)$  and  $a_p(\lambda)$ , some assumptions have to be made in order to calculate the spectral light field at depth:

- i). Gelbstoff absorption was constant for all depths;
- ii). Average of  $a_p$  for dawn and noon measurements was considered to represent the particle absorption coefficient for the whole day;
- iii). Due to the presence of clouds, it is difficult to estimate  $\mu_0$  for any given time. So an average sub-surface average cosine of  $\mu_0 = 0.77$  was used for these high-latitude sites for the whole day, including sunny, cloudy and overcast conditions;
- iv).  $b_b < a$  [Morel and Prieur, 1977].

Then we have

$$PAR(z) \sim \int_{\lambda} E_q(0) e^{-1.4[(a_w + a_p)z + \Sigma a_p \Delta z]} d\lambda, \quad (10)$$

where 1.4 in the exponent is  $\approx 1.08/0.77$ , and integration over time is implicitly combined into  $E_q(0)$ , and  $\Sigma \Delta z$  is  $\Sigma a_p \Delta z = \Sigma_i a_p(z_i)(z_{i+1} - z_i)$ .

In Eq. 10, vertical stratification of  $a_p$  is considered although most of the stations were quite well mixed [see Marra *et al.*, this issue]. Also, for Eq. 10,  $PAR(z)$  and  $a_p(z)$  were measured,  $a_w$  is known [Smith and Baker, 1981], and  $E_q(0)$  and  $a_p$  must be derived.

$a_p(\lambda)$  can be expressed as  $a_p(\lambda) = a_p(440)e^{-0.014(\lambda-440)}$  [Bricaud *et al.* 1981]. Since this variable is very difficult to measure at visible wavelengths for open ocean waters [Bricaud *et al.*, 1981], Walsh *et al.* [1992]

measured  $a_p(370)$  and used the above expression to extrapolate to  $a_p(440)$  for waters at the ML-ML site. The spectral slope  $0.014 \text{ nm}^{-1}$  for  $a_p$  is assumed and kept as constant for all the stations.

$E_q(0)$  is expressed as  $E_q(0) = PAR(0)_{der} * E_q^*(0)$ , where  $PAR(0)_{der}$  is the derived surface  $PAR$  in order to correct possible errors in measured  $PAR(z)$  due to sea-surface roughness, and  $E_q^*(0) = E_q(0)/PAR(0)$ .  $E_q(0)$  and  $PAR(0)$  are computed using the model of Gregg and Carder [1990]. There were typically 4 (3 for May 22)  $PAR$  measurements for each day, so  $PAR(0)_{der}$  and  $a_p(440)$  for each day can be derived by non-linear regression: i.e. minimize the variance between the modeled and measured  $PAR$ . The derived  $a_p(440)$  values are shown in Table 3.

After the derivation of  $PAR(0)_{der}$  and  $a_p(440)$ , quantum yield can be calculated for each depth through

$$\phi(z) = \frac{PP(z)}{PAR(0)_{der} \int_{\lambda} E_q^*(0) e^{-1.4[(a_w + a_p)z + \sum a_i \Delta z]} a_{ph} d\lambda} \quad (11)$$

### c. Remote sensing reflectance

With recent measurement techniques [e.g. Carder and Steward, 1985] and models for interpreting hyperspectral remote-sensing reflectance ( $R_{rs}$ ) data [Carder and Steward, 1985; Peacock et al., 1990; Lee et al., 1992; Lee et al., 1994(a), 1994(b)], it has been shown that by inversion of the measured  $R_{rs}$ , the total absorption coefficient for the surface layer can be derived [Lee et al., 1994(a), 1994(b)]. This measurement approach avoids the inherent problems of in-water reflectance measurements such as instrument-self shading [Gordon and Ding, 1992] and ship shadows [Gordon, 1985].

To use this approach, i.e. deriving the total absorption coefficient and then calculating the photons absorbed by phytoplankton at depth for a day, we still need most of those assumptions made for the non-linear regression method. However,  $PAR(0)_{der}$  is set to equal the measured surface  $PAR$ , and the total absorption  $a(\lambda)$  is derived by inverting  $R_{rs}(\lambda)$  data [see Lee et al., 1994(a)]. One approach for deriving  $a(\lambda)$  from  $R_{rs}$  is suggested by Gordon et al. [1988], Morel [1988], and Sathyendranath and Platt [1988]. They empirically derive the chlorophyll concentration first and use an empirical specific absorption coefficient to calculate the particle absorption coefficient. The gelbstoff absorption coefficient is assumed to covary with [chl  $a$ ]. This method only works well for "case 1"

waters [Morel and Prieur, 1977].

Recent studies [Gordon et al., 1988; Morel and Gentili, 1993; Lee et al., 1992, 1994(a)] show that  $R_{rs}$  can be expressed as

$$R_{rs} = \frac{G}{a_w + a_p + a_s} [b_{bw} + X(\frac{400}{\lambda})^Y] , \quad (12)$$

where  $G \approx 0.093(\tau/n)^2$ , the air-sea interface transmittance  $\tau \approx 0.97$  for most of the ocean [Austin, 1974], and  $n \approx 1.341$  is the refractive index of sea water. The two terms in brackets consist of scattering contributions due to water molecules and particles, respectively. The back-scattering coefficient of pure water,  $b_{bw}$ , is given by Smith and Baker [1981], and  $X$  and  $Y$  are site specific and can be derived from  $R_{rs}$  [Lee et al., 1994(a), 1994(b)].

By adjusting parameters affecting the modeled  $R_{rs}$  curve to achieve a close fit with the measured  $R_{rs}$  curve,  $a_s(\lambda)$  of the surface layer was derived. The derived  $a_s(440)$  values are shown in Table 3. In the derivation of  $a_s$  using  $R_{rs}$ , a multiplication factor  $f$  was applied to the surface  $a_p$  as in Lee et al. [1994(a)]. For the ML-ML waters  $f$  varied from 1.0 - 1.2. This factor accounts for possible errors in particle absorption due to plankton patchiness, vertical stratification, and the " $\beta$  factor".

After the inversion of  $R_{rs}$ , the sum  $a_w + f * a_p + a_s$  was used as the average total absorption coefficient for the water column to calculate *PAR* and *AP* at depth using measured profiles of  $a_{ph}(z)$ . Quantum yield values were then calculated based upon measured values of primary production.

## RESULTS and DISCUSSION

Figure 1 shows the pre-dawn (open symbols) and noon (filled symbols) measured chlorophyll values for the cruise. Notice that there was no strong vertical structure in the water column, if the average of the pre-dawn and noon profiles are considered. The differences between pre-dawn and noon chlorophyll values were larger for May 17 and 20, but much smaller for May 22 and 24, however.

Figure 2 shows the measured primary production for each of the four days. The surface production decreased from Day 1 to Day 3. This might be due in part to the progressive reduction in chlorophyll with time,

but the variation in  $PAR(0)$  values in Table 3 suggests a more complicated explanation.

Figures 3(a) and 3(b) show the measured spectra of remote-sensing reflectance and the pre-dawn particle absorption coefficients for the upper water column, respectively. May 17 had the lowest  $R_{rs}$  values around 440 nm, consistent with the highest noon chlorophyll concentration among the 4 days (Figure 1). Also notice the high  $R_{rs}(685)$  values for May 17, likely resulting from the contribution of chlorophyll *a* fluorescence. For the following 3 stations, the  $R_{rs}$  values were similar as their surface noon chlorophyll concentrations did not vary much (Figure 1).

The detritus-to-pigment ratio for absorption at 440 nm was in the range of 15 to 20 % with an average of about 18 %. The spectral curves were simulated using exponential functions with an average semi-log spectral slope for  $a_d$  of about  $-0.010 \text{ nm}^{-1}$ , similar to that found by Roesler et al. [1989].

Figures 4(a) to 4(d) show the measured and calculated  $PAR$  for the four days. In general,  $PAR$  values at greater depths calculated by the simple, non-spectral model were lower than those determined by non-linear regression and by  $R_{rs}$  methods. One reason why  $PAR$  estimates at greater depths were lower using the non-spectral model is that Beer's Law does not hold for  $K_{PAR}$  [Gordon, 1989]. The  $PAR$  values determined by non-linear regression and  $R_{rs}$  methods were quite close (average difference of 9%). Compared to the  $PAR$  values at 2 m, 12.5 m and 25 m, the average difference between the measured and  $R_{rs}$ -method calculations was 19%. Most of the difference was found at 2 m (see figure 4), where the measured values appeared to be low, especially on May 24. However, it is not clear what caused this.

Figures 5(a) to 5(d) show the calculated quantum yield  $\phi$  values for the four days. The simple, non-spectral model generates the highest  $\phi$  values at 30 and 40 m, some of which are much higher than the  $0.12 \text{ mol C (mol photons)}^{-1}$  theoretical maximum [Kok, 1960]. Possible reasons for these over-estimates include: 1) non-consideration of the spectral character of the light field [Morel, 1978; Kishino, 1986]; and 2)  $PAR(30)$  and  $PAR(40)$  were derived by extrapolation using  $K_{PAR}$ , which does not follow Beer's Law.

The differences in derived  $\phi$  values for the non-linear regression and  $R_{rs}$  methods are 2 to 28% (average 11%), with most of the differences occurring at 40 m near the bottom of the euphotic zone. This difference is largely due to the different derived  $a_d$  values. As there were no  $PAR$  measurements at 30 and 40 m, it is difficult



to judge which method is more accurate. The  $a_t$  values determined from the  $R_{tr}$  model inversion, however, are closer to the measured values reported by Walsh et al. [1992] with an average difference of only about 18%. The calculated  $\phi$  values by both methods are consistent with values reported elsewhere [Tyler, 1975; Dubinsky et al., 1984; Kishino, 1986], and are less than the  $0.12 \text{ mol C (mol photons)}^{-1}$  theoretical maximum.

Part of the error in  $\phi$  calculation comes from estimates of  $PAR(z)$  and measurements of  $a_{ph}(\lambda)$ . As the error of  $PAR$  was 19% using the  $R_{tr}$  method, if the error in measuring  $a_{ph}$  was 10%, then the error in  $\phi$  would be about 22%.

The error in  $\phi$  caused by errors in  $a_t$  varies with the relative contribution of  $a_t$  to the total absorption, and also varies with depth. For the waters studied, a 100% error in  $a_t(440)$  would cause a factor of 2 error in  $\phi$  at the bottom of the euphotic zone, whereas it would only contribute an error of about 10% in  $\phi$  for the surface layer. However, a recent study [Lee, 1994] shows that the average error of  $R_{tr}$ -derived total absorption is only about 30%. Therefore the error in  $\phi$  is expected to be much less than a factor of 2, especially when  $a_{ph}(\lambda)$  is measured.

Figure 6 shows calculated  $\phi$  versus  $PAR$  values: (a) results using the non-linear regression method; and (b) results by the  $R_{tr}$  method. These figures are similar in shape to those reported by Tyler [1975] and Kishino [1986]. If we ignore the  $\phi$  values at 40 m as being less reliable,  $\phi$  values for both methods can be expressed as suggested by Steele [1962]:

$$\phi = \phi_m e^{-\alpha PAR}, \quad (13)$$

where  $\phi_m$  and  $\alpha$ , derived from the  $\phi$  results of the two methods, are shown in Table 2 as a function of time. All the  $\phi_m$  values are consistent with the maximum quantum yield values reported by Welschmeyer and Lorenzen [1981] ( $0.040 - 0.074 \text{ mol C (mol photons)}^{-1}$ ), Kiefer and Mitchell [1983] ( $0.05 \text{ mol C (mol photons)}^{-1}$ ), Langdon [1988] ( $0.034 - 0.10 \text{ mol C (mol photons)}^{-1}$ ) and Cleveland et al. [1989] ( $0.033 - 0.102 \text{ mol C (mol photons)}^{-1}$ ). It is clear that the differences in  $\phi_m$  and  $\alpha$  as calculated by the two methods are smaller than the differences due to changes in the water column over the four days. The  $\phi_m$  values for the last three sampling days were fairly consistent and about 40% larger than on the first day, but the slope value  $\alpha$  increased more than two-fold between the first two days before dropping to an intermediate level. The daily change of  $\phi_m$  and  $\alpha$  can be caused by changes in

physiological parameters, such as nutrients, adaptation, species, and light level. For this cruise, however, nutrients were always abundant [Marra et al., this issue].

Table 3 summarizes the above results along with the column-integrated (within the euphotic zone) chlorophyll *a* and primary production. The column-integrated chlorophyll *a* decreased from the beginning to the end of the cruise. Also, for the four days, *PAR*(0) and chlorophyll *a* changed markedly ( $\approx 4 \times$  and  $3 \times$ , respectively), but the integrated primary production did not vary as much ( $< 2 \times$ ). This was especially interesting for the last three days, which included a sunny day (May 22) when the productivity near the surface on that day appeared to have been significantly reduced by photoinhibition.

May 22 was the only sunny day for the entire cruise, and the populations present would have been low-light adapted. The three to four-fold reduction in surface  $\phi$  values for the rare sunny day compared to values for the previous two stations suggests that great care must be taken in interpreting satellite estimates of primary production in light-changing environments. The occasional view of the ocean a satellite observes on a rare sunny day may be accompanied by perturbations in the photosynthetic performance of the phytoplankton because of a light-history factor that is not well understood at this time.

### SUMMARY

1. Three methods of estimating the absorbed photons at depth were evaluated, one of which was non-spectral.
2. The spectral methods (the non-linear regression and remote sensing reflectance approaches) both provide good alternatives to model the spectral light field at depth for reasonably well mixed water columns such as the ML-ML site. The *PAR* values for the non-spectral method were too low and resulted in theoretically unrealistic quantum yield values.
3. Calculated quantum yield values by the two spectral methods are consistent with each other and with values reported by other studies. The equation,
 
$$QY = \frac{\int_{\lambda} PAR(\lambda) d\lambda}{\int_{\lambda} PAR(\lambda) d\lambda}$$
 provides an estimate of the average quantum yield with *PAR* for the ML-ML site. Combining surface *PAR* values,

$$\phi(z) = 0.070e^{-0.075PAR(z)}, \quad (14)$$

either measured or modeled [e.g. Gregg and Carder, 1990; Bishop and Rossow, 1991], with Eq. 9 or Eq. 10 allows  $PAR(z)$  calculations to be made on the basis of remotely sensed data.

4. The daily  $PAR(0)$  varied four-fold, and the column-integrated chlorophyll  $a$  varied three-fold during the cruise. The column-integrated primary production varied only two-fold, however. This argues for the need to better understand factors affecting the quantum yield and the light field with depth in order to improve model simulations of primary production.

5. The methods suggested here for estimating of  $\phi$  provide alternatives for spectral measurements when only data of  $PAR(z)$  or  $R_{\tau}$  are available. If feasible, time-series measurements of the spectral light field at the incubation depths would be the best choice. Also, time series of  $R_{\tau}(\lambda)$ ,  $E_q(0,\lambda)$ , and  $a_{ph}(z,\lambda)$  would help to improve the suggested methods and to understand *in situ*  $\phi$ .

6. The reduction exhibited in surface  $\phi$  values for a rare sunny day suggests that primary production estimates based upon satellite measurements of ocean color for regions with a history of cloud-cover may be in serious error if light history of the region is not considered in assessing effects of photoinhibition.

# ACKNOWLEDGEMENTS

The authors wish to thank the Captain and crew of the R/V Endeavor for their help and professionalism on the ML-ML cruise. This research was supported by ONR grants N00014-89-J-1091 (K. Carder), N0004-89-c1150 (J. Marra), N00014-90-J-1091 (M. Perry), and NASA grant NAGW-465 (K. Carder).

## REFERENCES

- Austin, R.W., Inherent spectral radiance signatures of the ocean surface, Ocean color Analysis, *SIO Ref.* 7410, 1974.
- Balch, W., R. Evans, J. Brown, G. Feldman, C. McClain and W. Esaias, The remote sensing of ocean primary productivity: use of a new data compilation to test satellite algorithms, *J. Geophys. Res.*, **97**, C2, 2279-2293, 1992.
- Bannister, T.T., Production equations in terms of chlorophyll concentration, quantum yield, and upper limit to production, *Limnol. Oceanogr.*, **19**, 1-12, 1974.
- Bannister, T.T., Quantitative description of steady state, nutrient-saturated algal growth, including adaptation, *Limnol. Oceanogr.*, **24**, 76-96, 1979.
- Bannister, T.T. and A.D. Weidemann, The maximum quantum yield of phytoplankton photosynthesis *in situ*, *J. Plankton. Res.*, **6**, 275-294, 1984.
- Bishop, J.K. and W.B. Rossow, Spatial and temporal variability of global surface solar irradiance, *J. Geophys. Res.*, **96**, C9, 16,839-16,858, 1991.
- Bricaud, A., A. Morel, and L. Prieur, Absorption by dissolved organic matter of the sea (yellow substance) in the UV and visible domains, *Limnol. Oceanogr.*, **26**, 43-53, 1981.
- Bricaud, A. and D. Stramski, Spectral absorption coefficients of living phytoplankton and nonalgal biogenous matter: A comparison between the Peru upwelling area and the Sargasso Sea, *Limnol. Oceanogr.*, **35**, 562-582, 1990.
- Carder, K.L. and R.G. Steward, A remote-sensing reflectance model of a red tide dinoflagellate off West Florida, *Limnol. Oceanogr.*, **30**, 286-298, 1985.
- Cleveland, J.S., M.J. Perry, D.A. Kiefer and M.C. Talbot, Maximal quantum yield of photosynthesis in the northwestern Sargasso Sea, *J. Marine Res.*, **47**, 869-886, 1989.
- Cullen, J.J., On models of growth and photosynthesis in phytoplankton, *Deep-Sea Res.*, **37**, 667-683, 1990.
- Dubinsky, Z., T. Berman and F. Schanz, Field experiments for *in situ* measurements of photosynthetic efficiency and quantum yield, *J. Plankton Res.*, **6**, 339-349, 1984.
- Gordon, H.R., Ship perturbation of irradiance measurements at sea, 1: Monte Carlo simulations, *Appl. Optics*, **24**, 4172-4182, 1985.
- Gordon, H.R., O.B. Brown, R.H. Evans, J.W. Brown, R.C. Smith, K.S. Baker, and D.K. Clark, A semianalytic radiance model of ocean color, *J. Geophys. Res.*, **93**, D9, 10,909-10,924, 1988.
- Gordon, H.R., Can the Lambert-Beer law be applied to the diffuse attenuation coefficient of ocean water?, *Limnol. Oceanogr.*, **34**, 1389-1409, 1989.
- Gordon, H.R. and K. Ding, Self-shading of in-water instruments, *Limnol. Oceanogr.*, **37**, 491-500, 1992.
- Gregg, W.W. and K.L. Carder, A simple spectral solar irradiance model for cloudless maritime atmospheres, *Limnol. Oceanogr.*, **35**, 1657-1675, 1990.

Jones, B., L. Washburn, R. Smith, Spatial variability and physical and bio-optical properties in the sub-arctic North Atlantic during ML-ML, 1991, this issue.

Kiefer, A.D. and B.G. Mitchell, A simple, steady state description of phytoplankton growth based on absorption cross section and quantum efficiency, *Limnol. Oceanogr.*, 28, 770-776, 1983.

Kirk, J.T.O., Dependence of relationship between inherent and apparent optical properties of water on solar altitude, *Limnol. Oceanogr.*, 29, 350-356, 1984.

Kishino, M., M. Takahashi, N. Okami, and S. Ichimura, Estimation of the spectral absorption coefficients of phytoplankton in a thermally stratified sea, *Bull. Mar. Sci.*, 37, 634-642, 1985.

Kishino, M., N. Okami, M. Takahashi and S. Ichimura, Light utilization efficiency and quantum yield of phytoplankton in a thermally stratified sea", *Limnol. Oceanogr.*, 31, 557-566, 1986.

Kok, B., Efficiency of photosynthesis, p. 563-633. In W. Ruhland [ed.], *Handbuch der Pflanzenphysiologie*, v.5, part 1. Springer. 1960.

Lawes, E.A., G.R. Ditullio, K.L. Carder, P.R. Betzer and S.K. Hawes, Primary production in the deep blue sea, *Deep-Sea Res.*, 37, 715-730, 1990.

Lee, Z.P., K.L. Carder, S.K. Hawes, R.G. Steward, T.G. Peacock, and C.O. Davis, An interpretation of high spectral resolution remote sensing reflectance, *Optics of the Air-Sea Interface, Proc. SPIE. 1749*, 49-64, 1992.

Lee, Z.P., K.L. Carder, S.K. Hawes, R.G. Steward, T.G. Peacock, and C.O. Davis, A model for interpretation of hyperspectral remote sensing reflectance, *Appl. Optics*, in press, 1994(a).

Lee, Z.P., K.L. Carder and T.G. Peacock, Hyperspectral modeling of remote sensing reflectance: from the Florida Shelf to the Mississippi river, *EOS*, 75, January, 1994(b).

Lee, Z.P., Visible-infrared remote-sensing model and applications for ocean waters. Ph.D dissertation. University of South Florida. In preparation, 1994.

Langdon, C., On the causes of interspecific differences in the growth-irradiance relationship for phytoplankton, *J. Plankton Res.*, 10, 1291-1312, 1988.

Marra, J., T. Dickey, W.S. Chamberlin, C. Ho, T. Granata, D.A. Kiefer, C. Langdon, R. Smith, K. Baker, R. Bidigare, and M. Hamilton, Estimation of seasonal primary production from moored optical sensors in the Sargasso Sea, *J. Geophys. Res.*, 97, C5, 7399-7412, 1992.

Marra, J., C. Langdon, and C.A. Knudson, Primary production and water column changes and the demise of a *Phaeocystis* bloom at the Marine Light-Mixed Layers site (59°N/21°W, Northeast Atlantic Ocean), this issue.

Mitchell, B.G. and D.A. Kiefer, Chl-*a* specific absorption and fluorescence excitation spectra for light limited phytoplankton, *Deep-Sea Res.*, 35, 635-663, 1988.

Morel, A. and L. Prieur, Analysis of variations in ocean color, *Limnol. Oceanogr.*, 22, 709-722, 1977.

Morel, A., Available, usable, and stored radiant energy in relation to marine photosynthesis, *Deep-Sea Res.*, 25, 673-688, 1978.

- Morel, A., Optical modeling of the upper ocean in relation to its biogenous matter content (case I waters), *J. Geophys. Res.*, 93, C9, 10,749-10,768, 1988.
- Morel, A., Light and marine photosynthesis: a spectral model with geochemical and climatological implications, *Prog. Oceanogr.*, 26, 263-306, 1991.
- Morel, A. and B. Gentili, Diffuse reflectance of oceanic waters (2): Bi-directional aspects. *Appl. Opt.*, 32: 6864-6879.
- Peacock, T.G., K.L. Carder, C.O. Davis and R.G. Steward, Effects of fluorescence and water Raman scattering on models of remote-sensing reflectance, *Ocean Optics X, Proc. SPIE*, 1302, 303-319, 1990.
- Platt, T., C. Caverhill, and S. Sathyendranath, Basin-scale estimates of oceanic primary production by remote sensing: the North Atlantic", *J. Geophys. Res.*, 96, C8, 15,147-15,159, 1991.
- Plueddemann, A., R. Weller, T. Dickey, J. Marra and M. Stramska, Surface forcing and re-stratification in the sub-Arctic North Atlantic," this issue.
- Roesler, C.S., M.J. Perry and K.L. Carder, Modeling in situ phytoplankton absorption from total absorption spectra in productive inland marine waters, *Limnol. Oceanogr.* 34, 1510-1523, 1989.
- Sathyendranath S. and T. Platt, The spectral irradiance field at the surface and in the interior of the ocean: a model for applications in oceanography and remote sensing, *J. Geophys. Res.*, 93, C8, 9270-9280, 1988.
- Smith R.C. and K.S. Baker, Optical properties of the clearest natural waters, *Appl. Optics*, 20, 177-184, 1981.
- Steele, J.H., Environment control of photosynthesis in the sea, *Limnol. Oceanogr.*, 7, 137-150, 1962.
- Tyler, J.E., The *in situ* quantum efficiency of natural phytoplankton populations, *Limnol. Oceanogr.*, 20, 976-980, 1975.
- Walsh, J.J., K.L. Carder, and Frank E. Muller-Karger, Meridional fluxes of dissolved organic matter in the North Atlantic Ocean, *J. Geophys. Res.*, 97, C10, 15,625-15,637, 1992.
- Welschmeyer, N.A. and Lorenzen, C.J., Chlorophyll-specific photosynthesis and quantum efficiency at subsaturating light intensities, *J. Phycol.*, 17, 283-293, 1981.

## FIGURE LEGENDS

1. Depth profiles of chlorophyll values.  
Open symbols: pre-dawn measured, filled symbols: noon measured.
2. Depth profiles of measured production values.
3. Measured spectra of water properties.  
3(a): remote-sensing reflectance  
3(b): particle absorption coefficients
4. Depth profiles of measured *PAR* vs. calculated *PAR*.  
4(a): May 17, 4(b): May 20, 4(c): May 22, 4(d): May 24.
5. Depth profiles of quantum yield.  
5(a): May 17, 5(b) May 20, 5(c): May 22, 5(d): May 24.
6. Quantum yield vs. *PAR*.  
6(a): calculated by non-linear regression method,  
6(b): calculated by  $R_{rs}$  method.



Table 1: Symbols and units

$a(\lambda)$	Total absorption coefficient, $\text{m}^{-1}$ ; $a(\lambda) = a_w(\lambda) + a_d(\lambda) + a_p(\lambda)$
$a_d(\lambda)$	Absorption coefficient of detritus, $\text{m}^{-1}$
$a_t(\lambda)$	Absorption coefficient of gelbstoff, $\text{m}^{-1}$
$a_{ph}(\lambda)$	Absorption coefficient of phytoplankton pigments, $\text{m}^{-1}$
$a_w(\lambda)$	Absorption coefficient of pure water, $\text{m}^{-1}$
$AP$	Absorbed photons by phytoplankton, $\text{mol photons/m}^3/\text{day}$
$b_b(\lambda)$	Backscattering coefficient, $\text{m}^{-1}$
$E_q^*(\lambda)$	Specific quantum irradiance, $E_q(\lambda)/PAR(0)$ , $\text{nm}^{-1}$
$E_q(\lambda)$	Quantum irradiance, $\mu\text{mol photons/m}^2/\text{nm/s}$
$K_{PAR}$	Attenuation coefficient for $PAR$ , $\text{m}^{-1}$
$\{K(\lambda)\}$	Vertically-averaged attenuation coefficient for downwelling irradiance, $\text{m}^{-1}$
$n$	Refractive index of sea water
$PAR$	Photosynthetically available radiation (integrated from 400 - 700 nm), $\text{mol photons/m}^2/\text{day}$
$PP$	Primary production, $\text{mol C/m}^3/\text{day}$
$PAR(0)_{der}$	Derived surface $PAR$ , $\text{mol photons/m}^2/\text{day}$
$Rrs(\lambda)$	Remote sensing reflectance, ratio of upwelling radiance to downwelling irradiance above the sea surface, $\text{sr}^{-1}$
$T$	Integration or incubation period of time, hours or day
$\alpha$	Slope to describe $\phi$ changes with $PAR$ , $(\text{mol photons/m}^2/\text{day})^{-1}$
$\phi$	Quantum yield, $\text{mol C (mol photons)}^{-1}$
$\phi_m$	Maximum quantum yield, $\text{mol C (mol photons)}^{-1}$
$\lambda$	Wavelength, nm
$\tau$	Air-sea surface transmittance
$\mu_0$	Sub-surface average cosine for downwelling irradiance

Table 2. Calculated maximum quantum yield

Day	Non-linear reg. method		$R_r$ method		Average of methods	
	$\phi_m$	$\alpha$	$\phi_m$	$\alpha$	$\phi_m$	$\alpha$
May 17	0.047	0.038	0.056	0.049	$0.052 \pm 8.8\%$	$0.044 \pm 12.6\%$
May 20	0.091	0.118	0.085	0.106	$0.088 \pm 3.4\%$	$0.112 \pm 5.4\%$
May 22	0.058	0.071	0.074	0.088	$0.066 \pm 12.1\%$	$0.080 \pm 13.2\%$
May 24	0.069	0.056	0.081	0.073	$0.075 \pm 8.0\%$	$0.065 \pm 13.2\%$
Average over days	$0.066 \pm 20.8\%$	$0.071 \pm 33.6\%$	$0.074 \pm 12.2\%$	$0.079 \pm 22.8\%$	$0.070 \pm 18\%$	$0.075 \pm 29\%$

Note:  $\phi_m$  is in units mol C (mol photons)<sup>-1</sup>,  $\alpha$  is in units (mol photons/m<sup>2</sup>/day)<sup>-1</sup>.

Table 3: Summary of Results

Day	PAR(0) mol photons/m <sup>2</sup> /day	Int. [chl <i>a</i> ] mg/m <sup>2</sup>	Int. PP g C/m <sup>2</sup> /day	<i>a<sub>p</sub></i> (440)	
				non-linear	<i>R<sub>r</sub></i>
May 17	38.27	162.2	2.3	0.013	0.026
May 20	16.25	108.2	1.2	0.024	0.021
May 22	65.72	56.0	1.1	0.018	0.029
May 24	28.73	50.6	1.2	0.017	0.028

# Available Irradiance of ML-ML

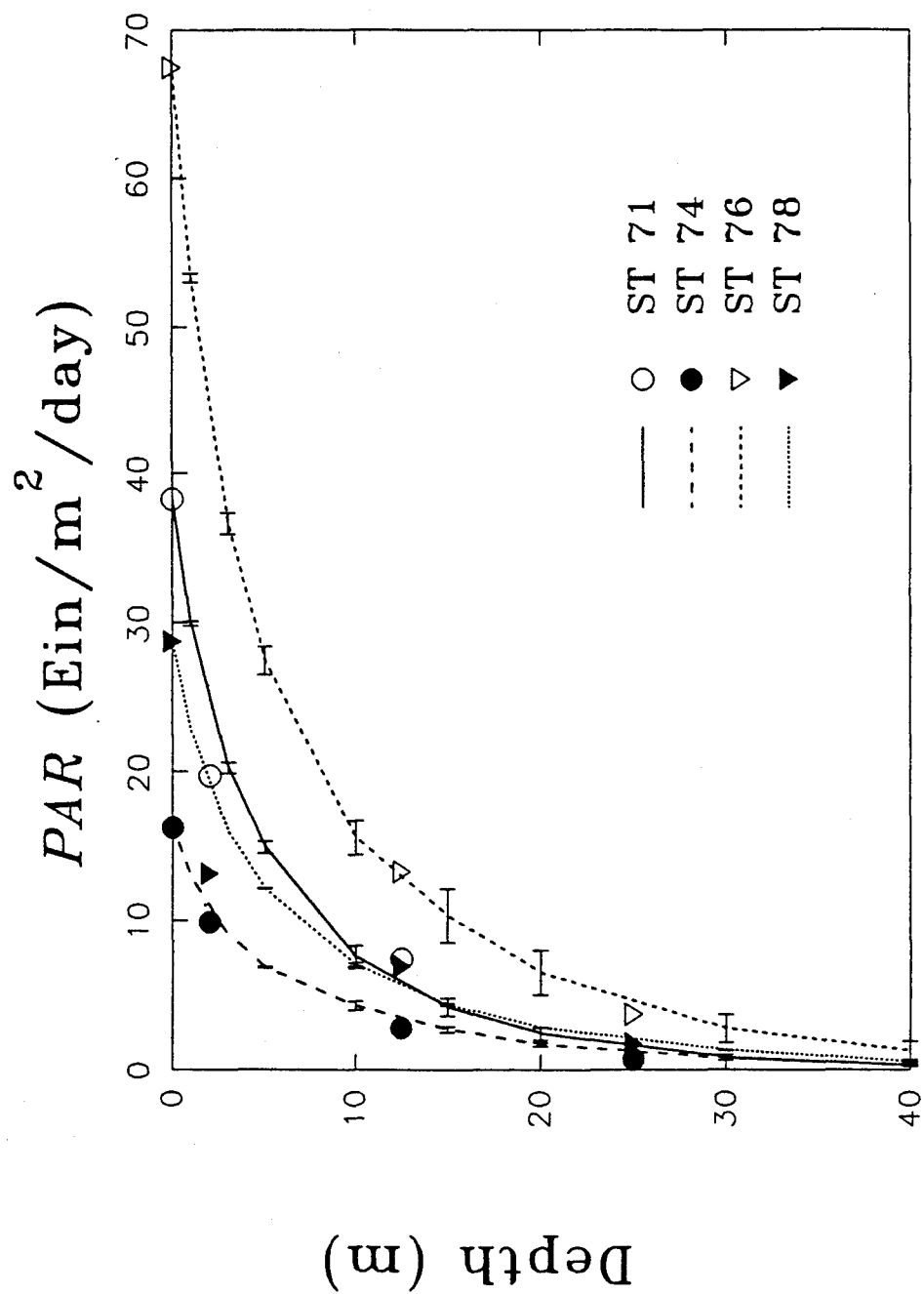


Fig.1

# Chlorophyll profile of ML-ML

Chlorophyll ( $\mu\text{g/l}$ )

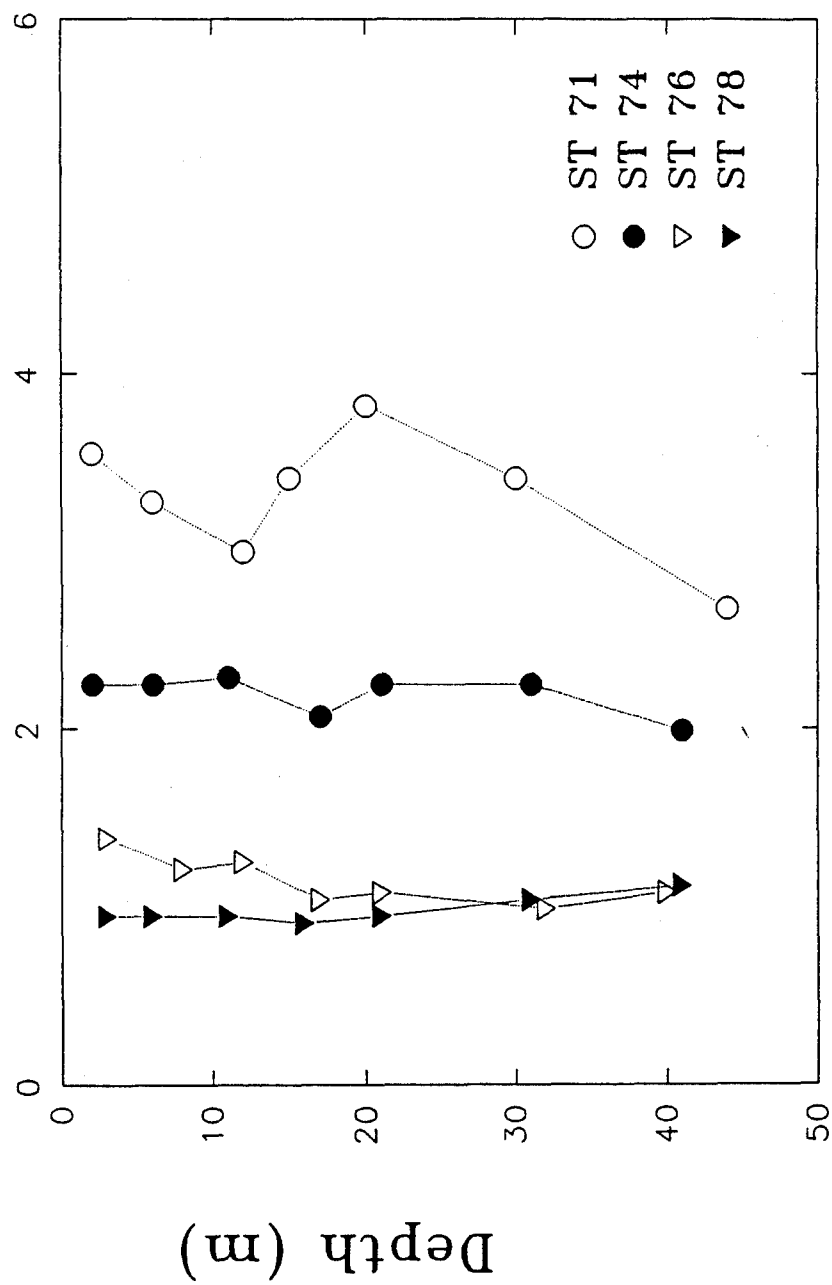


Fig. 2

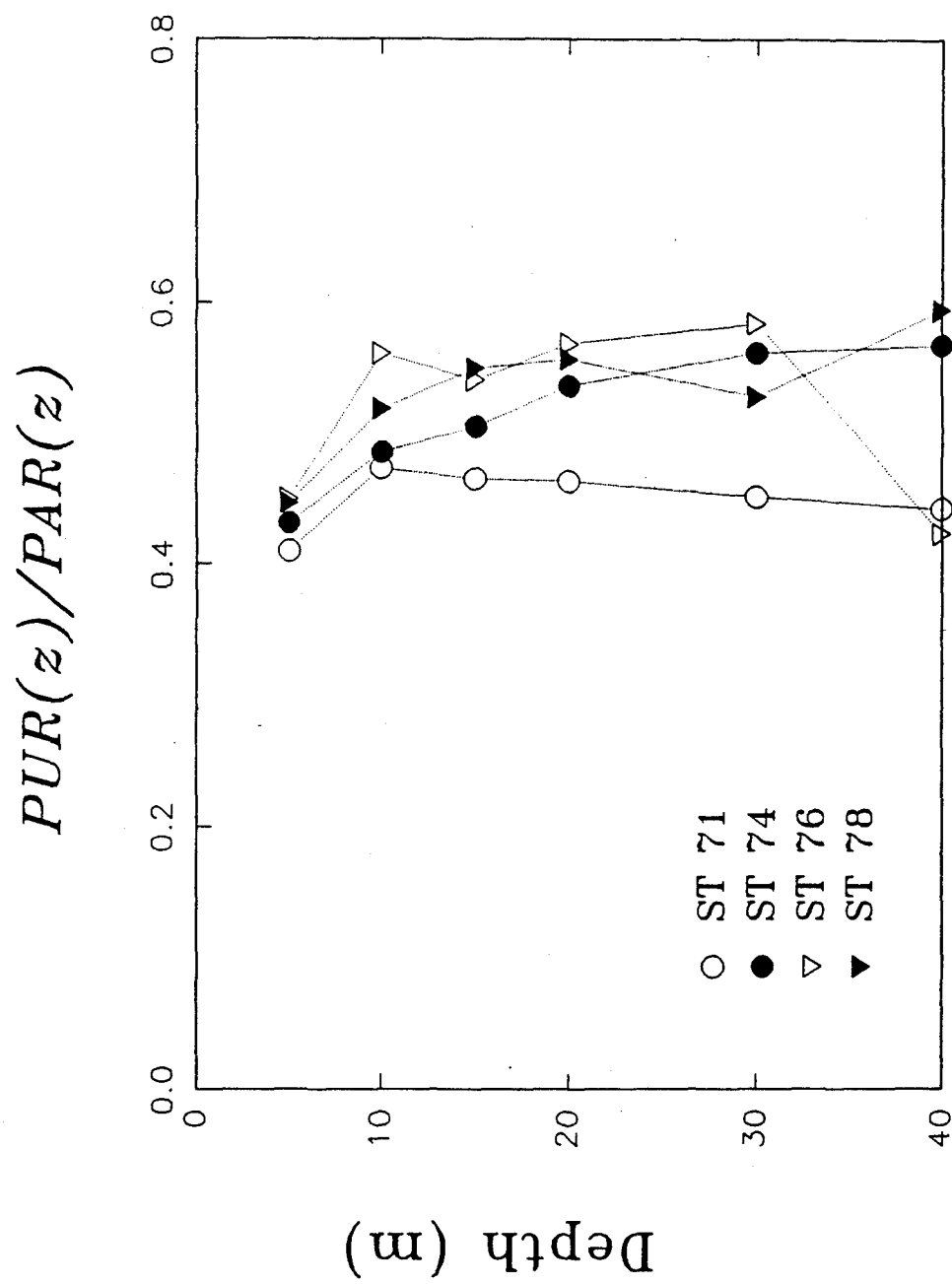


Fig. 3

# Production of ML-ML

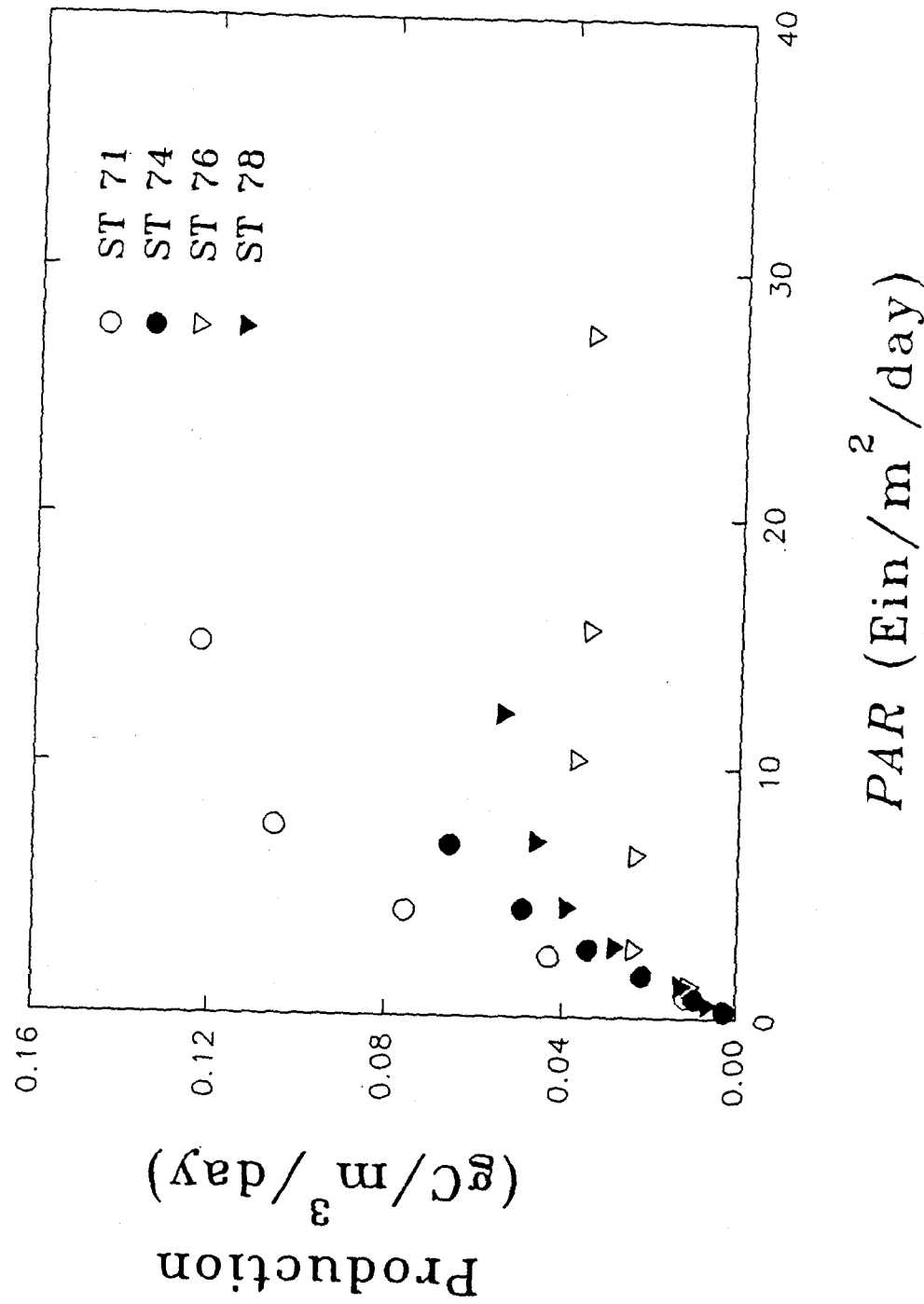


Fig. 4(a)

# Production of ML-ML

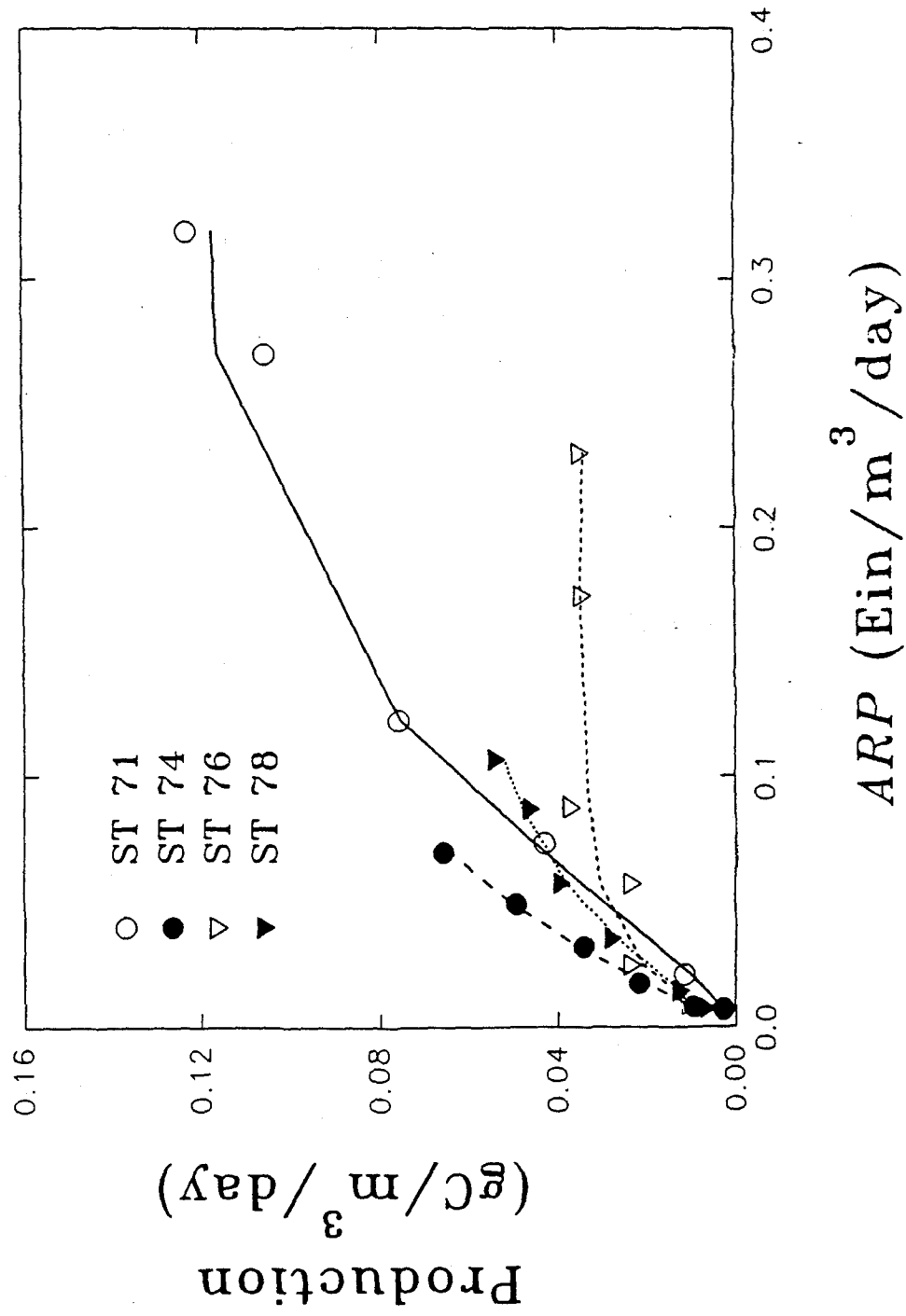


Fig. 4(b)



# Quantum Yield of ML-ML

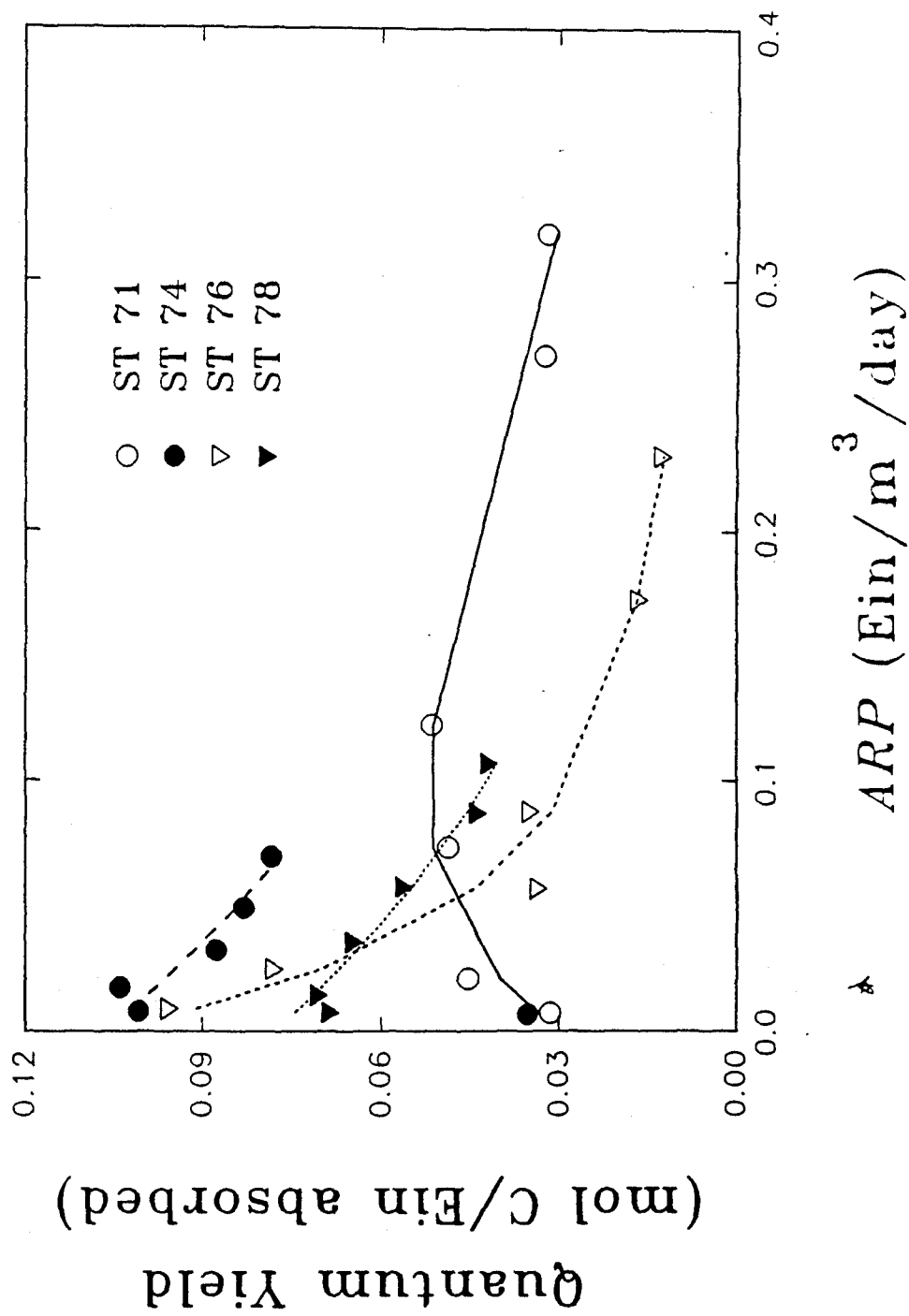


Fig. 5

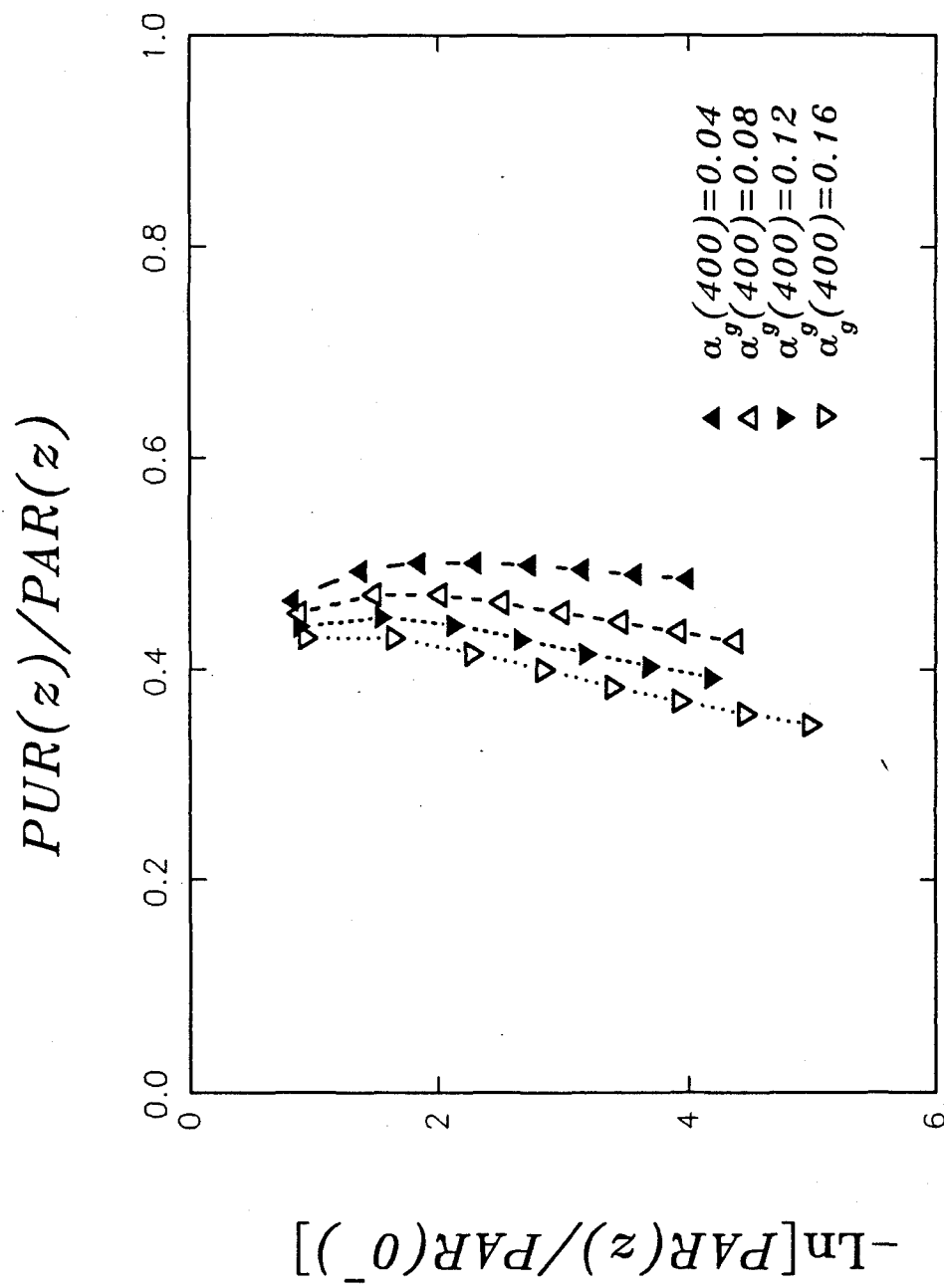


Fig. 6(a)

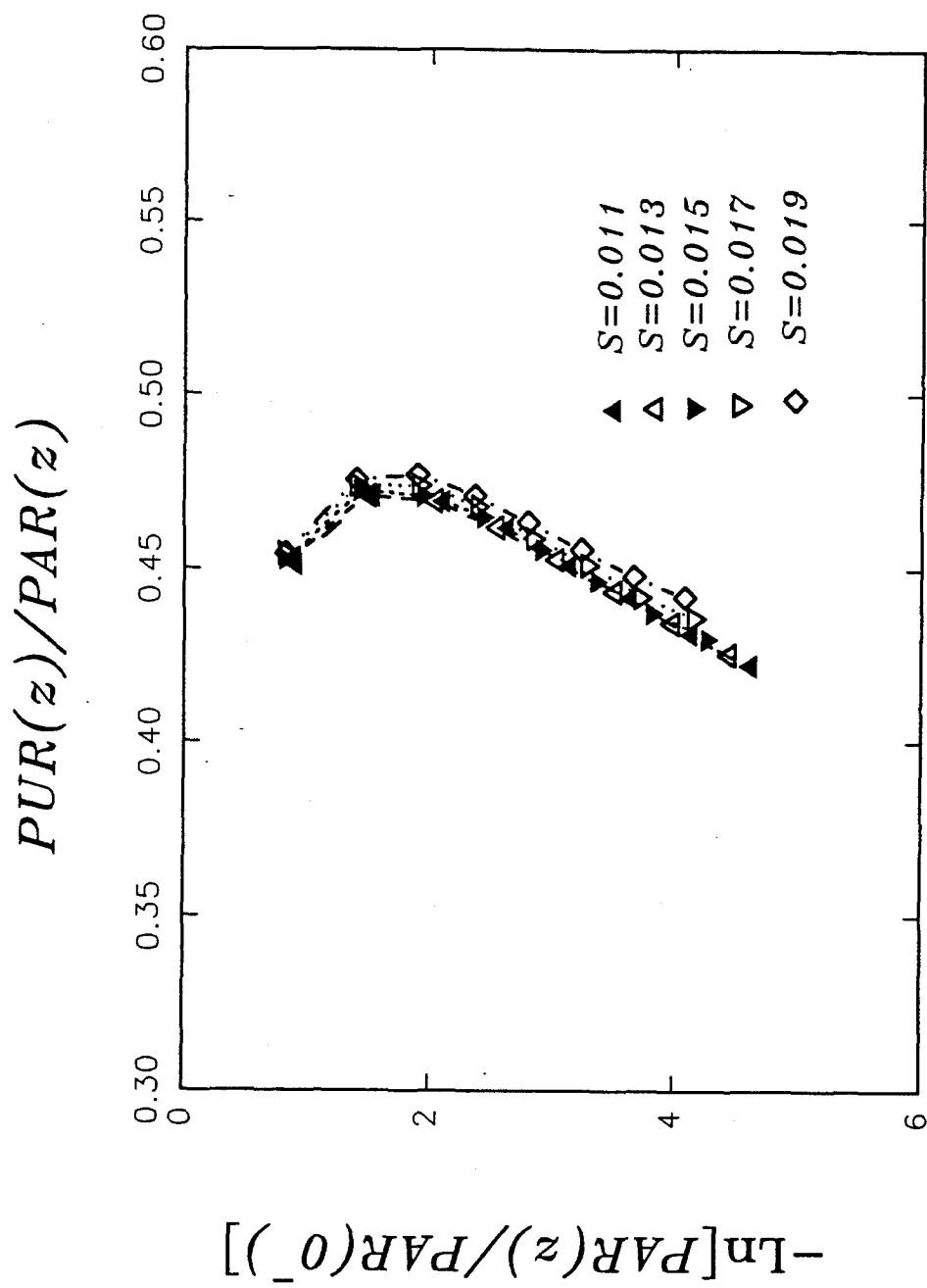


Fig. 6(b)

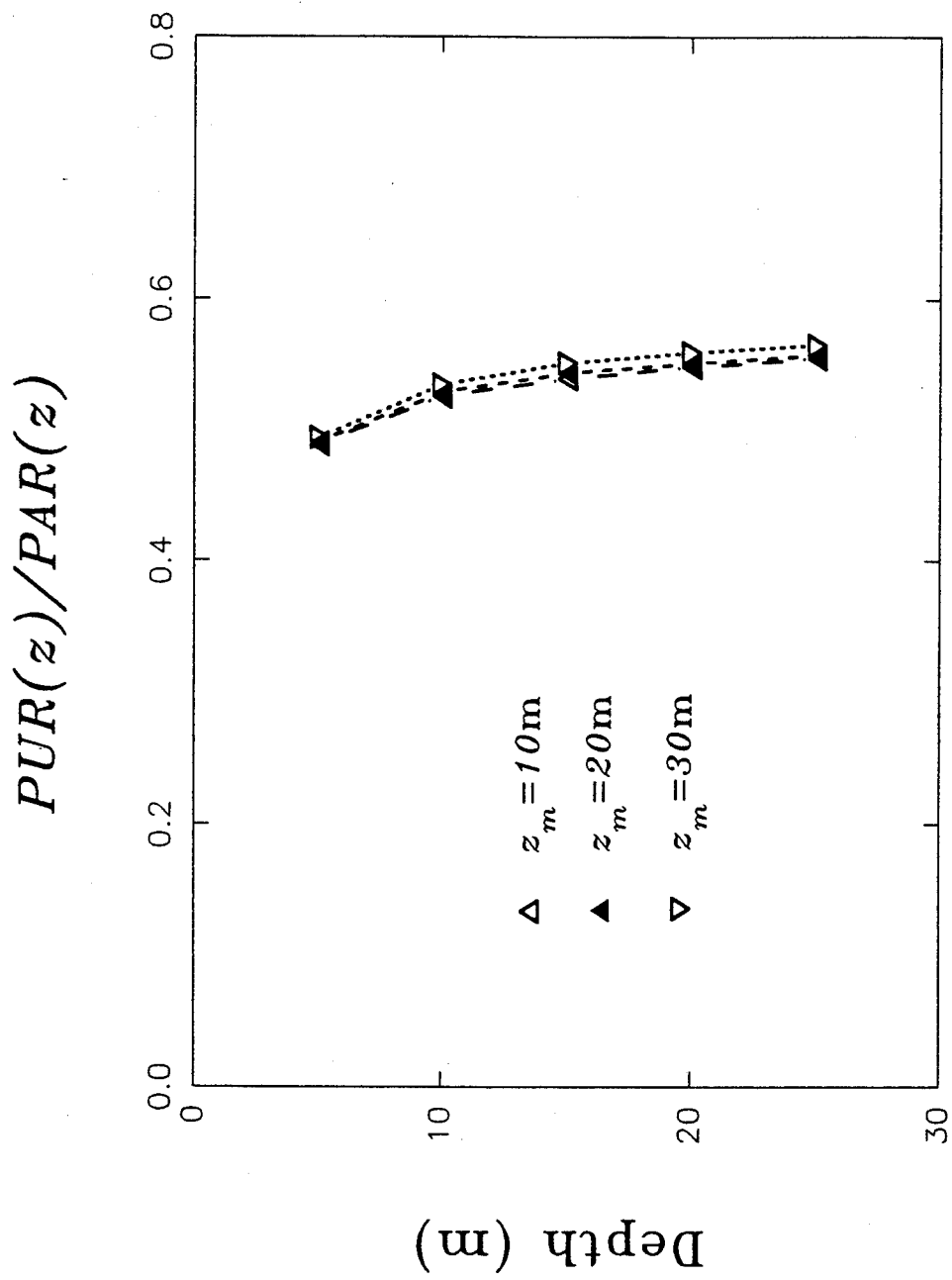


Fig. 7(a)

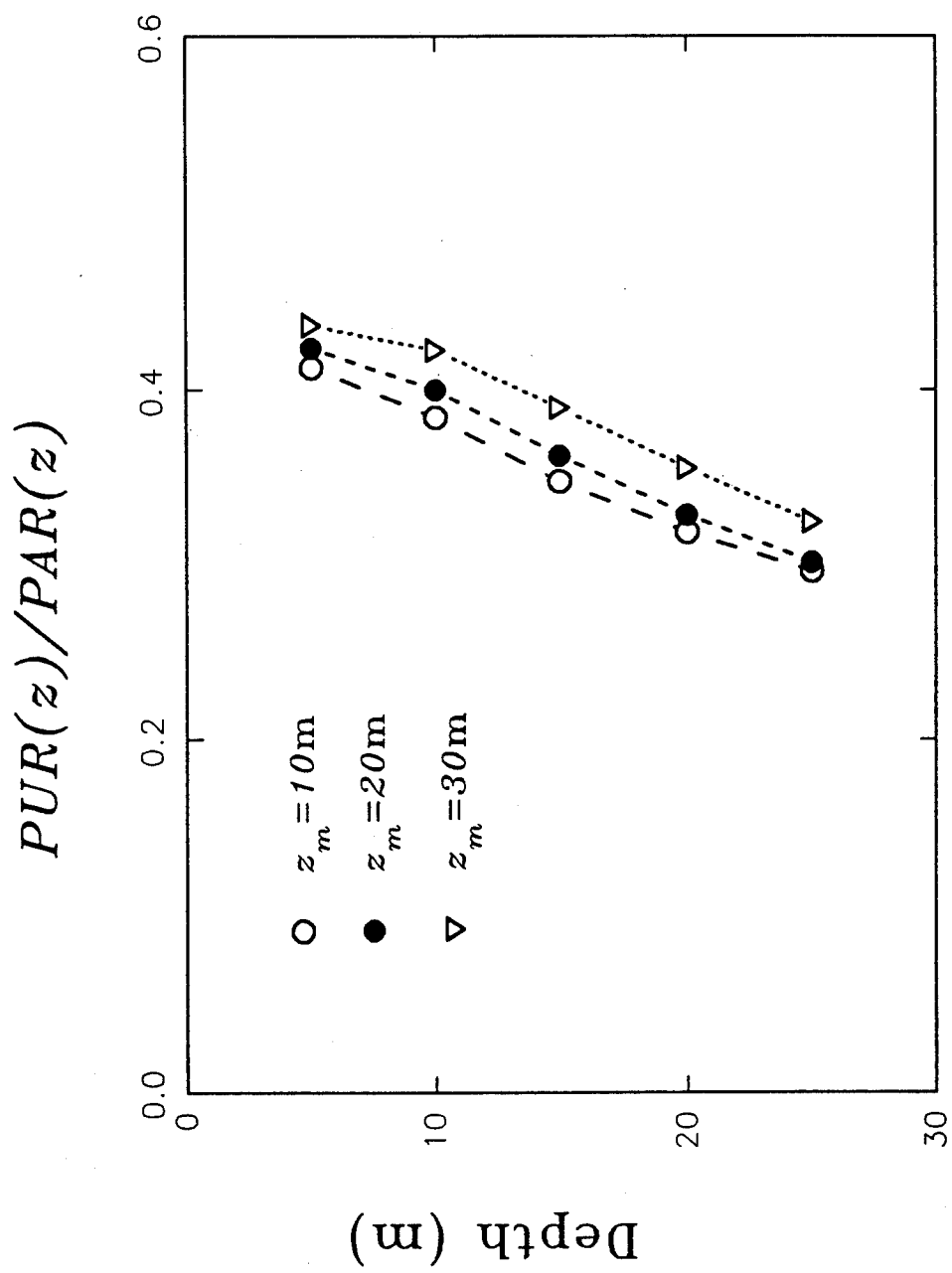


Fig. 7(b)

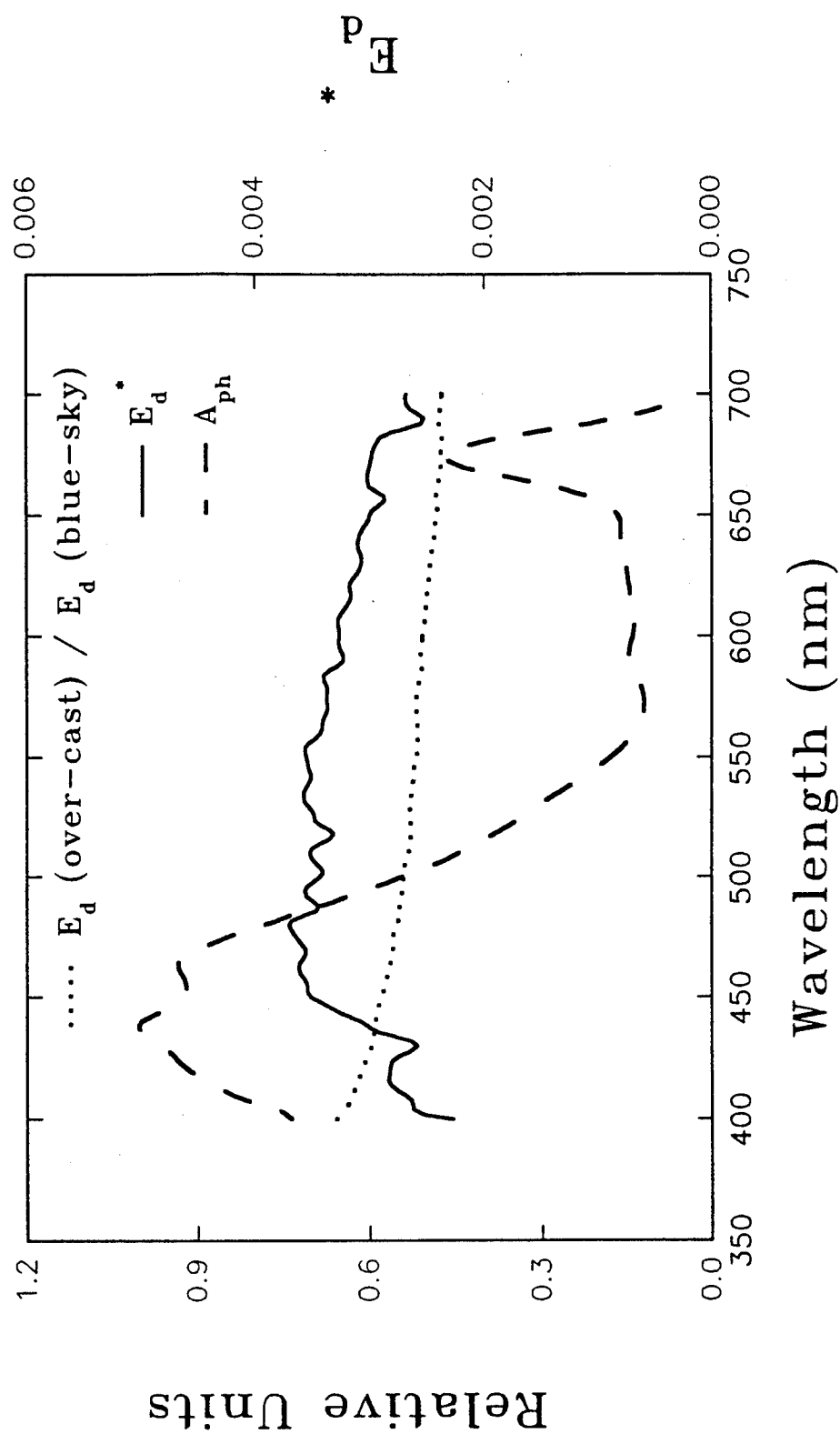


Fig. 8

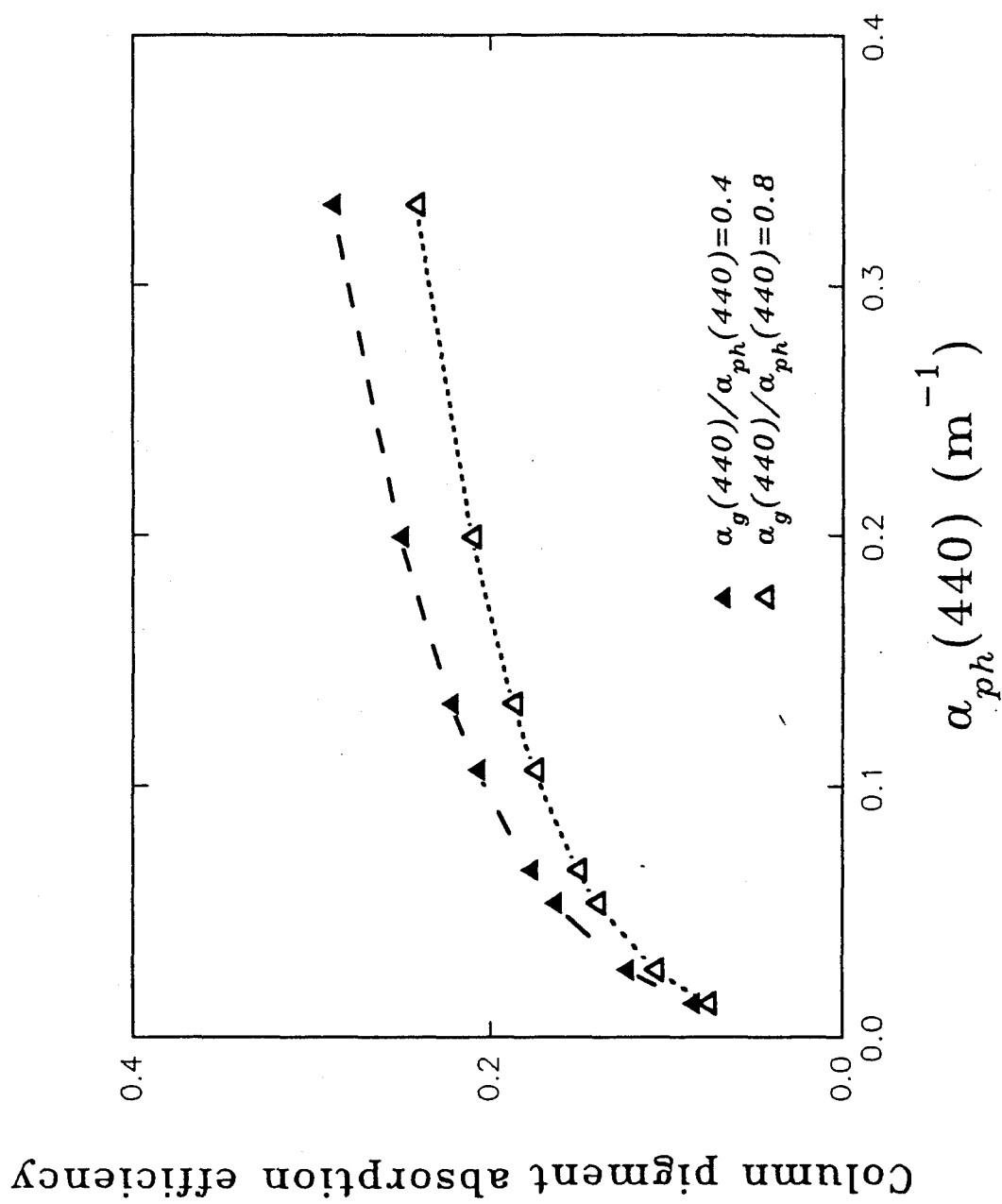


Fig. 9

**Estimating primary production from remote sensing: a new approach**

Z. P. Lee<sup>1</sup>, K. L. Carder<sup>1</sup>, J. Marra<sup>2</sup>, R. G. Steward<sup>1</sup> and M. J. Perry<sup>3</sup>

<sup>1</sup>Department of Marine Science  
University of South Florida  
140 7th Avenue North  
St. Petersburg, FL 33701

<sup>2</sup>Lamont-Doherty Earth Observatory of Columbia University  
Palisades, New York 10964

<sup>3</sup>School of Oceanography, WB-10  
University of Washington  
Seattle, WA 98195

running heading:     *primary production, remote sensing*



*Acknowledgements*

The authors wish to thank the Captain and crew of the R/V Endeavor for their help and professionalism on the ML-ML cruise. We appreciate the comments and suggestions made by Dr. Gabriel Vargo. This research was supported by the ONR grant N00014-89-J-1091 and NASA NAGW-465 to the University of South Florida and ONR grant N0004-89-1150.

*Abstract*

A mathematical simulation of the absorption coefficient of phytoplankton pigments is used to estimate the primary production in the euphotic zone based on the measured remote-sensing reflectance and surface solar irradiance. In the suggested approach here, it is not necessary to know the pigment concentration and the chlorophyll-specific absorption coefficient, which are essential in traditional methods. This approach is tested against measurements made in the high-latitude North Atlantic in May 1991. A comparison of the calculated and measured daily primary production in the euphotic zone had an  $r^2 = 0.95$  ( $n=24$ ), with a slope of 1.26 and + 32% difference. Using the traditional method yielded an  $r^2 = 0.85$  ( $n=24$ ) with a slope of 0.34 and - 78% difference. These results mean that there is a factor of 3 improvement in estimation accuracy for the phytoplankton photosynthesis of waters studied; it also suggests that it is preferable to shift the primary production model from traditional pigment-concentration base to pigment-absorption base.

## Introduction

In the past decades, primary production models are based on pigment concentration, either using light available expression (e.g. P-I relation in Platt et al. 1991) or light absorbed expression (e.g. P-AQ relation in Bidigare et al. 1992), or by non-spectral or spectral model (see Bidigare et al. 1992). Recent popular models use the light absorbed approach, i.e., chlorophyll *a* concentration multiplied by the irradiance and two factors: averaged chlorophyll-specific absorption coefficient, and the quantum yield for carbon fixation. Thus the photosynthesis rate at depth *z* is (Kishino et al. 1986; Smith et al. 1989; Cullen 1990; Morel 1991; Marra et al. 1992; Zaneveld et al. 1993):

$$PP(z) = \phi(z)[chl\ a]\bar{a}_\phi^* PAR(z), \quad (1)$$

where  $\phi(z)$  is the quantum yield for carbon fixation, and  $[chl\ a]$  is the chlorophyll *a* concentration in mg/m<sup>3</sup> (important symbols used in this text are summarized in Table 1).

$\bar{a}_\phi^*$  is the spectrally-averaged chlorophyll-specific absorption coefficient over 400 - 700 nm (m<sup>2</sup>(mg chl *a*)<sup>-1</sup>):

$$\bar{a}_\phi^* = \frac{\int_{400}^{700} a_\phi^*(\lambda) E_0(z, \lambda) d\lambda}{\int_{400}^{700} E_0(z, \lambda) d\lambda}, \quad (2)$$

and  $a_\phi^*(\lambda) = a_\phi(\lambda)/[chl\ a]$  is the chlorophyll-specific absorption coefficient.

$PAR(z)$  is the photosynthetically available irradiance, computed as

$$PAR(z) = \int_{400}^{700} E_o(z, \lambda) d\lambda, \quad (3)$$

where  $E_o(z, \lambda)$  in equations 2 and 3 is the spectral scalar irradiance in quanta/m<sup>2</sup>/nm/s. From Sathyendranath and Platt (1988),

$$E_o(z, \lambda) \approx E_o(0, \lambda) e^{-K_d(\lambda)z}. \quad (4)$$

Recently, Bannister (1992) pointed out that Equation 4 is a rough approximation for high-scattering media. However, the waters studied here show a low scattering-to-absorption ratio, and the sub-surface solar zenith angle was large. That means there was not much variation between the sub-surface average cosine and the average cosine at depth (see Fig. 3 of Bannister 1992). So, equation 4 can still be used for the situation described, especially when an vertically-averaged  $K_d$  is used.

Quantum yield (Langdon 1988; Cleveland et al. 1989; Smith et al. 1989),  $\phi$ , varies with light intensity and physiological status of the phytoplankton population. We chose the empirical formula suggested by Kiefer and Mitchell (1983) to express how  $\phi$  changes with  $PAR$ ,

$$\phi(z) = \phi_m \frac{PAR_\phi}{PAR_\phi + PAR(z)}, \quad (5)$$

where  $\phi_m$  is the maximum quantum yield,  $PAR_\phi$  is the  $PAR$  value at which  $\phi = \phi_m/2$ .

Therefore, combined with the photoinhibition expression suggested by Platt et al. (1980), primary production at depth  $z$  can be expressed as

$$PP(z) = APP(z) \frac{\phi_m PAR_\phi}{PAR_\phi + PAR(z)} e^{-v PAR(z)}, \quad (6)$$

with

$$APP(z) = \rho[C]\bar{a}_\phi^* PAR(z) \quad (7)$$

where  $\nu$  is a parameter to describe photoinhibition, the influence of which will be discussed in the section on results and discussion.

Eq. 7 accounts for the absorbed photons by the phytoplankton pigments, in which  $\rho$  determines the fraction of chlorophyll *a* relative to chlorophyll *a* + phaeophytin *a* concentration  $[C]$ .

Often, estimation of primary production based upon remote measurements are accomplished using Eqs. 6 and 7. Traditionally,  $[C]$  is estimated first (one of the important reasons for the development of pigment algorithm from remote sensing) from remotely measured signals (Platt et al. 1991; Balch et al. 1992) using for example the CZCS (Coastal Zone Color Scanner) algorithm:

$$[C] = A \left[ \frac{L_w(443)}{L_w(550)} \right]^B \approx 0.95^B A \left[ \frac{R_{rs}(443)}{R_{rs}(550)} \right]^B \quad (8)$$

where  $A = 1.13 \text{ mg/m}^3$  and  $B = -1.71$  (Gordon et al. 1983). The 0.95 comes from  $E_d(443)/E_d(550) \approx 0.95$ . Using  $[C]$ , the diffuse attenuation coefficient of irradiance can be approximated by the empirical relationship suggested by Morel (1988), which is:

$$K_d(\lambda) = K_w(\lambda) + d(\lambda)[C]^{e(\lambda)} \quad (9)$$

in which values for  $K_w$ ,  $d$  and  $e$  are found in tables calculated by Morel (1988).

With  $K_d$  and measured or calculated  $E_o(0)$  (e.g. converted from Gregg and Carder (1990) or Bishop and Rossow (1991)),  $PAR$  at any depth can then be estimated. However  $\rho$ ,  $\nu$ ,  $\phi_\pi$ ,  $PAR_\phi$  and  $\bar{a}_\phi^*$  must be estimated for the calculation of  $PP$ .  $\rho$  varies from 0.3 to 0.9, with an

average value of 0.75 (Morel and Berton 1989; Balch et al. 1992), the value used for our calculation.  $\nu$ ,  $\phi_m$  and  $PAR_\phi$  vary with phytoplankton physiological status, which at this point cannot be derived based upon remotely sensed measurements, but must be estimated from other information.  $\phi_m$  has been reported to range from 0.03 mol C (Ein absorbed)<sup>-1</sup> to 0.1 mol C (Ein absorbed)<sup>-1</sup> (Bannister and Weidemann 1984; Smith et al. 1989; Morel 1991). As a kind of average for productive waters,  $\phi_m$  is assumed to equal 0.074 mol C (Ein absorbed)<sup>-1</sup>, a value suggested by Cullen (1990). In Marra et al. (1993), however, a  $\phi_m$  value of 0.06 mol C (Ein absorbed)<sup>-1</sup> was used. There is little literature information, however, about the values of  $\nu$  and  $PAR_\phi$ . Platt et al. (1980) found  $\nu$  varied from 0 to 0.0028 (W m<sup>-2</sup>)<sup>-1</sup>. If we choose 0.0028 (W m<sup>-2</sup>)<sup>-1</sup> for  $\nu$ , its equivalent value is  $\nu \approx 0.01$  (Ein/m<sup>2</sup>/day)<sup>-1</sup>. Kiefer and Mitchell (1983) found that  $PAR_\phi$  equals about 10 Ein/m<sup>2</sup>/day, a value assumed for the waters in this study.

The only unknown variable remaining is  $\bar{a}_\phi^*$ . This value varies with phytoplankton condition and the light environment (Kishino et al. 1986). If only remote-sensing information is available,  $\bar{a}_\phi^*$  must be estimated from other data, or an empirical value has to be picked for  $\bar{a}_\phi^*$ . In many calculations, an  $\bar{a}_\phi^*$  value of  $\sim 0.015$  (m<sup>2</sup>(mg chl *a*)<sup>-1</sup>) was measured (Marra et al. 1992) or has been used (Bannister 1974; Dubinsky et al. 1984; Smith et al. 1989) and assumed to be vertically constant.

As we know, [C] using the CZCS algorithm is accurate to about a factor of 2 (Gordon and Morel 1983), and  $\bar{a}_\phi^*$  can vary by a factor of 4 (Morel and Bricaud 1981; Kishino et al. 1986; Bricaud et al. 1988; Laws et al. 1990; Carder et al. 1991) because of the pigment composition, the "package effect," and the color of the light field. On a global scale, the combined variation of [C] and  $\bar{a}_\phi^*$  for APP could potentially range over a factor of 8 when other

terms are known.

Actually Eq. 1 is a simplified version of a complete expression as noted by Sathyendranath et al. (1989), Morel (1991), Platt et al. (1991) and Bidigare et al. (1992); i.e.

$$PP(z) = \phi(z) \int_{400}^{700} a_{\phi}(\lambda) E_0(z, \lambda) d\lambda, \quad (10)$$

and the absorbed photons by phytoplankton are

$$APP(z) = \int_{400}^{700} a_{\phi}(\lambda) E_0(z, \lambda) d\lambda. \quad (11)$$

However, the  $a_{\phi}(\lambda)$  curves in those full spectral models were directly dependent upon  $a_{\phi}^*(\lambda)$  and chlorophyll  $a$  concentration, which means the determination of  $[C]$  and/or  $[chl\ a]$  is still the first step in the  $PP$  calculation, and empirical curves for  $a_{\phi}^*(\lambda)$  must be selected. Due to uncertainties in both  $[C]$  and  $a_{\phi}^*(\lambda)$  estimates using remote sensing, if  $a_{\phi}(\lambda)$  and  $a(\lambda)$  can be obtained directly and analytically from remotely measured signals (e.g. remote-sensing reflectance), the problems involved in the estimation of  $[C]$  and choosing values for  $\rho$  and  $\bar{a}_{\phi}^*$  will be avoided. The accuracy of estimating  $APP$  and  $PP$  can then be improved when  $E_0(0)$ ,  $\phi_m$ ,  $PAR_{\phi}$  and  $\nu$  are certain.

For a study carried out in the North Atlantic, where both primary production and above-surface remote-sensing reflectance were measured, two sets of primary production calculations were made. One used Eqs. 6 and 7 (hereafter referred to as the "pigment" method), and the other used Eqs. 6 and 11 (hereafter referred to as the "absorption" method). Comparisons of the calculated to the measured daily primary production were then made, using identical input parameters for the light field and the  $PP$  model.

### *The new approach*

For remote-sensing reflectance  $R_{rs}$  (ratio of the water-leaving radiance to the downwelling irradiance above the surface) at  $N$  wavelengths, recent studies (Gordon et al. 1988; Morel and Gentili 1993; Lee et al. 1994a; Lee 1994) show that:

$$R_{rs}(\lambda_1) \approx \frac{0.17}{a_w(\lambda_1) + a_{dg}(\lambda_1) + a_\phi(\lambda_1)} \left[ \frac{b_{bm}(\lambda_1)}{3.4} + X \left( \frac{400}{\lambda_1} \right)^Y \right],$$

$$\vdots$$

$$R_{rs}(\lambda_N) \approx \frac{0.17}{a_w(\lambda_N) + a_{dg}(\lambda_N) + a_\phi(\lambda_N)} \left[ \frac{b_{bm}(\lambda_N)}{3.4} + X \left( \frac{400}{\lambda_N} \right)^Y \right],$$
(12)

where  $a_w$  and  $b_{bm}$  are the absorption and backscattering coefficients of pure sea water, respectively, and can be found in Smith and Baker (1981);  $a_{dg}$  is the absorption coefficient of detritus and gelbstoff, and can be expressed as (Roesler et al. 1989; Carder et al. 1991):

$$a_{dg}(\lambda) = a_{dg}(440)e^{-S(\lambda-440)}.$$
(13)

$X$  and  $Y$  describe the scattering effects of suspended particles.

Eq. 12 is a series of  $N$  equations, which in total have at least  $N + 4$  unknowns ( $N$  for  $a_\phi$ , 2 for  $a_{dg}$  and 2 for particle scattering) given only  $R_{rs}$ . For the  $N$  equations, unless we can dramatically reduce the unknowns regarding  $a_\phi$ , there will be no certain solutions for  $a_\phi$  and the total absorption  $a$ .

Bidigare et al. (1990) suggested that  $a_\phi$  can be reconstructed by knowing concentrations of the pigments and the specific absorption for each pigment, but these analyses cannot be performed remotely. Hoepffner and Sathyendranath (1991) suggest that the pigment spectrum



can be simulated by a sum of 11 Gaussian bands. For these 11 Gaussian bands, their center wavelengths and half bandwidths vary from species to species. Even if the center wavelengths and half bandwidths are fixed, we still need to derive 11 parameters to obtain  $a_\phi$ . Morel (1980) suggested the use of averaged chlorophyll-specific absorption coefficient while Roesler and Perry (1994) suggested the use of a single, averaged, spectral shape for phytoplankton absorption. Using these approaches, only one unknown (the concentration of pigments or a scale factor) is needed to model  $a_\phi$ . However, due to the "package effect" and variable pigment composition, it is well known that the shape of  $a_\phi$  curve can vary widely from region to region, and no single  $a_\phi$  curve shape can be used globally. So, a simpler expression with adequate accuracy for describing the different shape of  $a_\phi$  curves is necessary.

By analyzing surface  $a_\phi$  curves collected for waters from the Gulf of Mexico with a pigment range of  $0.07 \text{ mg/m}^3 \leq [\text{chl } a] \leq 40 \text{ mg/m}^3$ , a mathematical expression was derived from a combination of 3 simple functions (Lee et al. 1994b), which involves 6 parameters. Figure 1 shows examples of the  $a_\phi(\lambda)$  simulation. Among the 6 parameters, 2 parameters vary only slightly for different waters, and only 2 parameters have strong effects on  $APP$  (Eq. 11). For the wavelength range of  $400 \text{ nm} \leq \lambda \leq 700 \text{ nm}$ , the expression is (Lee 1994; Lee et al. 1994b):

$$400 \leq \lambda \leq 590, \quad a_\phi(\lambda) = a_{\phi 1} e^{-F \left( \ln \frac{\lambda - \lambda_1}{100} \right)^2}, \quad (14)$$

$$590 < \lambda < 656, \quad a_\phi(\lambda) = a_\phi(590) + \frac{a_\phi(656) - a_\phi(590)}{656 - 590} (\lambda - 590), \quad (15)$$

and

$$656 \leq \lambda \leq 700, \quad a_{\phi}(\lambda) = a_{\phi 2} e^{-\frac{(\lambda - \lambda_2)^2}{2\sigma_2^2}} \quad (16)$$

Parameter  $F$  describes the width of the  $a_{\phi}$  curvature from 400 nm to  $\sim 560$  nm,  $\lambda_1$  is the reference needed to obtain the blue peak wavelength,  $100 + \lambda_1$ , for a log-normal curve,  $\lambda_2$  is the red peak wavelength of a Gaussian curve, and  $2.355\sigma_2$  determines the half width of the band around the red peak. For the examples given in their report,  $F$  varied from 1.6 to 4.2,  $\lambda_1$  from 338 - 342 nm with 80% at 340 nm,  $\lambda_2$  ranged from 672 to 675 nm, and  $2.355\sigma_2$  varied from 21 to 35 nm.  $a_{\phi 1}$  varied widely from 0.01 to 0.83  $\text{m}^{-1}$  while  $a_{\phi 2}/a_{\phi 1}$  ranged from 0.21 to 0.85. The root-mean-square (rms) difference between the measured and simulated  $a_{\phi}$  values was 11%. This difference dropped to 2% when comparing the calculated  $APP$  using measured versus simulated  $a_{\phi}$  curves (Lee et al. 1994b), meaning the  $a_{\phi}$  expression works well for the calculation of phytoplankton- absorbed photons. Using this expression in the  $R_{rs}$  inversion to analytically derive  $a_{\phi}$  and  $a$  allows calculation of  $PP$  at any depth simply from  $R_{rs}$  when  $\phi_m$ ,  $PAR_{\phi}$ ,  $\nu$  and  $E_o(0)$  are determined for a euphotic layer that is well-mixed. This is often true for high-latitude waters and upwelling regions.

By analyzing the measured  $a_{\phi}(440)$  and the simulation parameters, Lee (1994) found that for  $a_{\phi}(440)$  in the range of 0.01 to 1.0  $\text{m}^{-1}$ ,

$$\begin{aligned} a_{\phi 2}/a_{\phi 1} &\approx .86 + .16 \ln(a_{\phi 1}), & \text{normalized rms error: 17.2\%,} \\ F &\approx 2.89 \exp[-.505 \tanh[.56 \ln(a_{\phi 1}/.043)]], & \text{normalized rms error: 12.4\%,} \\ \sigma_2 &\approx 14.17 + .9 \ln(a_{\phi 1}), & \text{normalized rms error: 5.6\%.} \end{aligned}$$

Thus whenever  $a_{\phi 1}$  is determined, the full  $a_{\phi}$  spectrum can be estimated with the change of the curve shape considered, at least to first order. Instead of attempting to statistically relate

$a_{\phi_i}$  with ratios of  $R_{rs}$ , it is possible to analytically derive it if  $N$  is equal to or greater than 5. So, the absorption coefficient of pigments as well as the total absorption coefficient can be obtained when there are  $R_{rs}$  values at more than 5 wavelengths.

After the retrieval of  $a_{\phi}$  and  $a$  from measured  $R_{rs}$ , scalar irradiance at depth  $z$  can be calculated (Eq. 4) with  $K_d \approx 1.08 D_d(0) a$  (Gordon 1989), where  $D_d(0)$  is the sub-surface distribution function.  $E_o(0)$  can be calculated using modifications to the models of Gregg and Carder (1990), Bishop and Rossow (1991), or using in situ mooring or drifter *PAR* data. Thus, when  $\phi_m$ ,  $PAR_{\phi}$  and  $\nu$  are known, *PP* for any depth can be calculated through Eqs. 6 and 11.

For data collected from the Marine Light-Mixed Layer (ML-ML) study (21°W/59°N) of May 1991, two sets of calculations were made. The traditional set is derived using Eqs. 6, 7, 8 and 9 (the "pigment" method) as discussed in the introduction. The other is derived by Eqs. 6 and 11 (the "absorption" method), where the absorption coefficients of the pigments and the total absorption coefficients are analytically derived just from measured remote-sensing reflectance.

In both calculations, measured  $PAR(0)$  values for each station were used for the  $PAR(z)$  calculations and comparison of the two methods because most of the stations were taken during cloudy weather.  $D_d(0)$  is approximated as 1.2 (Platt et al. 1991) in the "absorption" method as most of the station days were cloudy. The calculated results for each day at each depth were compared with the measured primary production values, and the water-column-integral production.

### *Data and measurements*

Data for  $PAR(z)$ ,  $PP(z)$ , and  $R_r(\lambda)$  were collected on an ML-ML cruise from May 17 to May 24, 1991 in the waters south of Iceland (21°W/59°N).  $PAR$  and  $PP$  measurements were carried out on floating array for each of four days: May 17, 20, 22 and 24. The sampling site, conditions, wind, mixing, and nutrients are presented in Marra et al. (1994) and Plueddemann et al. (1994). In general, it was windy for the stations, and the euphotic zone was well mixed.

*Shipboard measurements* -  $PAR(z)$  at four depths (0, 2, 12.5 and 25 m) was monitored and averaged for every 10 minute interval throughout the day using a Biospherical  $PAR$  sensor attached to each incubation array (Marra et al. 1994).

Dawn-to-dusk incubations (17 hours) with four replicates were carried out *in situ* at each of six depths (5, 10, 15, 20, 30 and 40 m) chosen to span the euphotic zone. Primary production ( $PP$ ) measurements were made using the  $^{14}C$  technique (Marra et al. 1994).

*Remote-sensing reflectance,  $R_r(\lambda)$*  - Hyperspectral remote-sensing reflectance  $R_r(\lambda)$  was measured for the noon site by the method developed by (Carder and Steward 1985). The instrument was the Spectron Engineering spectral radiometer (model SE-590). It has 253 channels and covers the wavelength range from 370 - 1100 nm with a spectral resolution of 7 nm using a 200  $\mu m$  entrance slit. With this instrument the water-leaving radiance and downwelling sky radiance were directly measured, downwelling irradiance was measured by viewing a standard diffuse reflector (Spectralon,  $\sim 8.5\%$ ). Reflected sky radiance was corrected by the method of Carder and Steward (1985) when calculating  $R_r(\lambda)$ .

## Results and discussion

Comparisons of calculated and measured *PAR* and calculated and measured *PP* are presented in Figures 2a - 2d and Figures 3a - 3d, respectively. All data are summarized in Table 2 and all *PP* data in Figure 4a, with Figure 4b shows the results when  $\nu$  is 0 (i.e. no photoinhibition considered).

It can be seen that the "absorption" method yields close estimates of *PAR*(*z*), while *PAR*(*z*) values calculated by the "pigment" method were consistently higher, particularly at depth. One reason for this is that the CZCS pigment algorithm estimated [chl *a*] as much as a factor of 5 lower than the measured surface values for these waters. This had the consequence that  $K_d$  values (Eq. 9) calculated from these [*C*] ([chl *a*]/0.75) were small. This difference could be the result of an incorrect CZCS algorithm for that environment (e.g. Balch et al. 1989; Mitchell and Holm-Hansen 1991) or less likely that there were substantial errors or discrepancies in the measurements of  $R_{rs}$  or "sea truth" [chl *a*]. Also, the empirical relationship between  $K_d$  and [*C*] might not hold for these waters. However, the same field data are used for both methods, so models and algorithms will be largely responsible for differences between the methods.

Calculated primary production values by the "absorption" method were highly comparable to the measured values, whereas the "pigment" method significantly underestimated *PP*, particularly in the surface waters. The average difference of the water-column-integrated *PP* is 20% between the measured and the "absorption" method, while it is 61% between the measured and the "pigment" method (Table 2). The  $r^2$  is 0.95 ( $n=24$ ) for a linear regression between the

values calculated by the "absorption" method and that of the measurements, with a slope of 1.26 and + 32% difference. The  $r^2$  is 0.85 ( $n=24$ ) between the values calculated by the "pigment" method and that of the measurements, with a slope of 0.34 and - 78% difference (see Figure 4). These results indicate that there is about a factor of 3 improvement in the accuracy of *PP* calculation from remote sensing for ML-ML waters using the "absorption" method suggested here.

For May 17 (Figure 3a), the calculated *PP* values by the "absorption" method in the euphotic zone were generally greater than the measured values. Factors that can account for these differences include possible errors in measurement and  $R_{\infty}$  inversion, grazing effects on the measured values, and either the photoinhibition factor used was smaller than the "real" situation, or  $\phi_m$  and/or  $PAR_{\phi}$  used was higher than the "actual" values.

For May 20 and May 24 (Figures 3b and 3d), the *PP* values calculated by the "absorption" method were very close to those measured, which suggest that our assumed values of  $\phi_m$ ,  $PAR_{\phi}$  and  $\nu$  for these two days were probably close to reality.

The greatest differences between measured and calculated values from both the "pigment" and "absorption" methods occurred on the only sunny day of the cruise, May 22 (Figure 3c), where measured surface layer production was smaller than the second layer. Other than measurement errors, this is an indication of increased photoinhibition, as suggested by the calculated values of the "absorption" method, which was also discussed in Carder et al. (1994) and Marra et al. (1994). However, the calculated *PP* values by the "absorption" method are greater than the measured values for the first four depths (~40%). Possible reasons for this difference might be an overestimation of  $\phi_m$  and/or an underestimation of  $\nu$  for the phytoplankton

in this environment, since  $\phi_m$  and/or  $\nu$  might be a function of light history. The other 3 cruise days were overcast with an expected adaptation of the plants to a low light level. The sudden exposure to the bright light probably caused extreme photoinhibition in the dark-adapted phytoplankton population with the resultant overestimation of *PP* by the "absorption" method.

The *PP* values calculated by the "pigment" method for the sunny day, however, do not show a photoinhibition response in the surface waters (Figure 3c). One reason for this is that  $\bar{a}_\phi^*$  not only varies with the chlorophyll-specific absorption coefficient, it also varies with the light field (Eq. 2). An  $\bar{a}_\phi^*$  value for surface water is not necessarily appropriate for the whole water column, even for a well-mixed ocean (Kishino et al. 1986). So, the  $\bar{a}_\phi^*$  value is one of the major sources of error in *PP* calculations by the traditional method.

For the waters studied, *PP* values calculated by the "pigment" method were lower than measured rates by a factor of 3. Since *PP* values calculated by the "absorption" method were close to measured values, our value of  $\phi_m$ ,  $0.074 \text{ mol C (Ein absorbed)}^{-1}$ , is apparently close to the actual value. Therefore, the differences between calculated and measured *PP* for the "pigment" method are largely due to the estimation of  $[C]$  and the product of  $\rho[C]\bar{a}_\phi^*$ . However, when only remote-sensing data are available, it is difficult to know which are the "correct"  $\bar{a}_\phi^*$  and  $\rho[C]$  values, as they depend upon empirical values. What makes things interesting is that a factor of 2 increase in both  $[C]$  and  $\bar{a}_\phi^*$  will make calculated *PAR* and *PP* both close to the measured values. The pigment data in Table 2, however, suggest that the CZCS algorithm accounts for most of the error. This is consistent with the conclusion of Platt et al. (1988) that determination of biomass by remote sensing dominates the error in primary production estimation. So, it is preferable to shift the primary production models from pigment-

concentration base to pigment-absorption base.

Comparing Eqs. 7 and 11, the main difference between the "absorption" and "pigment" methods is how  $APP(z)$ , the absorbed energy by phytoplankton pigments, is obtained from remote-sensing data. In the traditional method, calculation of  $APP$  depends heavily on 4 numbers:  $\rho$ ,  $A$ ,  $B$ , and  $\overline{a}_\phi$ . When there are only remote-sensing signals, it is difficult to verify which values should be used for each of these parameters, although each of them could be tuned empirically to specific regions and specific seasons (Platt et al. 1991). Since there are errors associated with each number, the cumulative error in  $APP$  could then be very high, even if  $PAR$  is correct.

In the  $APP$  calculation by the "absorption" method, however, the single most important parameter ( $a_{\phi_l}$ ) is analytically derived from measured  $R_{rs}$ . Thus, most of the error comes from the  $R_{rs}$  inversion process. It is believed that absorption coefficients derived from  $R_{rs}$  inversion have an accuracy better than 50% for "case 1" and "case 2" waters (Lee 1994). This means that the accuracy in the  $APP$  calculation by the "absorption" method could be within 50%. Values derived using the traditional method were only 1/3 of the measured values, however. In the "absorption" method, the mid-step, i.e. deriving [chl  $a$ ] and estimating a value for  $\overline{a}_\phi$ , is eliminated. The result is highly improved accuracy in deriving  $APP$  and  $PP$ .

How to remotely obtain accurate estimations of the physiological parameters such as  $\phi_m$ ,  $PAR_\phi$  and  $\nu$ , however, remains a challenge for the calculation of  $PP$  through remote sensing (Balch et al. 1992). Including light history and surface temperature anomalies (e.g. see Kamykowski and Zentara 1986) in future  $PP$  models may reduce this deficiency. Among the three parameters,  $\phi_m$  might be the most important for a  $PP$  model, since  $PP$  is proportional to



the value of  $\phi_m$ . Only when  $PAR(z)$  is very high is there a strong influence on  $PP$  due to  $PAR$ , and  $\nu$ . For example, for  $\nu = 0.01 \text{ (Ein/m}^2\text{/day)}^{-1}$ ,  $e^{-\nu PAR(z)}$  is 0.90, 0.82, 0.67, 0.55 and 0.45 for  $PAR(z)$  values of 10, 20, 40, 60 and 80  $\text{Ein/m}^2\text{/day}$ , respectively. This means that by dropping the photoinhibition term, the calculated  $PP$  will increase 10% to about 55%. Such an increase could be compensated by using a smaller  $\phi_m$  value, but, without the photoinhibition term, the increase then decrease vertical profile of  $PP$  with depth would not be simulated. Without consideration of photoinhibition for the waters studied,  $r^2$  decreased from a value of 0.95 to 0.93 ( $n=24$ ), and the slope increased from 1.26 to 1.39 (see Figure 4b). This suggests that the photoinhibition term is important for primary production model applications to the ML-ML site.

### Conclusions and expectations

1. Based on the results presented here, the  $a_p$  simulation works very well in modeling  $PAR(z)$  based on  $PAR(0)$  and  $R_{\infty}$ . Combined with parameters regarding phytoplankton photosynthesis, the  $PP$  values calculated by the "absorption" method were close to the measured ones with  $r^2 = 0.95$ , a slope = 1.26, and average difference of 32%. This means a great improvement in  $PP$  estimation accuracy, where the modeled values were three-fold smaller than the measured ones using the traditional method. So, it is preferable to shift the primary production models from pigment-concentration base to pigment-absorption base. These results also indicate that the combined  $PP$  model,

$$PP(z) = APP(z) \frac{\phi_m PAR_{\phi}}{PAR_{\phi} + PAR(z)} e^{-\nu PAR(z)}, \quad (17)$$

works fine for the waters studied.

2. It is not necessary to know  $[chl\ a]$  for the calculation of  $PP$ . In the traditional method, the estimation of  $[C]$  and  $\bar{a}_{\phi}^*$  separately is an inherent disadvantage in calculating  $PP$  based upon satellite or aircraft remote-sensing measurements of ocean color. What is really needed for models of  $PP$  is the absorbed energy by phytoplankton, and the physiological parameters of phytoplankton photosynthesis.

3. Coupled investigations between  $PP$  and  $R_{\infty}$  measurements need be carried out widely to generate more data to test and improve the method.

4. Cloud-covered marine environments such as the ML-ML site in the spring cannot often be viewed from space. They can, however, be measured using drifters or moorings or from

aircraft flying beneath the cloud base. Autonomously piloted aircraft (Montgomery et al. 1994) are becoming available that could provide spectral observations of the ocean *in the future* to increase our knowledge of cloud-fast environments. Methods such as developed in this contribution can provide improved estimates of primary production and ultimately pigments if combined with appropriate drifters, moorings, or aircraft and sensor packages.

5. For space-based measurements, methods must be pursued to remotely estimate the physiological parameters, perhaps by their covariance with some remotely measured variable such as sea surface temperature anomalies, wind-stress history, and light history.

## References

- Balch, W. M., R. W. Epply, M. R. Abbott, and F. M. H. Reid. 1989. Bias in satellite-derived pigment measurements due to coccolithophores and dinoflagellates. *J. Plankton Res.* **11**: 575-581.
- Balch, W. M., R. Evans, J. Brown, G. Feldman, C. McClain, and W. Esaias. 1992. The remote sensing of ocean primary productivity: use of a new data compilation to test satellite algorithms. *J. Geophys. Res.* **97**: 2279-2293.
- Bannister, T. T. 1974. Production equations in terms of chlorophyll concentration, quantum yield, and upper limit to production. *Limnol. Oceanogr.* **19**: 1-12.
- Bannister, T. T., and A.D. Weidemann. 1984. The maximum quantum yield of phytoplankton photosynthesis *in situ*. *J. Plankton. Res.* **6**: 275-294.
- Bannister, T. T. 1992. Model of the mean cosine of underwater radiance and estimation of underwater scalar irradiance. *Limnol. Oceanogr.* **37**: 773-780.
- Bidigare, R. R., M. E. Ondrusek, J. H. Morrow, and D. A. Kiefer. 1990. In vivo absorption properties of algal pigments. *In Ocean Optics X. Proc. SPIE 1302*: 290-302.
- Bidigare, R. R., B. B. Prezelin, and R. C. Smith. 1992. Bio-optical models and the problems of scaling, p. 175-212. *In* P. G. Falkowski and A. D. Woodhead [ed.], *Primary Production and Biogeochemical Cycles in the Sea*. Plenum Press.
- Bishop, J. K., and W. B. Rossow. 1991. Spatial and temporal variability of global surface solar irradiance. *J. Geophys. Res.* **96**: 16,839-16,858.
- Carder, K. L., and R. G. Steward. 1985. A remote-sensing reflectance model of a red tide

dinoflagellate off West Florida. *Limnol. Oceanogr.* 30: 286-298.

Carder, K. L., S. K. Hawes, K. S. Baker, R. C. Smith, R. G. Steward, and B. G. Mitchell.

1991. Reflectance model for quantifying chlorophyll *a* in the presence of productivity degradation products, *J. Geophys. Res.* 96: 20,599-20,611.

Carder, K. L., Z. P. Lee, J. Marra, R. G. Steward, and M.J. Perry. 1994. Calculated quantum yield of photosynthesis of phytoplankton in the Marine Light-Mixed Layers (59°N/21°W). *J. Geophys. Res.* Accepted.

Cleveland, J. S., M. J. Perry, D. A. Kiefer, and M. C. Talbot. 1989. Maximal quantum yield of photosynthesis in the northwestern Sargasso Sea. *J. Marine Res.* 47: 869-886.

Cullen, J. J. 1990. On models of growth and photosynthesis in phytoplankton. *Deep-Sea Res.* 37: 667-683.

Dubinsky, Z., T. Berman, and F. Schanz. 1984. Field experiments for *in situ* measurements of photosynthetic efficiency and quantum yield, *J. Plankton Res.* 6: 339-349.

Gordon, H. R., and A. Morel. 1983. Remote assessment of ocean color for interpretation of satellite visible imagery: A review. Springer. 114 p.

Gordon, H. R., O. B. Brown, R. H. Evans, J. W. Brown, R. C. Smith, K. S. Baker, and D. K. Clark. 1988. A semianalytic radiance model of ocean color. *J. Geophys. Res.* 93: 10,909-10,924.

Gordon, H. R. 1989. Can the Lambert-Beer law be applied to the diffuse attenuation coefficient of ocean water? *Limnol. Oceanogr.* 34: 1389-1409.

Gregg, W. W., and K. L. Carder. 1990. A simple spectral solar irradiance model for cloudless maritime atmospheres. *Limnol. Oceanogr.* 35: 1657-1675.

- Hoepffner, N., and S. Sathyendranath. 1991. Effect of pigment composition on absorption properties of phytoplankton. *Marine Ecology Progress Series* 73: 11-23.
- Kamykowski, D., and S. Zentara. 1986. Predicting plant nutrient concentrations from temperature and sigma-t in the upper kilometer of the world ocean. *Deep-Sea Res.* 33: 89-105.
- Kiefer, D. A., and B. G. Mitchell. 1983. A simple, steady state description of phytoplankton growth based on absorption cross section and quantum efficiency. *Limnol. Oceanogr.* 28: 770-776.
- Kishino, M., N. Okami, M. Takahashi, and S. Ichimura. 1986. Light utilization efficiency and quantum yield of phytoplankton in a thermally stratified sea. *Limnol. Oceanogr.* 31: 557-566.
- Laws, E. A., G. R. Ditullio, K. L. Carder, P. R. Betzer, and S. K. Hawes. 1990. Primary production in the deep blue sea. *Deep-Sea Res.* 37: 715-730.
- Langdon, C. 1988. On the causes of interspecific differences in growth-irradiance relationship for phytoplankton, II, A general review. *J. Plankton Res.* 10: 1291-1312.
- Lee, Z. P., K. L. Carder, S. K. Hawes, R. G. Steward, T. G. Peacock, and C. O. Davis. 1994a. A model for interpretation of hyperspectral remote sensing reflectance. *Appl. Opt.* 33: 5721-5732.
- Lee, Z. P., K. L. Carder, and T. G. Peacock. 1994b. Hyperspectral modeling of remote sensing reflectance: from the Florida Shelf to the Mississippi river. *EOS Trans. AGU* 75: 193.
- Lee Z. P. 1994. Visible-infrared remote-sensing model and applications for ocean waters. Ph.D. dissertation. University of South Florida. 145 p.

- Marra, J., T. Dickey, W. S. Chamberlin, C. Ho, T. Granata, D. A. Kiefer, C. Langdon, R. C. Smith, K. S. Baker, R. R. Bidigare, and M. Hamilton. 1992. Estimation of seasonal primary production from moored optical sensors in the Sargasso Sea. *J. Geophys. Res.* **97**: 7399-7412.
- Marra, J., W. S. Chamberlin, and C. A. Knudson. 1993. Proportionality between in situ carbon assimilation and bio-optical measures of primary production in the Gulf of Maine in summer. *Limnol. Oceanogr.* **38**: 232-238.
- Marra, J., C. Langdon, and C. A. Knudson. 1994. Primary production and water column changes and the demise of a *phaeocystis* bloom at the Marine Light-Mixed Layers site (59°N/21°W, North Atlantic Ocean). *J. Geophys. Res.* Accepted.
- Mitchell, B. G., and O. Holm-Hansen. 1991. Bio-optical properties of Antarctic Peninsula waters: Differentiation from temperate ocean models. *Deep-Sea Res.* **38**: 1009-1028.
- Montgomery, K., J. J. Petrovic, and N. P. Murarka. 1994. Guidance and control of unmanned air vehicles. Association for Unmanned Vehicle Systems Symposium. Detroit, MI. May 23-25.
- Morel, A., and A. Bricaud. 1981. Theoretical results concerning light absorption in a discrete medium and application to the specific absorption of phytoplankton. *Deep-Sea Res.* **28**: 1357-1393.
- Morel, A. 1980. In-water and remote measurements of ocean color. *Boundary-Layer Meteorology* **18**: 177-201.
- Morel, A. 1988. Optical modeling of the upper ocean in relation to its biogenous matter content (case I waters). *J. Geophys. Res.* **93**: 10,749-10,768.

- Morel, A., and J. F. Berton. 1989. Surface pigments, algal biomass profiles, and potential production of the euphotic layer: relationships reinvestigated in review of remote-sensing applications. *Limnol. Oceanogr.* 34: 1545-1562.
- Morel, A. 1991. Light and marine photosynthesis: a spectral model with geochemical and climatological implications. *Prog. Oceanogr.* 26: 263-306.
- Morel A., and B. Gentili. 1993. Diffuse reflectance of oceanic waters (2): Bi-directional aspects. *Appl. Opt.* 32: 6864-6879.
- Platt, T., C. L. Gallegos, and W.G. Harrison. 1980. Photoinhibition of photosynthesis in natural assemblages of marine phytoplankton. *J. Marine Res.* 38: 687-701.
- Platt, T., S. Sathyendranath, C. M. Caverhill, and M.R. Lewis. 1988. Ocean primary production and available light: further algorithms for remote sensing. *Deep-Sea Res.* 35: 855-879.
- Platt, T., C. M. Caverhill, and S. Sathyendranath. 1991. Basin-scale estimates of oceanic primary production by remote sensing: The North Atlantic. *J. Geophys. Res.* 96: 15,147-15,159.
- Plueddemann, A., R. Weller, T. Dickey, J. Marra, and M. Stramska. 1994. Surface forcing and re-stratification in the sub-Arctic North Atlantic. *J. Geophys. Res.* Submitted.
- Roesler, C. S., M. J. Perry, and K. L. Carder. 1989. Modeling in situ phytoplankton absorption from total absorption spectra in productive inland marine waters. *Limnol. Oceanogr.* 34: 1510-1523.
- Roesler, C. S., and M. J. Perry. 1994. A robust model for determining *in situ* phytoplankton absorption and fluorescence emission spectra from reflectance. *J. Geophys. Res.* Submitted.



Sathyendranath, S., and T. Platt. 1988. The spectral irradiance field at the surface and in the interior of the ocean: a model for applications in oceanography and remote sensing.

J. Geophys. Res. 93: 9270-9280.

Smith, R. C., and K. S. Baker. 1981. Optical properties of the clearest natural waters. Appl. Opt. 20: 177-184.

Smith, R. C., B. B. Prezelin, R. R. Bidigare, and K. S. Baker. 1989. Bio-optical modeling of photosynthetic production in coastal waters. Limnol. Oceanogr. 34: 1524-1544.

Zaneveld, J. R. V., J. C. Kitchen, and J. L. Mueller. 1993. Vertical structure of productivity and its vertical integration as derived from remotely sensed observations. Limnol. Oceanogr. 38: 1384-1393.

Table 1: Symbols and units.

---

$a(\lambda)$	Total absorption coefficient, $\text{m}^{-1}$ ; $a(\lambda) = a_w(\lambda) + a_{dg}(\lambda) + a_\phi(\lambda)$
$a_{dg}(\lambda)$	Absorption coefficient of detritus and gelbstoff, $\text{m}^{-1}$
$a_\phi(\lambda)$	Absorption coefficient of phytoplankton pigments, $\text{m}^{-1}$
$a_\phi^*(\lambda)$	Pigment-specific absorption coefficient, $\text{m}^2 (\text{mg chl } a)^{-1}$
$a_{\phi 1, \phi 2}$	$a_\phi(440)$ and $a_\phi(675)$ , respectively, $\text{m}^{-1}$
$a_w(\lambda)$	Absorption coefficient of pure water, $\text{m}^{-1}$
$APP$	Absorbed photons by phytoplankton, $\text{Ein}/\text{m}^3/\text{day}$
$b_b(\lambda)$	Backscattering coefficient, $\text{m}^{-1}$
$[\text{chl } a]$	chlorophyll $a$ concentration, $\text{mg}/\text{m}^3$
$[C]$	chlorophyll-like pigment concentration, $\text{mg}/\text{m}^3$
$D_d(0)$	Subsurface downwelling distribution function
$E_o$	Quantum scalar irradiance, $\text{quanta}/\text{m}^2/\text{s}$
$K_d$	Diffuse attenuation coefficient for downwelling irradiance, $\text{m}^{-1}$
$L_w$	Water-leaving radiance, $\text{W}/\text{m}^2$
$PAR$	Photosynthetically available radiation (integrated from 400 - 700 nm), $\text{Ein}/\text{m}^2/\text{day}$
$PAR(0)$	Surface $PAR$ , $\text{Ein}/\text{m}^2/\text{day}$
$PAR_\phi$	Value of $PAR$ where $\phi = \phi_m/2$ , $\text{Ein}/\text{m}^2/\text{day}$
$PP$	Primary production, $\mu\text{mol C}/\text{l}$
$R_{rs}$	Remote-sensing reflectance, $= L_w/E_d$ , $\text{sr}^{-1}$

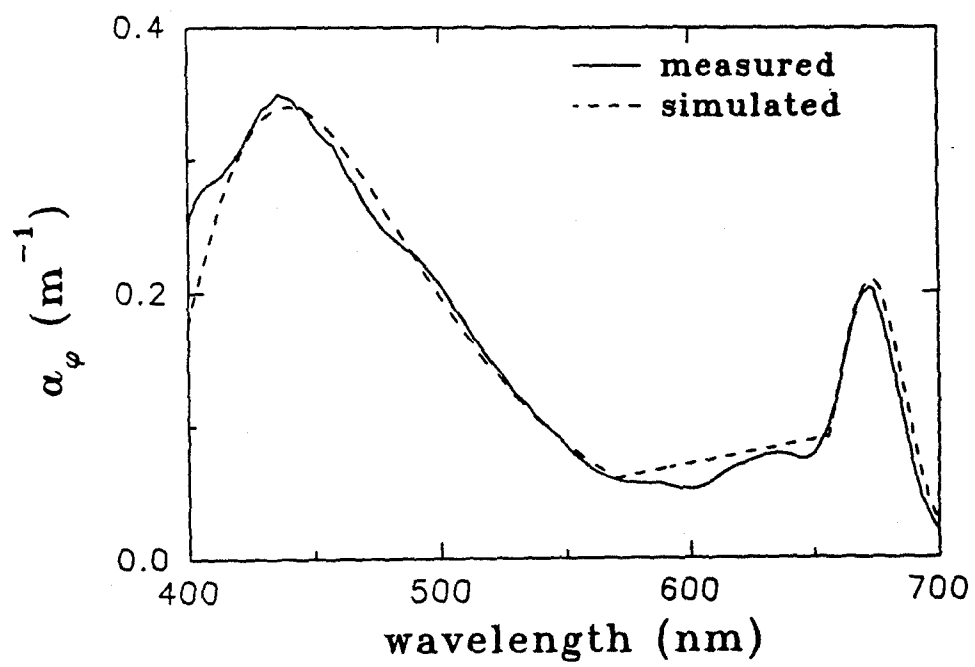
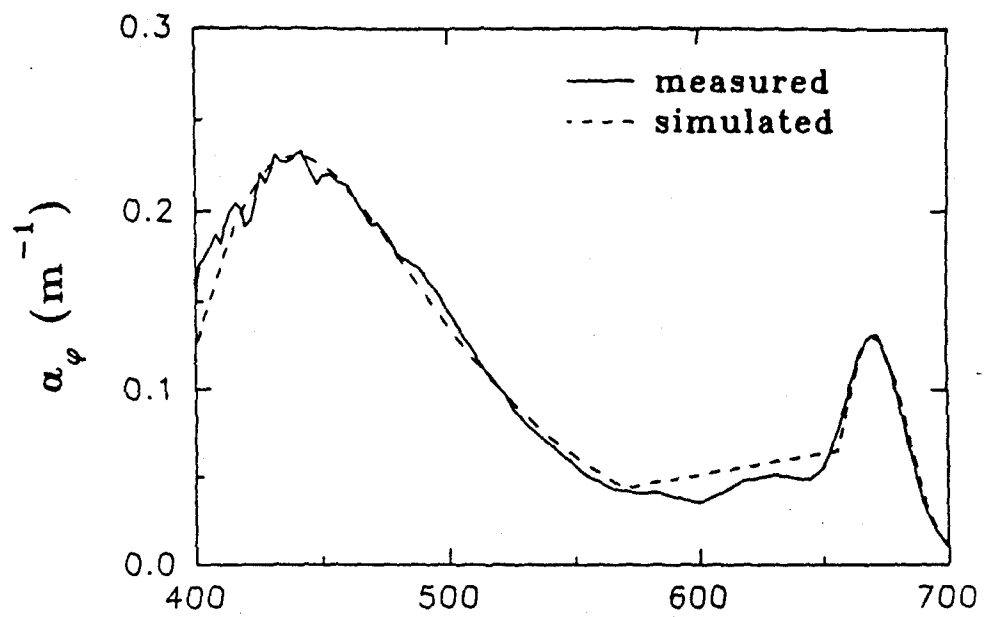
---

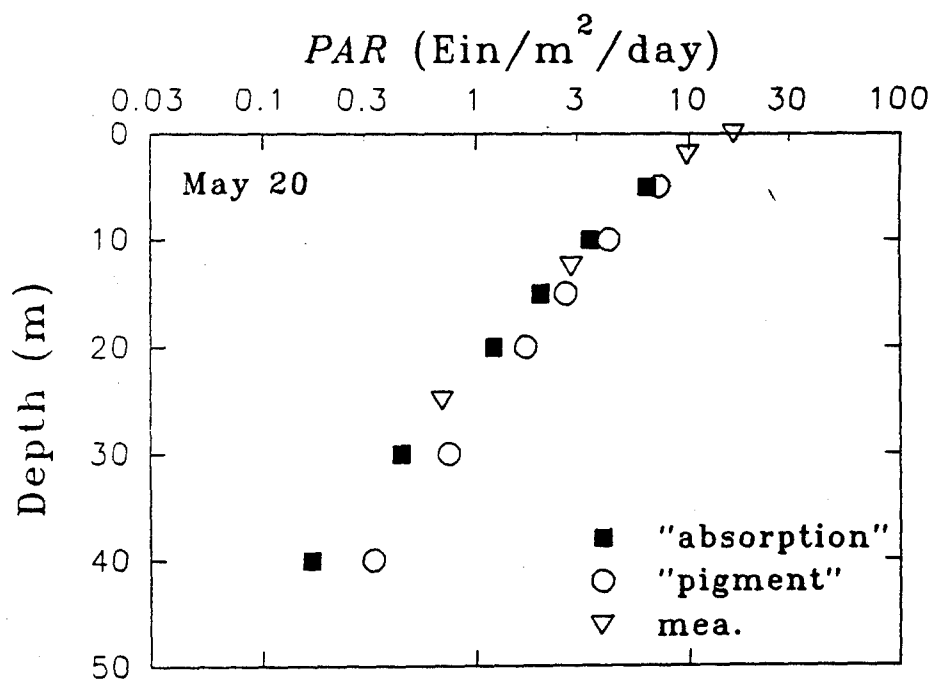
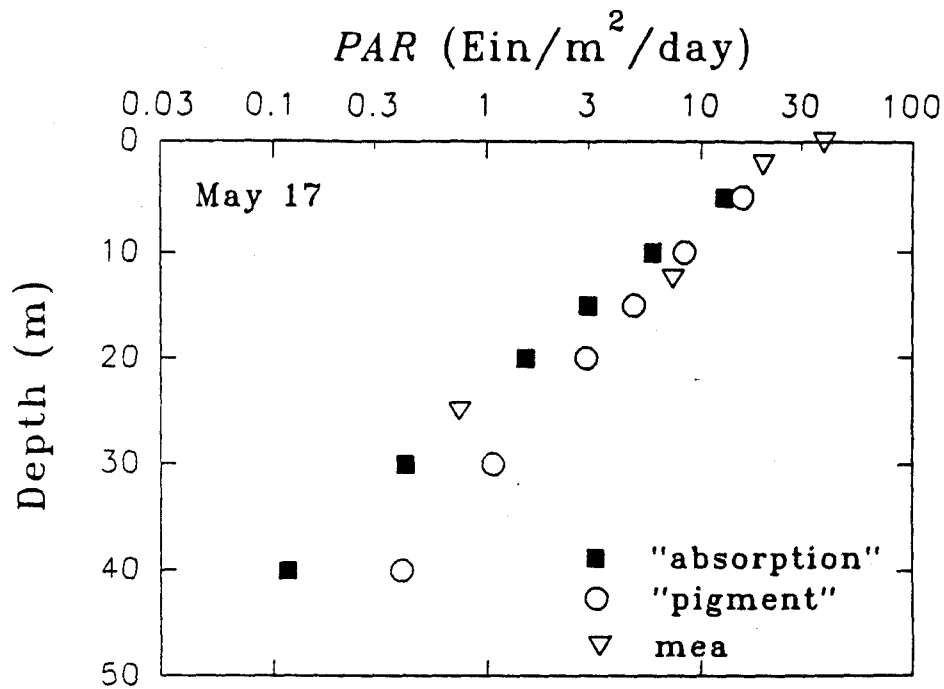
$\phi$	Quantum yield, mol C (Ein absorbed) <sup>-1</sup>
$\phi_m$	Maximum quantum yield, mol C (Ein absorbed) <sup>-1</sup>
$\lambda$	Wavelength, nm
$\rho$	fraction of [chl <i>a</i> ] in [C]
$\nu$	Photoinhibition factor, (Ein m <sup>-2</sup> day <sup>-1</sup> ) <sup>-1</sup>

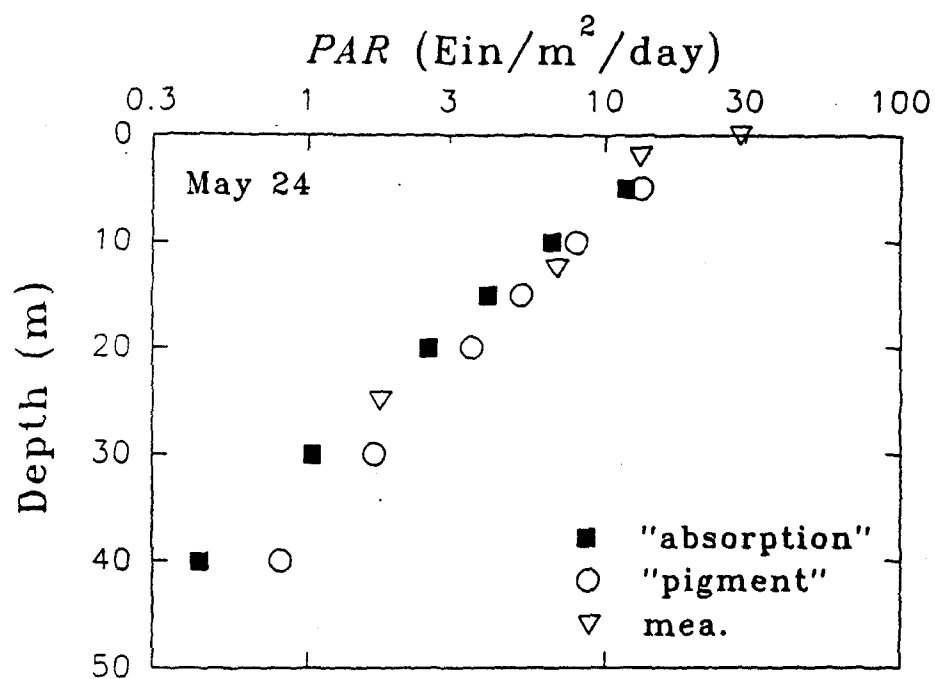
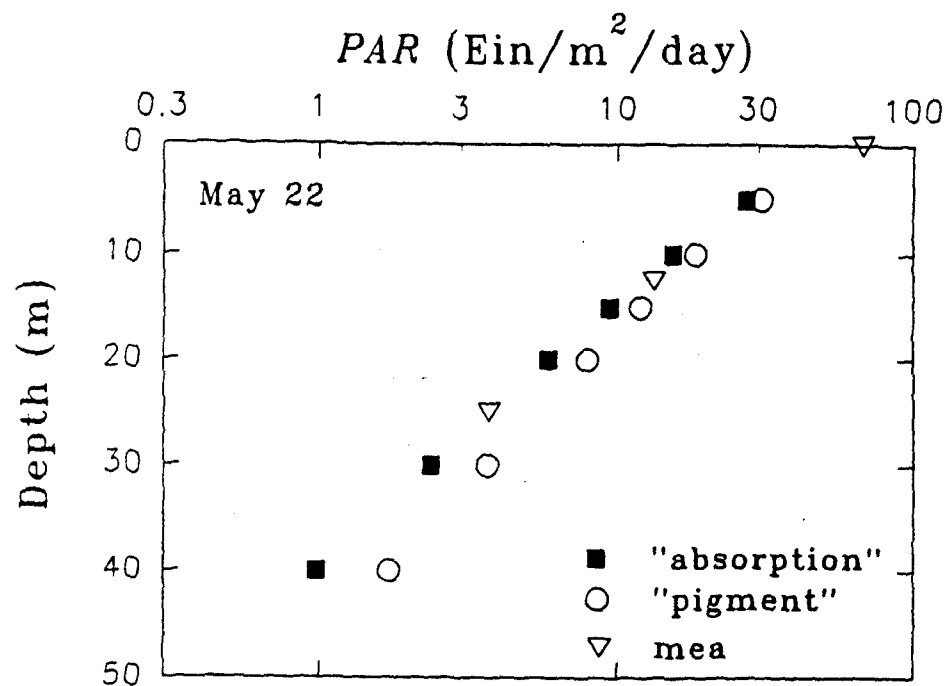
---

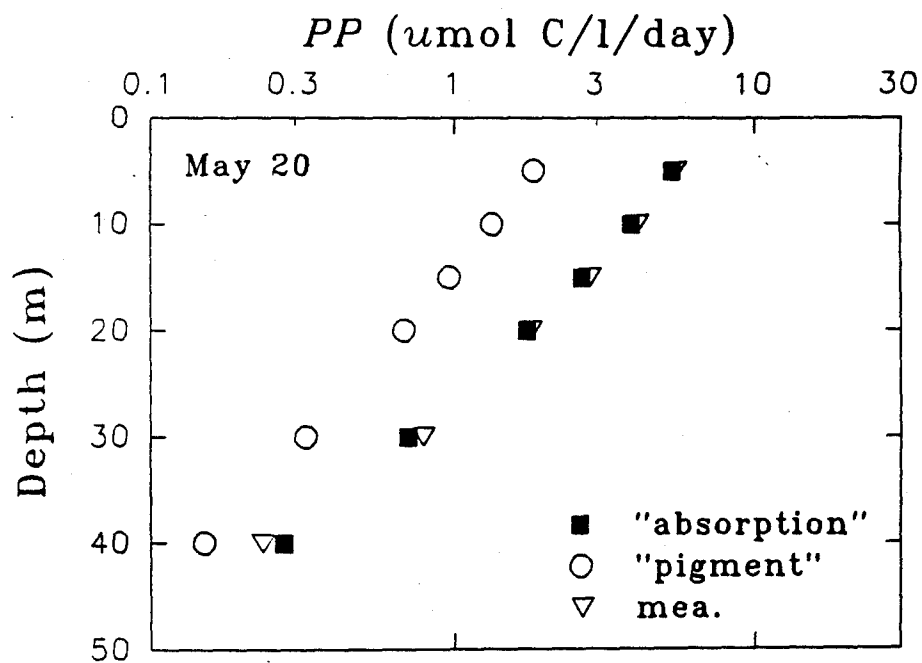
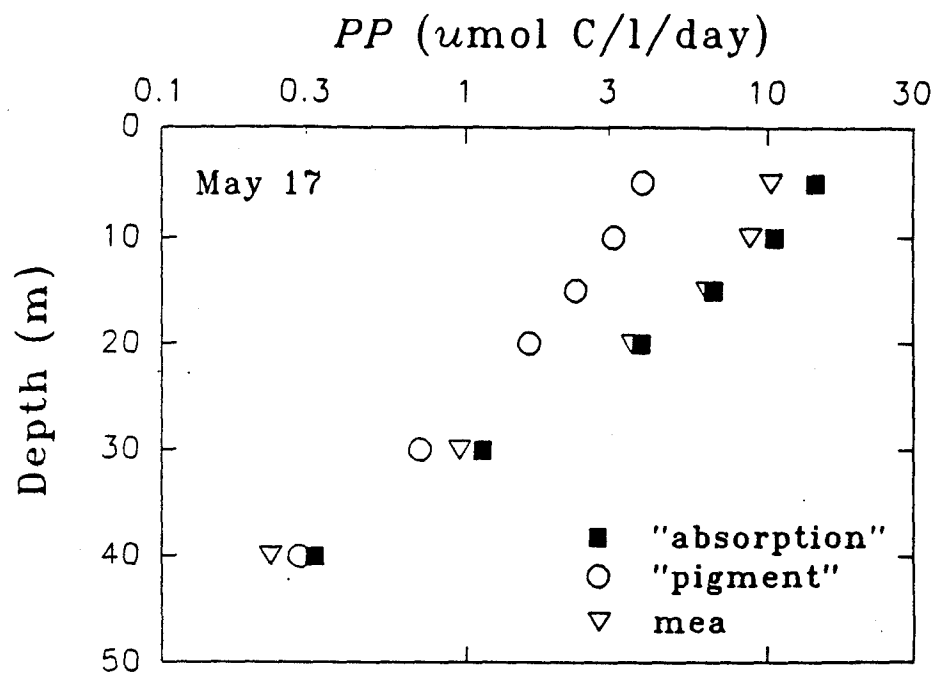
Table 2. Result summary.

Day	May 17	May 20	May 22	May 24
$PAR(0)$ (Ein/m <sup>2</sup> /day)	38.27	16.25	65.72	28.73
$R_{rs}(443)/R_{rs}(550)$	1.2	1.6	1.8	1.8
surface [chl <i>a</i> ] (mg/m <sup>3</sup> )	2.9	1.3	1.5	1.0
CZCS [chl <i>a</i> ] (mg/m <sup>3</sup> )	0.67	0.43	0.36	0.34
Mea. integral <i>PP</i> ( <i>m</i> mol C/m <sup>2</sup> /day)	190	98	89	99
Est. integral <i>PP</i> : "absorption" ( <i>m</i> mol C/m <sup>2</sup> /day)	235	94	105	89
Est. integral <i>PP</i> : "pigment" ( <i>m</i> mol C/m <sup>2</sup> /day)	77	34	62	40

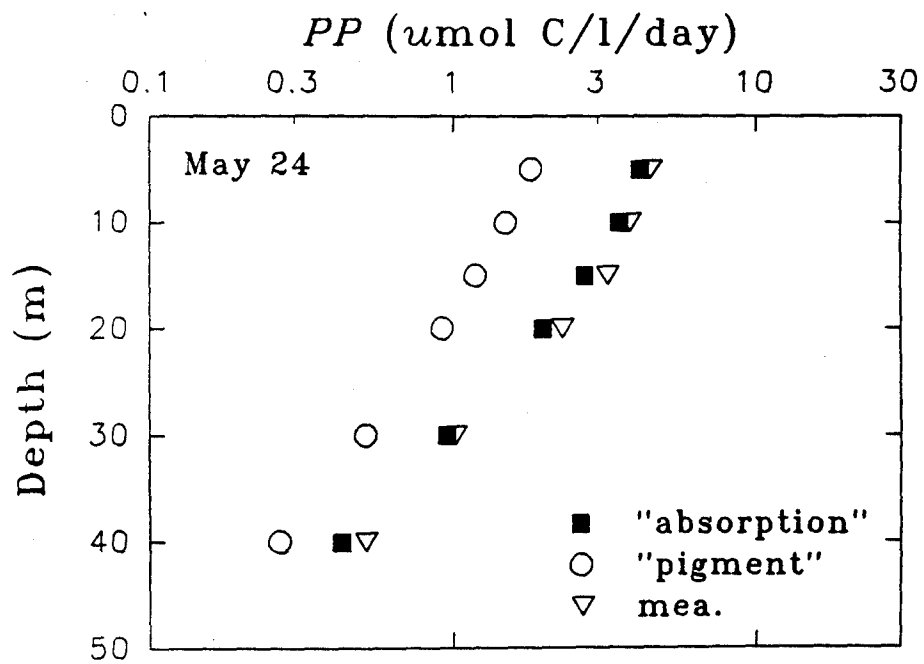
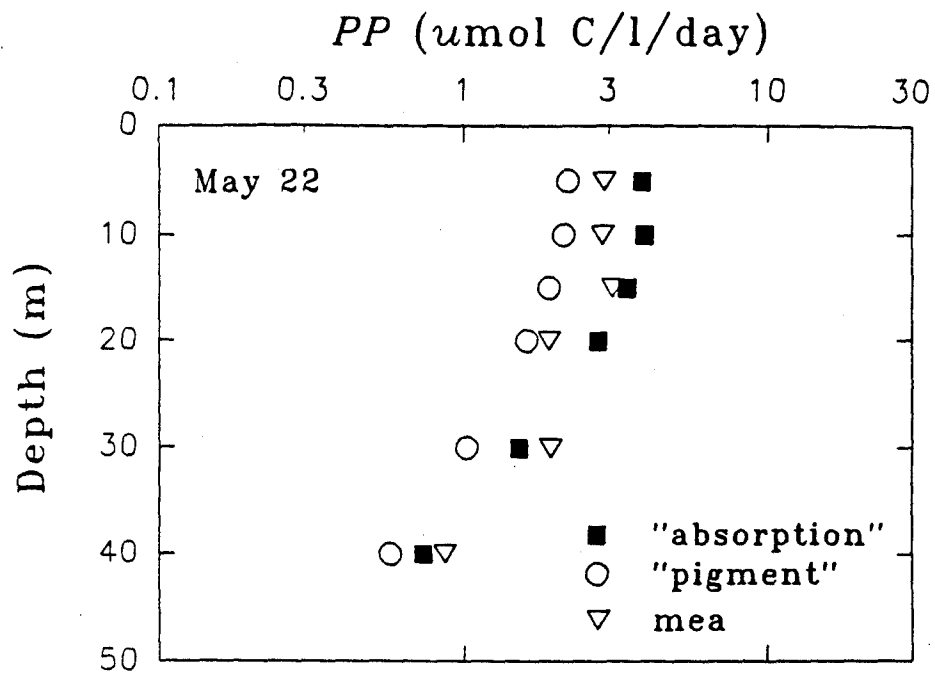




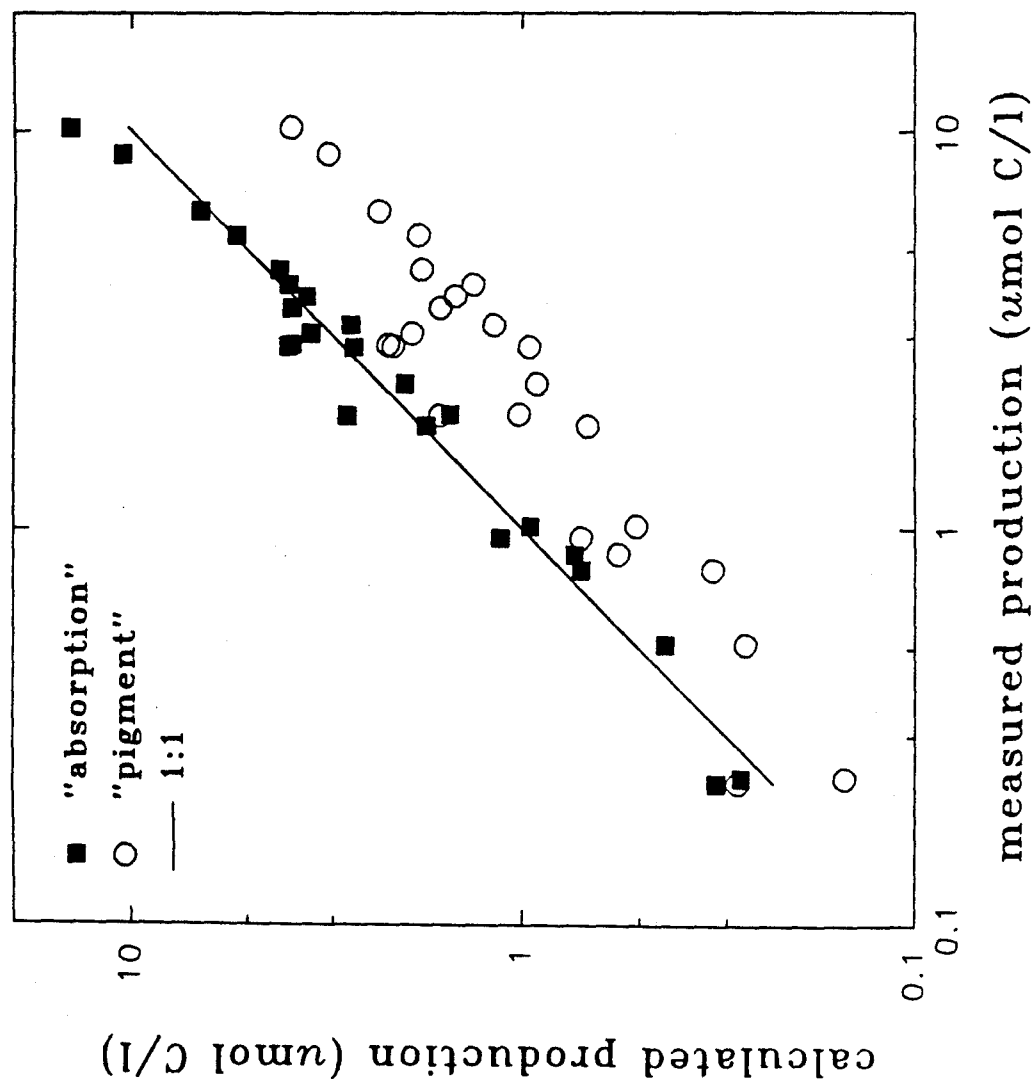








# Primary production of ML-ML, May 91



# Primary production of ML-ML, May 91

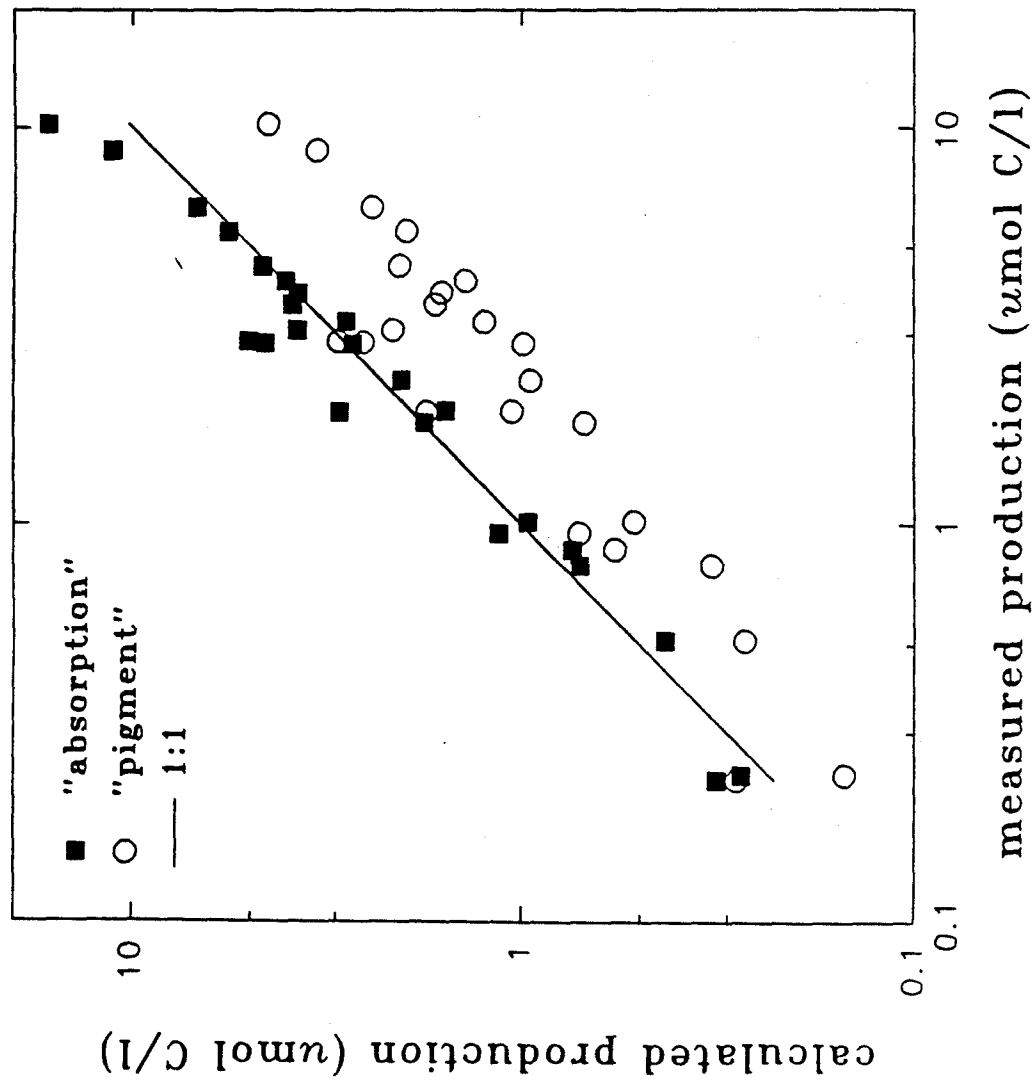


### *Figure legends*

Figure 1a - 1b. Examples for the  $a_p(\lambda)$  simulation.

Figure 2a - 2d. Depth profiles of *PAR* for May 17, May 20, May 22 and May 24, respectively.

Open triangle-down: measured. Filled square: estimated by the "absorption" method.

Open circle: estimated by the "pigment" method.

Figure 3a - 3d. Depth profiles of *PP* for May 17, May 20, May 22 and May 24, respectively.

Symbols as in Figure 2.

Figure 4a - 4b. Comparison of all measured and calculated *PP*.

In 4a, photoinhibition was considered; in 4b, photoinhibition was not considered (details see text).

Symbols as in Figure 2.

## MERIDIONAL FLUXES OF DISSOLVED ORGANIC MATTER IN THE NORTH ATLANTIC OCEAN

John J. Walsh, Kendall L. Carder, and Frank E. Müller-Karger

Department of Marine Science, University of South Florida, St. Petersburg

**Abstract.** Using bio-optical estimates of gelbstoff and a few platinum measurements of dissolved organic carbon ( $\text{DOC}_{\text{pt}}$ ), a budget of the meridional flux of DOC and dissolved organic nitrogen (DON) across  $36^{\circ}25'N$  in the North Atlantic is constructed from previous inverse models of water and element transport. Distinct southward subsurface fluxes of dissolved organic matter (DOM) within subducted shelf water, cabelled slope water, and overturned basin water are inferred. Within two cases of a positive gradient of  $\text{DOC}_{\text{pt}}$  between terrestrial/shelf and offshore stocks, the net equatorward exports of  $\text{O}_2$  and  $\text{DOC}_{\text{pt}}$  from the northern North Atlantic yield molar ratios of 2.1 to 9.1, compared to the expected Redfield  $\text{O}_2/\text{C}$  ratio of 1.3. In the first case, 63% of the apparent oxygen utilization demands of the water column may be met by DOC, instead of only 14% in the second scenario, preserving a role for falling particles in the sea. With a DOC/DON ratio of 10, the larger net southward export of DON across  $36^{\circ}25'N$  balances the postulated net northward input of  $1.7 \times 10^3 \text{ kg NO}_3 \text{ s}^{-1}$  of unutilized nitrate within the Gulf Stream. Without an enhanced supply of DOM from the shelves, a zero seaward gradient of DOM in the third case suggests that none of the poleward nitrate flux is returned southward as DON, but instead a net poleward flux of DON prevails as well. Our present estimates are confounded, however, by the seasonal and multiyear variability of sinking processes in the North Atlantic. Future active and passive remote sensors, field programs, and simulation models must now discriminate between particulate and dissolved components of surface color signals to verify the importance of both continental margins and DOM in global biogeochemical cycles.

## 1. Introduction

Recent measurements of dissolved organic carbon (DOC) and nitrogen (DON) in sea water, involving varying amounts of a platinum catalyst [Suzuki *et al.*, 1985, 1992; Sugimura and Suzuki, 1988] have rekindled controversies [Williams and Druffel, 1988; Jackson, 1988], ignited at the turn of the century [Putter, 1909], about the roles of dissolved organic matter (DOM) in the ocean. Prior large estimates of DOC in the ocean, obtained with different methods [Plunkett and Rakestraw, 1955; Skopintsev *et al.*, 1966; Gordon and Sutcliffe, 1973; Melnikov and Pavlov, 1978] had been rejected in favor of the lower values obtained with ultraviolet and peroxodisulfuric acid techniques of wet combustion [Armstrong *et al.*, 1966; Menzel and Vaccaro, 1964], although unmeasured organic acids could account for differences in potentiometric and

manometric estimates of total  $\text{CO}_2$  in seawater [Bradshaw and Brewer, 1988]. If the even larger values of DOC measured with the platinum technique are correct, they raise questions about prior estimates of regional sources and sinks of the global carbon budget [Tans *et al.*, 1990], particularly in the North Atlantic, which is the subject of our analysis.

Using depth profiles of Apparent Oxygen Utilization (AOU) and the platinum estimates of DOC, 80% [Toggweiler, 1989] to 100% [Sugimura and Suzuki, 1988] of the respiration in the aphotic zone is now attributed to consumption of DOC, rather than of falling particles in the western Pacific. This hypothesis is a sharp contrast to a previous estimate for the same region [Ogura, 1970], which suggested that at most 25% of AOU demands were met by a DOC source, based on a Redfield molar  $\text{O}_2/\text{C}$  ratio of 1.3 [Redfield *et al.*, 1963] and the wet combustion method [Menzel and Vaccaro, 1964]. These new findings imply that the global downward flux of DOC may be equivalent to the particulate rain of marine carbon, representing 50-67% of new production in simple models of the open ocean [Toggweiler, 1989; Bacastow and Maier-Reimer, 1991; Najjar *et al.*, 1992].

Local invasion of most of the deep sea by surface DOM must occur at slower rates than the settling velocities ( $\sim 100 \text{ m d}^{-1}$ ) of large particles [Aldredge and Gotschalk, 1989], however. At similar rates to those of nitrate infusion up the oceanic nutricline [Walsh, 1991], for example, diffusive invasion by surface DOM at a rate of  $1 \text{ cm}^2 \text{ s}^{-1}$  is equivalent to a penetration speed of  $\sim 37 \text{ m yr}^{-1}$  over the upper 100 m of the water column. At this rate, it would take at least 27 years to arrive at a depth of 1000 m; eddy diffusion of DOM across the main pycnocline would be even slower. Over this time, lateral advection, particularly that of western boundary currents ( $>100 \text{ km d}^{-1}$ ), may allow pilgrimage of tropical and subtropical DOC pools to polar latitudes [Toggweiler, 1989], where convective mixing may accelerate the descent of DOC.

Otherwise, photodegradation [Keiber *et al.*, 1990] and bacterial utilization [Kirchman *et al.*, 1991] of DOC in surface waters may return most of this dissolved form of photosynthate back to the atmosphere as biogenic  $\text{CO}_2$ , leaving behind a relatively inert component of DOC. The  $^{14}\text{C}$  age [Williams and Druffel, 1987] and C/N ratio [Jackson and Williams, 1985] of deep-sea pools of DOM determined by UV-radiation are 6000 years and 25, for example, instead of the C/N ratios of 5-7 [Sugimura and Suzuki, 1988] and a bomb-label [Druffel *et al.*, 1989] for DOC measured with the platinum method. The more recent observations imply a younger and less refractory component of DOC as well, at least in offshore waters [Kirchman *et al.*, 1991; Suzuki and Tanoue, 1991; Benner *et al.*, 1992]. In contrast, the radiocarbon age of near-surface humic and fulvic acids, comprising 20-50% of the DOC

Copyright 1992 by the American Geophysical Union

Paper number 92JC01177.  
0148-0227/92/92JC-01177\$05.00

sampled by UV-oxidation [Harvey et al., 1983; Meyers-Schulte and Hedges, 1986; Williams and Druffel, 1987], is about 4000 years [Druffel et al., 1989].

The identity of these additional labile pools of DOM, if and whether they really exist in soluble, colloidal (0.005-0.050  $\mu\text{m}$  diameter), or fine particle (0.050-1.000  $\mu\text{m}$ ) form, remains an unresolved issue [Benner et al., 1992]. Their sources (terrestrial, coastal, and oceanic) and fates (photodegradation, remineralization, and storage as inert forms of DOC) are also open questions, which underscore our inadequate understanding of temporal-spatial variance in the biogeochemical cycles of carbon and nitrogen [Walsh, 1991].

To qualify as a dynamic storage reservoir in global carbon budgets [Tans et al., 1990], however, DOM stocks, like those of dissolved inorganic carbon (DIC), must be removed from surface regions of the ocean by sinking water, if not by falling particles, to avoid respiration back to  $\text{CO}_2$  at the sea-surface. We explore this mechanism by considering (1) the possible DOC stocks in shelf, slope, and basin regions of the North Atlantic Ocean as estimated with both platinum ( $\text{DOC}_{\text{pt}}$ ) and ultraviolet ( $\text{DOC}_{\text{uv}}$ ) techniques; (2) their potential annual sinking fluxes in relation to freshwater and photosynthetic supplies; and (3) the implied net southward transfer of subsurface DOC and DON in relation to other meridional fluxes of oxygen and nitrate across  $36^\circ 25' \text{N}$ .

## 2. Methods

In a previous study, Rintoul and Wunsch [1991] suggested that the net poleward transfer of nitrate by the Gulf Stream System across  $36^\circ 25' \text{N}$  (the location of this section is shown in Figure 1) might be balanced by a southward transport of DON. Rintoul [1988] provides zonally averaged estimates of meridional transport of water over 17 vertical levels (Table 1) at this latitude, based on an inverse model, which conserves both mass and silicate below a depth of 750 m and has a reference

level of 3000 dbar. Using their results, we construct budgets of the possible southward export of DOC and DON from the North Atlantic at four of the depth intervals, over which sinking water may exit this basin towards the equator. The net exchange over the whole water column is then obtained by summing the  $\text{DOC}_{\text{pt}}$  and  $\text{DOC}_{\text{uv}}$  transports in each of the 17 levels (Table 1).

For example, as a result of heat extraction from the Gulf Stream and influx of polar water within the East Greenland Current, a precursor of North Atlantic Deep Water (NADW) is formed in the Iceland Sea [Swift, 1984]. South of Denmark Strait, NADW sinks to depths  $>4000$  m and moves south as part of the Deep Western Boundary Current (DWBC) off North America [Broecker et al., 1991]. This source of sinking water is a likely mechanism for the export of DOC from surface waters of the Arctic Seas [Duursma, 1965], providing a sequestration time scale of thousands of years.

Similarly, mixing of Labrador Current Water (LCW) with the western boundary current to the east of the Grand Banks (note the packed isopleths of salinity in Figure 1) results in about 4 Sv of water cabelling to depths  $>2000$  m [Krauss et al., 1990], the same as previously estimated for sinking surface waters of the Labrador Sea [Sverdrup et al., 1942; Wright, 1972]. Seasonal convective overturn of additional North Atlantic Current (NAC) waters farther east in the North Atlantic basin also leads to surface mixed layer depths of  $>400$  m [Levitus, 1982] in the northeast end of the subtropical gyre, where Ekman pumping and lateral induction [Pedlosky, 1990; Huang, 1990] may further sequester DOC. Finally, some of the southward flow from the Greenland, Iceland, and Labrador Seas exits the Middle Atlantic Bight (MAB) at Cape Hatteras [Chapman and Beardsley, 1989], where the shelf water is subducted to depths  $>100$  m along the northwest wall of the Gulf Stream [Lillibridge et al., 1990].

The Arctic Ocean is analogous to the head of a large North Atlantic estuary [Walsh et al., 1989], where 74% of the freshwater discharge (Figure 1) and associated terrestrial DOC loading of the northern hemisphere occur [Walsh, 1988]. A significant part of the total sequestration of DOC released within coastal, slope, and basin ecosystems may thus take place along the northwestern edges of the Gulf Stream System in the North Atlantic. This could occur within sinking surface waters via NADW formation, LCW cabelling, basin convective mixing, and shelf water subduction, part of which may flow south across  $36^\circ 25' \text{N}$  at respective depths of perhaps 3400-4300 m, of 1600-3100 m, of 600-750 m, and of 100-350 m (Table 1).

At other depths, currents flow north, of course, such that the net exchange of water across  $36^\circ 25' \text{N}$  is negligible (Table 1). Is the net exchange of DOM also zero? In an attempt to answer this question, we estimate the possible stocks of both  $\text{DOC}_{\text{pt}}$  and  $\text{DOC}_{\text{uv}}$  at each depth interval along  $36^\circ 25' \text{N}$ .

To place the southward transfer of DOM within sinking water of different origins in the context of its surface supply, we also estimate the possible excretory release of DOM by various groups of plankton, as a function of particulate primary production of each shelf, slope, and basin region [Platt et al., 1991]. An implicit assumption of this analysis is that oxidation of the excreted DOM within sinking waters takes place at depth, such

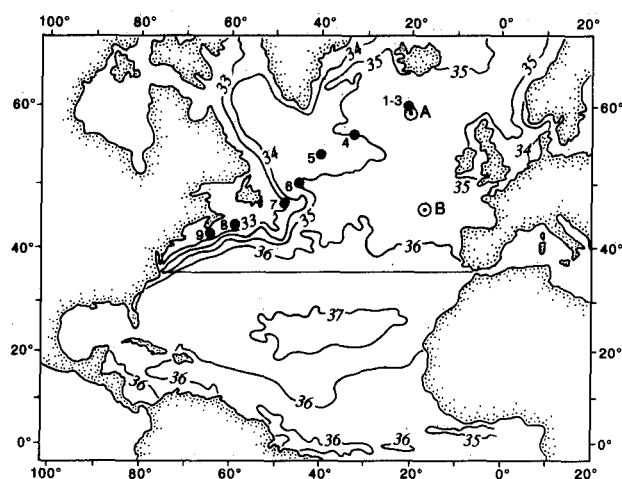


Fig. 1. The distribution of salinity in the North Atlantic at a depth of 30 m (after Worthington [1976]) in relation to (1) a trans-Atlantic hydrographic section at  $36^\circ 25' \text{N}$ , (2) observations of  $\text{DOC}_{\text{pt}}$  at  $46^\circ 30' \text{N}$  (point B) and  $59^\circ 30' \text{N}$  (point A), and (3) bio-optical estimates of Gelbstoff between Iceland and Nova Scotia (stations 1-9).

TABLE 1. The Estimated Meridional Fluxes of  $\text{DOC}_{\text{pt}}$  and  $\text{DOC}_{\text{uv}}$  Across  $36^{\circ}25'N$  in the North Atlantic

Depth Layer, m	Transport, Sv	Water Type	$\text{DOC}_{\text{pt}}(\text{DOC}_{\text{uv}})$ Stock, $\text{g m}^{-3}$	$\text{DOC}_{\text{pt}}(\text{DOC}_{\text{uv}})$ Flux, $\times 10^3 \text{ kg s}^{-1}$
0-100	15.2	GS	2.83	(0.80)
100-350	-1.5	shelf	[20.00 11.32 2.83]	[(10.80), (6.12), (1.53)]
350-600	2.2	GS	2.83	(0.80)
600-750	-4.1	NAC	1.50	(0.42)
750-900	2.4	GS	1.20	(0.34)
900-1200	3.1	AIW	0.90*	(0.25)
1200-1400	1.6	GS	1.20	(0.34)
1400-1800	-2.1	LCW/GS	2.10	(0.59)
1800-2100	-3.3	LCW	3.00	(0.85)
2100-2400	-1.4	LCW	3.00	(0.85)
2400-2800	-0.5	LCW	3.00	(0.85)
2800-3100	-0.2	LCW	3.00	(0.85)
3100-3400	1.1	ACPW	1.25	(0.35)
3400-3700	-0.1	NADW	1.65	(0.47)
3700-4000	-5.3	NADW	1.65	(0.47)
4000-4300	-6.6	NADW	1.35	(0.38)
4300-4600	-0.4	AABW	1.25	(0.35)
Total	+0.1			[-16.87 -3.85 +8.88]
				(-12.50), (-5.48), (+1.40)]

The layer transports (Sv) are from Rintoul [1988] and the  $\text{DOC}_{\text{pt,uv}}$  concentrations are from Bauer [1991] and the text. The water types are subducting shelf water within the Gulf Stream (GS), convecting North Atlantic Current (NAC) water, cabelling Labrador Current Water (LCW), and sinking North Atlantic Deep Water (NADW), Antarctic Intermediate Water (AIW), Antarctic Circumpolar Water (ACPW), and Antarctic Bottom Water (AABW). A negative sign denotes southward transport of water and  $\text{DOC}_{\text{pt,uv}}$ .

\*From Bauer [1991].

that losses of photo-oxidation and bacterial degradation in the euphotic zone are ignored.

### 3. Results

#### 3.1. Shelf Waters

We first use aircraft and ship bio-optical data to infer possible DOC stocks near Cape Hatteras (Figure 2), where perhaps 72% of the particulate organic carbon (POC) flux of the Gulf Stream is derived from the adjacent South and Middle Atlantic shelves [Walsh, 1992]. In contrast, the disparity in half-lives of the long-lived DOC and the short-lived POC pools [Legendre and Gosselin, 1989] should lead to much longer residence for DOC, such that some of the DOM off Cape Hatteras may have a multiyear origin, both from waters within the East Greenland Current [Chapman and Beardsley, 1989] and the Mississippi River plume [Atkinson and Wallace, 1975]. This situation would, of course, violate spatial assumptions of linear covariation of DOC, chlorophyll, and phaeopigments, needed for accurate satellite algorithms within coastal and perhaps oceanic waters [Gordon and Morel, 1983].

Using Coastal Zone Color Scanner (CZCS) imagery, for example, the mean primary production of North Atlantic shelf waters, between  $11^{\circ}$ - $70^{\circ}N$  (Table 2), is estimated to be  $732 \text{ g C m}^{-2} \text{ yr}^{-1}$  [Platt et al., 1991], with the assumption that the upwelling

radiance, sampled by the satellite radiometer, represent mainly chlorophyll. This is not always true, of course, particularly in Case 2 coastal waters [Morel and Prieur, 1977], where humic matter

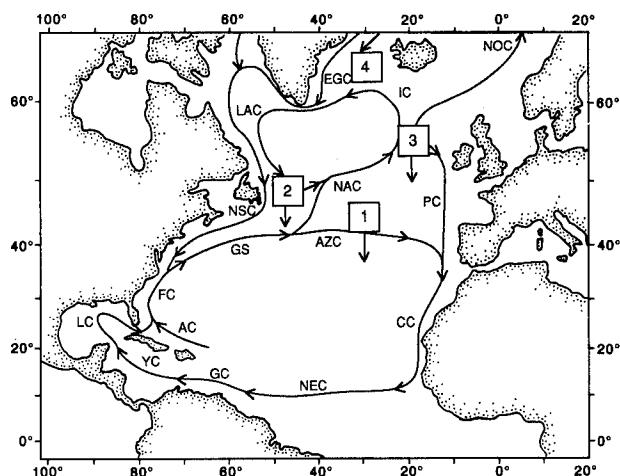


Fig. 2. A prospectus for DOM sequestration within sinking waters of the North Atlantic during subduction of shelf water (area 1), cabelling of slope water (area 2), convective overturn and lateral induction of basin water within NAC (area 3), and formation of NADW (area 4).

TABLE 2. Mean Carbon Fixation ( $\text{g C m}^{-2} \text{ yr}^{-1}$ ), Total Photosynthesis ( $\times 10^{15} \text{ g C yr}^{-1}$ ), Terrestrial Input ( $\times 10^{15} \text{ g DOC}_{\text{pt,uv}} \text{ yr}^{-1}$ ), Marine Excretion ( $\times 10^{15} \text{ g DOC yr}^{-1}$ ), and NAC Contribution to NADW ( $\times 10^{15} \text{ g DOC}_{\text{pt,uv}} \text{ yr}^{-1}$ ) With Respect to Sinking Waters Within Shelf, Slope, and Basin Areas ( $\times 10^6 \text{ km}^2$ ) of the North Atlantic Ocean

Sinking Water	Origin	Latitude	Mean C Fixation	Area	Total Production	Excretion/Advection
GS	shelf	11°-70°N	732[366]	2.5	1.83[0.92]	0.37[0.19]
	land	11°-70°N	-	-	0.35 Sv $\times$ 12(6.5) $\text{g m}^{-3}$	0.13(0.07)
LCW	slope	38°-70°N	329	3.4	1.12	0.22
	basin	38°-50°N	319	3.1	0.99	0.20
NAC	basin	51°-70°N	185	5.4	1.00	0.20
NADW	shelf	71°-80°N	150	0.7	0.11	0.02
	basin	71°-80°N	150	0.5	0.08	0.02
	NAC	71°-80°N	-	-	2.00 Sv $\times$ 3(0.85) $\text{g m}^{-3}$	0.19(0.05)

prevails [Carder et al., 1989]. The Gelbstoff, or colored dissolved organic carbon (CDOC), absorption coefficient on the Alabama-Florida shelves, for example, is as large as  $0.054 \text{ m}^{-1}$  [Carder et al., 1989], and is equivalent in absorption to a chlorophyll concentration of  $1 \text{ mg chl m}^{-3}$ .

More traditional  $^{14}\text{C}$  estimates of carbon fixation on North Atlantic shelves, between 11°-70°N, instead suggest a mean annual production of  $159 \text{ g C m}^{-2} \text{ yr}^{-1}$  [Walsh, 1988]. We will evaluate these different estimates of primary production, and associated DOC release, after estimation of the stocks and sinking fluxes of DOM of different shelf origins. If DOC is a major factor in the contamination of color signals detected by passive satellite and active aircraft remote sensors [Walsh, 1988], what are the implications for regional carbon budgets?

3.1.1. *DOC stocks.* Away from coastal regions, where terrestrial DOM signals are the strongest, the abundance of marine Gelbstoff, and therefore light absorption, generally increases with the amount of annual primary production [Carder et al., 1989]. Within the Sargasso Sea during December 1984, an unproductive time of year [Menzel and Ryther, 1960], for example, the ratio of the diffuse attenuation coefficients,  $k_d$ , for Gelbstoff or CDOD, and  $k_p$ , for the particulate matter (chlorophyll and its degradation products), at 441 nm ranged from 0.3 to 0.7, depending on the optical model [Topliss et al., 1989]. This range is consistent with a mean value of 0.6 at 440 nm for the respective absorption coefficients,  $a_d/a_p$ , in the Gulf of Mexico [Carder et al., 1989], since  $a \approx k \cdot \cos \theta$ , where  $\theta$  is the subsurface solar zenith angle.

At December shelf and slope stations in the MAB,  $k_d/k_p$  was instead a mean of 2.1 [Topliss et al., 1989], with ratios ranging as high as 3.6, the value of  $a_d/a_p$  observed after bloom senescence in coastal waters of the Gulf of Mexico [Carder et al., 1989]. High values of this ratio imply excess amounts of colored dissolved organic matter (CDOM) on the continental margins, compared to steady state conditions. This situation results from an unknown time integral of both terrestrial influxes

of CDOD and marine CDOD byproducts of previous local shelf primary production.

The winter Topliss et al. [1989] data can be converted to estimates of  $\text{DOC}_{\text{pt,uv}}$  by first estimating the amount of CDOD. Using mass-specific absorption coefficients for marine humic and fulvic acids [Carder et al., 1989], an average cosine of  $\cos \theta \approx 0.82$ , the spectral slope of  $0.013 \text{ nm}^{-1}$  for the winter Topliss et al. [1989] data, and a CDOD mixture of 16% humic and 84% fulvic acids [Carder et al., 1989], we compute the entries of Table 3 from

$$a_d(\lambda) = a_d(450) e^{[0.013 (450-\lambda)]} \quad (1)$$

where  $a_d(450) = 0.031 \text{ CDOM}$ , and  $\text{CDOM} = 2 \text{ CDOD}$ . We obtain means of 2.2 and  $0.17 \text{ g CDOD m}^{-3}$  due to marine humus within respective shelf/slope and basin waters (Table 3).

Is such a 10-fold winter gradient of CDOD between shelf and basin waters representative of all seasons, and does it reflect similar gradients of total DOC? The previous wet oxidation techniques, which yield full recovery of humic and fulvic acids (all of our computed CDOD in Table 3), suggest that CDOD constitutes 20-50% of the total  $\text{DOC}_{\text{uv}}$  [Harvey et al., 1983], with a C/N ratio of 34 [Meyers-Schulte and Hedges, 1986]. However, humic matter, measured by the platinum method, may account for only 6-14% and 11-27% of the total  $\text{DOC}_{\text{pt}}$ , since Suzuki and Tanoue [1991] indicate that  $\text{DOC}_{\text{pt}}$  may be  $3.54 \times \text{DOC}_{\text{uv}}$  in unproductive areas and  $1.85 \times \text{DOC}_{\text{uv}}$  in rich regions.

As much as 33% of the  $\text{DOC}_{\text{pt}}$  may instead be reactive polysaccharides [Benner et al., 1992]. Furthermore, the photo-chemical production of low molecular-weight organic compounds from humic substances in natural waters [Keiber et al., 1989, 1990] suggests that the ratio of humic (H) and fulvic (F) acids to total DOC decreases with time in surface waters, given no other sources or sinks. This process is perhaps discernable within Harvey et al.'s [1983] observations for depths  $\leq 20 \text{ m}$  in the Gulf of Mexico, during fertile (spring) and unproductive (fall) periods of the year.

Except for one measurement during a senescent bloom off Cape San Blas, their spring data [Harvey



TABLE 3. Mean Pigment Concentrations ( $\text{mg m}^{-3}$ ), Absorption Coefficients ( $\text{m}^{-1}$ ), and Colored Dissolved Organic Carbon ( $\text{g m}^{-3}$ ) Within MAB Shelf/Slope and Sargasso Sea Waters

	Chl a	Phaeo a	$a_p(441)$	$a_d(441)$	CDOC	$\text{DOC}_{\text{pt}}$
MAB shelf/ slope	1.84	0.59	0.072	0.153	2.20	20.00
Sargasso Sea	0.35	0.22	0.025	0.012	0.17	2.83

These values are based on both *Topliss et al.* [1989] measurements and models, and on mass-specific absorption coefficients for a mixture of 15% humic and 85% fulvic acids [*Carder et al.*, 1989], consistent with a spectral slope,  $S_\lambda$ , of  $0.013 \text{ nm}^{-1}$  for the absorption by colored dissolved organic matter (CDOM) in December 1984. Diffuse attenuation coefficients were converted to absorption coefficients by  $a = 0.82 k$ , while  $\text{CDOC}/\text{CDOM} = 0.5$ , and  $\text{DOC}_{\text{pt}}$  is computed from  $1.85 \text{ DOC}_{\text{uv}}$  in coastal waters and from  $3.54 \text{ DOC}_{\text{uv}}$  in oceanic waters.

*et al.*, 1983] can be expressed by the regression

$$\text{DOC}_{\text{uv}} = 0.30 + 0.78(\text{H}+\text{F}), \quad (2)$$

whereas the fall data fall along a line expressed by

$$\text{DOC}_{\text{uv}} = 0.90 + 0.43(\text{H}+\text{F}) \quad (3)$$

The intercept value of (3) for fall conditions, i.e., the portion of  $\text{DOC}_{\text{uv}}$  which does not covary with  $(\text{H}+\text{F})$ , is threefold that of (2) for spring waters. Such a trend may reflect photolysis of some of the light-absorbing  $(\text{H}+\text{F})$ , which would be reflected in a smaller  $\text{CDOC}/\text{DOC}$  ratio.

Accordingly, we compute the offshore stock of  $2.83 \text{ g DOC}_{\text{pt}} \text{ m}^{-3}$  (Table 3) in the Gulf Stream with a  $\text{CDOC}/\text{DOC}_{\text{pt}}$  ratio of 0.06, and the shelf stock of  $20 \text{ g DOC}_{\text{pt}} \text{ m}^{-3}$  with a ratio of 0.11. We employ these smaller ratios to emphasize both photolysis of CDOC and the other labile fractions of DOM, captured with the platinum method, since our  $\text{CDOC}/\text{DOC}_{\text{uv}}$  ratio is 0.20, when  $\text{DOC}_{\text{pt}} = 1.85 \text{ DOC}_{\text{uv}}$  in coastal waters, and 0.21, when  $\text{DOC}_{\text{pt}} = 3.54 \text{ DOC}_{\text{uv}}$  in oceanic waters [*Suzuki and Tanoue*, 1991]. Except for the shelf estimates of Table 1, all other values of  $\text{DOC}_{\text{uv}}$  at different depths assume oceanic  $\text{DOC}_{\text{pt}} = 3.54 \text{ DOC}_{\text{uv}}$ .

Our estimated  $\text{DOC}_{\text{pt}}$  stock for offshore surface waters (Table 1) approximates the previous dry combustion measurements of about  $3.6 \text{ g DOC m}^{-3}$  at the edge of the Nova Scotian shelf and  $2.4 \text{ g DOC m}^{-3}$  in the Sargasso Sea [*Gordon and Sutcliffe*, 1973]. How realistic is the nearshore estimate of  $\text{DOC}_{\text{pt}}$  stocks (Table 3), however? Riverine concentrations of as much as  $42.6 \text{ g DOC}_{\text{pt}} \text{ m}^{-3}$  ( $1.85 \times$  prior  $\text{DOC}_{\text{uv}}$  of *Wei-Bin et al.* [1983]) evidently suffer rapid dilution on the adjacent shelf of the East China Sea, with only  $5.8 \text{ g DOC}_{\text{pt}} \text{ m}^{-3}$  found at mid-shelf in the Yangtze River plume and  $3.1 \text{ g DOC}_{\text{pt}} \text{ m}^{-3}$  in the Kuroshio [*Suzuki and Tanoue*, 1991]. We thus consider a range of three  $\text{DOC}_{\text{pt,uv}}$  stocks for shelf waters in Table 1 and compute their offshore fluxes within sinking water, for comparison with the total inputs of DOC from land and from release by the marine food web (Table 2).

3.1.2. *Sinking water.* Containing a distinct diatom assemblage of nearshore species, the shelf

water at Cape Hatteras is subducted to depths  $>100 \text{ m}$  underneath the western boundary current [*Lillibridge et al.*, 1990]. Along a downstream distance of  $150 \text{ km}$ , for example, the subsurface core of low salinity water (and associated DOC stock) descended from a depth of  $\sim 75 \text{ m}$  at  $50 \text{ km}$  seaward of the Cape Hatteras shelf-break to  $\sim 125 \text{ m}$  during an October 1985 study of the Gulf Stream. Eastward transfer within the downstream North Atlantic and Azore Currents over months to years will smear such land/shelf DOC signals, of course, like that of radium 228 [*Sarmiento et al.*, 1990].

We estimate the possible sinking loss, however, by assuming a surface width of low-salinity waters of shelf origin to be perhaps  $15 \text{ km}$  along the northwest wall of the Gulf Stream at  $37^\circ\text{N}$ . Over a depth interval of at least  $100 \text{ m}$  at a speed of  $1 \text{ m s}^{-1}$ , the transport within the first  $15 \text{ km}$  of the nearshore Gulf Stream would be  $1.5 \text{ Sv}$  of water. This transport is similar to that of  $1 \text{ Sv}$  estimated for the combined water fluxes from the South and Middle Atlantic shelves at the  $100\text{-m}$  isobath off Cape Hatteras [*Walsh*, 1992].

If subduction were to occur all year, continued storage of a combination of terrestrial and shelf DOC, like radium 228 and  $\text{O}_2$  [*Sarmiento et al.*, 1982, 1990], may occur within the main pycnocline of the subtropical gyre of the North Atlantic. Here, arguments about local oxygen utilization and primary production rates off Bermuda [*Jenkins and Goldman*, 1985; *Platt and Harrison*, 1986] may be confounded by these lateral supplies of organic matter, albeit DOC rather than non-sinking POC [*Martin et al.*, 1987]. Depending upon transit time and subsurface respiration losses, the southward dispersion of the shelf DOC signals may be a seasonal, or a multiyear, process.

To employ a suitable averaging scheme across these time scales, we construct a zonal mean of the possible meridional transport, over  $17$  depth intervals, of  $\text{DOC}_{\text{pt,uv}}$  across  $36^\circ 25' \text{N}$  latitude. A southward transport in Table 1 of  $1.5 \text{ Sv}$  of water over a depth interval of approximately  $100\text{--}350 \text{ m}$  (a density interval of  $26.4$  to  $26.8 \sigma$  from *Roemmich and Wunsch* [1985]) is obtained by averaging over the  $6000\text{-km}$  length of this section (Figure 1). Such a southward transport of water and oxygen at this depth interval [*Rintoul*, 1988] is assumed by

us to also represent the fate of shelf and land DOC, subducted at the surface (Figure 2) along  $\sim 40^\circ\text{N}$  between  $20^\circ\text{--}70^\circ\text{W}$  [Huang, 1990], with possible equatorward transfers of  $4.25$  to  $30 \times 10^3 \text{ kg DOC}_{\text{pt}} \text{ s}^{-1}$  into the upper pycnocline of the subtropical gyre (Table 1).

Although the vertical structure of the  $^{14}\text{C}$  age of  $\text{DOC}_{\text{pt}}$  in the water column off Bermuda has not yet been sampled with the same resolution as Table 1, early results [Bauer, 1991] confirm our assumptions of a recent source of DOC within the upper pycnocline. At a depth of about  $500 \text{ m}$ , a subsurface minimum in the radiocarbon age of  $\text{DOC}_{\text{pt}}$  was observed (about  $-275\%$ ), indicating a relatively young origin. In contrast, a  $\Delta^{14}\text{C}$  value of  $-450\%$  was measured for a DOC stock of  $0.9 \text{ g DOC}_{\text{pt}} \text{ m}^{-3}$  (Table 1) within the oxygen minimum layer near a depth of  $850 \text{ m}$  [Bauer, 1991].

**3.1.3. Excretory supply.** If we first assume the combined land and shelf DOC stock to be  $20 \text{ g DOC}_{\text{pt}} \text{ m}^{-3}$ , the southward DOC flux along the north-west wall of the Gulf Stream might be as high as  $30 \times 10^3 \text{ kg DOC}_{\text{pt}} \text{ s}^{-1}$  (Table 1), or  $0.9 \times 10^{15} \text{ g DOC}_{\text{pt}} \text{ yr}^{-1}$  on an annual basis. This is presumably an upper bound, since it is almost twice the larger estimate of land and shelf supply of DOC to the North Atlantic shelves (Table 2). A smaller  $\text{DOC}_{\text{uv}}$  shelf stock of  $10.8 \text{ g m}^{-3}$  and the same water transport of  $1.5 \text{ Sv}$  yield instead an export of  $16.2 \times 10^3 \text{ kg DOC}_{\text{uv}} \text{ s}^{-1}$  (Table 1), or  $0.5 \times 10^{15} \text{ g DOC}_{\text{uv}} \text{ yr}^{-1}$ ; this is still larger than the estimated inputs of terrestrial and marine  $\text{DOC}_{\text{uv}}$ .

A very large total primary production of  $1.83 \times 10^{15} \text{ g C yr}^{-1}$  over a shelf area of  $2.5 \times 10^6 \text{ km}^2$  [Platt et al., 1991], for example, and a phytoplankton excretion rate of  $20\%$  of this carbon fixation yield a marine excretory input of  $0.37 \times 10^{15} \text{ g DOC yr}^{-1}$  (Table 2). A total freshwater discharge of  $1.1 \times 10^{13} \text{ m}^3 \text{ yr}^{-1}$  to the North Atlantic shelves between  $11^\circ\text{--}70^\circ\text{N}$  [Walsh, 1988] and a mean terrestrial DOC concentration of  $12 \text{ g DOC}_{\text{pt}} \text{ m}^{-3}$  ( $1.85 \times 6.5 \text{ g DOC}_{\text{uv}} \text{ m}^{-3}$  of Spitzzy et al. [1991]) suggest a possible land input of either  $0.7 \times 10^{15} \text{ g DOC}_{\text{uv}} \text{ yr}^{-1}$ , or  $1.3 \times 10^{15} \text{ g DOC}_{\text{pt}} \text{ yr}^{-1}$ . If these estimates of photosynthesis, excretion, and terrestrial supplies of DOC are all correct, the combined sources sum to  $0.44 \times 10^{15} \text{ g DOC}_{\text{uv}} \text{ yr}^{-1}$  and  $0.50 \times 10^{15} \text{ g DOC}_{\text{pt}} \text{ yr}^{-1}$  (Table 2).

Mean excretion rates of shelf phytoplankton range from  $5\%$  ( $n=21$ ) of primary production in the South Atlantic [Thomas, 1971],  $17\%$  ( $n=838$ ) in the Middle Atlantic [Thomas et al., 1979], to  $38\%$  ( $n=4$ ) in the North Atlantic [Choi, 1972] Bights, suggesting an average of  $20\%$ . Such a shelf DOC release rate is similar to respective means of  $22\text{--}23\%$  for phytoplankton excretion of DOC in slope ( $n=4$ ) and basin ( $n=5$ ) regions of the western North Atlantic [Thomas, 1971; Choi, 1972]. When these data are pooled with the results of 14 other regional studies [Sharp, 1977], a grand mean excretion rate of  $23\%$  is obtained.

Sharp [1977] suggested that the high excretion rates of phytoplankton might be experimental artifacts, but analysis of more recent data suggests a mean rate of  $13\%$ , which meets less than half of the substrate demands of coexisting bacterial populations [Baines and Pace, 1991]. Thus far, we have ignored releases of DOC by zooplankton [Jumars et al., 1989] and bacterioplankton [Brophy and Carlson, 1989], thereby underestimating the biotic supply of DOC. An excretory release rate of  $20\%$  approximates the numerous observations of phyto-

plankton excretion in the MAB [Thomas et al., 1979] and allows for some heterotrophic input of DOC as well [Baines and Pace, 1991].

We believe that the satellite estimate of a shelf primary production of  $732 \text{ g C m}^{-2} \text{ yr}^{-1}$  [Platt et al., 1991] may be too large, however, because of coastal stocks of DOC, sensed as chlorophyll biomass by the CZCS. If the remotely sampled DOC concentrations constitute half of the color signal of coastal waters [Hochman, 1992], and the specific photosynthetic rate ( $\text{yr}^{-1}$ ) remains the same, the actual primary production might be  $366 \text{ g C m}^{-2} \text{ yr}^{-1}$  (Table 2). A smaller excretory input of  $0.19 \times 10^{15} \text{ g DOC yr}^{-1}$  would follow (Table 2), supporting less of a shelf export of DOC to be subducted beneath the Gulf Stream. We thus consider the case of an intermediate seaward DOC flux, estimated by aircraft sensors, and then a third scenario of no difference between shelf and basin stocks of DOC.

Active remote sensors on aircraft [Hoge and Swift, 1981] sample at  $10^3$  faster rates than shipboard surveys [Walsh et al., 1988], such that the laser-induced measurement of a fourfold range in Gelbstoff concentrations, between coastal and offshore waters in December [Topliss et al., 1989], may be more accurate than the spatial assessment of DOC abundance from a few ship stations. Accordingly, we estimate that the shelf stock of DOM might instead be an intermediate  $11.32 \text{ g DOC}_{\text{pt}} \text{ m}^{-3}$ , fourfold the basin concentration (Table 1). In this case, the offshore fluxes of DOM would be  $17 \times 10^3 \text{ kg DOC}_{\text{pt}} \text{ s}^{-1}$  and  $9.2 \times 10^3 \text{ kg DOC}_{\text{uv}} \text{ s}^{-1}$  (Table 1). Over a year, these possible sinking fluxes of  $0.3 \times 10^{15} \text{ g DOC}_{\text{uv}} \text{ yr}^{-1}$   $-0.5 \times 10^{15} \text{ g DOC}_{\text{pt}} \text{ yr}^{-1}$  represent all of the combined terrestrial and shelf supplies of  $0.26\text{--}0.32 \times 10^{15} \text{ g DOC yr}^{-1}$  (Table 2).

Finally, the no-DOC-gradient scenario yields offshore fluxes of  $2.3 \times 10^3 \text{ kg DOC}_{\text{uv}} \text{ s}^{-1}$  and  $4.2 \times 10^3 \text{ kg DOC}_{\text{pt}} \text{ s}^{-1}$  (Table 1), or  $0.07\text{--}0.13 \times 10^{15} \text{ g DOC yr}^{-1}$ , i.e., only  $27\text{--}41\%$  of the coastal supplies of DOC at a reduced annual rate of photosynthesis of  $366 \text{ g C m}^{-2} \text{ yr}^{-1}$  (Table 2). The offshore decline of primary production, from  $732$  [366] to  $329 \text{ g C m}^{-2} \text{ yr}^{-1}$  (Table 2), may reflect less contamination by DOC of the satellite estimates of chlorophyll biomass in slope regions. Within basin regions between  $38^\circ\text{--}50^\circ\text{N}$  and  $51^\circ\text{--}70^\circ\text{N}$ , the respective rate of photosynthesis is even smaller, from  $319$  to  $185 \text{ g C m}^{-2} \text{ yr}^{-1}$  (Table 2); we thus assume that the estimates of primary production in slope and basin waters [Platt et al., 1991] are correct for the purposes of our carbon budgets.

### 3.2. Slope Waters

**3.2.1. DOC stocks.** We next consider how much surface DOC stocks might be cabelled downward as a mixture of the Labrador and North Atlantic Currents to depths of  $1400\text{--}2400 \text{ m}$  on the Newfoundland slope [Krauss et al., 1990]. Of the  $90\text{--}100 \text{ Sv}$  transport of the Gulf Stream at  $70^\circ\text{W}$  [Johns et al., 1989] and  $55^\circ\text{W}$  [Richardson, 1985], part recirculates to the west, part moves southeast as the Azores Current (Figure 2), and about  $33 \text{ Sv}$  proceeds northeastward as the NAC [Krauss et al., 1990].

With movement towards the northeast at  $0.5\text{--}1.0 \text{ m s}^{-1}$ , between the subarctic and subtropical gyres of the North Atlantic [Smith et al., 1990], this downstream western boundary current, east of the Grand Banks, should still have a Gulf Stream DOC content of  $2.83 \text{ g DOC}_{\text{pt}} \text{ m}^{-3}$  (Table 1), assuming a half-life for the labile DOC of about  $25\text{--}50$  years

[Keiber et al., 1990; Toggweiler, 1990; Bacastow and Maier-Reimer, 1991]. We then need an estimate of the DOC content of the coastal end member of this mixing pair.

The actual source regions of shelf DOC entrained at Cape Hatteras may extend from north of Greenland [Chapman and Beardsley, 1989] to at least the Mississippi River [Atkinson and Wallace, 1975] as a result of longshore coherence of flow and the long half-life of some DOC components. In contrast to the Mississippi and Hudson Rivers, where urban DOC fluxes constitute as much as 90% of the daily carbon loading of 8-10 g DOC<sub>uv</sub> m<sup>-3</sup> [Mueller et al., 1976; Segar and Berberian, 1976; Thomas et al., 1979; Leenheer, 1982], the DOC content of the relatively pristine St. Lawrence River is now less than half, about 2-4 g DOC<sub>uv</sub> m<sup>-3</sup> [Pocklington and Tan, 1983]. We might thus expect the additional DOC loading of the western North Atlantic from subarctic shelf waters (Figure 2), partially derived from pristine Arctic Rivers, to be less than at mid-latitudes.

Accordingly, we assume that the 2 Sv of shelf water, draining the Canadian Archipelago via Davis Strait [Chapman and Beardsley, 1989; Walsh et al., 1989] contains 6 g DOC<sub>pt</sub> m<sup>-3</sup> (1.85 x 3.24 g DOC<sub>uv</sub> m<sup>-3</sup> [Pocklington and Tan, 1983]). A mixture of 2 Sv of this shelf water, with 6 g DOC<sub>pt</sub> m<sup>-3</sup>, and 33 Sv of prior Gulf Stream water, with 2.83 g DOC<sub>pt</sub> m<sup>-3</sup>, yields a recirculating NAC transport (Figure 2) of 35 Sv, containing 3 g DOC<sub>pt</sub> m<sup>-3</sup> (Table 1). Part of this augmented NAC sinks in the Labrador Sea as cabelled slope water, and part sinks in the eastern Atlantic as convected basin water (Figure 2).

**3.2.2. Sinking water.** At least 4 Sv of water cabells along the Newfoundland slope to join the DWBC at depths >2400 m [Krauss et al., 1990]. This estimate is similar to prior transport calculations of sinking surface water in this region [Sverdrup et al., 1942; Wright, 1972]. Over a year, continuous sinking of this amount of water would yield an annual slope DOC sequestration of  $0.1 \times 10^{15}$  g DOC<sub>uv</sub> yr<sup>-1</sup> to  $0.4 \times 10^{15}$  g DOC<sub>pt</sub> yr<sup>-1</sup>, i.e., half, or double, the estimated excretory supply of DOC within just slope regions over 38°-70°N (Table 2).

**3.2.3. Excretory supply.** Over the northern slope area of  $3.4 \times 10^6$  km<sup>2</sup>, a total photosynthesis of  $1.12 \times 10^{15}$  g C yr<sup>-1</sup> [Platt et al., 1991] and a 20% excretion rate yield an excretory release of  $0.22 \times 10^{15}$  g C yr<sup>-1</sup> within the nearshore mixing member (Table 2). Over a similar basin area of  $3.1 \times 10^6$  km<sup>2</sup>, between 38°-50°N, more primary production of  $0.99 \times 10^{15}$  g C yr<sup>-1</sup> yields another excretory input of  $0.20 \times 10^{15}$  g C yr<sup>-1</sup> (Table 2). Their sum balances the advective loss of DOC<sub>pt</sub> within 4 Sv of sinking Labrador Current Water (LCW).

If the DOC<sub>pt</sub> measurements are artifacts, however, as a result of organic contaminants of the catalysts or poor blanks, for example, less biotic supply of DOC is required to balance sinking losses of DOC<sub>uv</sub> within LCW. The sequestration of  $0.1 \times 10^{15}$  g DOC<sub>uv</sub> yr<sup>-1</sup> within 4 Sv of LCW only requires the supply of dissolved photosynthate over a smaller area of  $\sim 1.6 \times 10^6$  km<sup>2</sup>, i.e., along the Labrador slope between 50°-60°N. On the other hand, if all of the southward transport of 6.8 Sv of LCW across 36°25'N (Table 1) represents just one year of ventilation of surface waters, and the DOC<sub>pt</sub> stocks are not artifacts, the associated equatorward flux of DOC would be  $0.6 \times 10^{15}$  g DOC<sub>pt</sub> yr<sup>-1</sup>, i.e., 150% of the sum of slope and basin supplies of DOC (Table 2).

**3.2.4. Southern Ocean supply.** In terms of a meridional flux of DOC across 36°25'N, we thus assume that 5.4 Sv of LCW, over a depth range of 1800-3100 m, represents a recent influx from the Labrador Sea. The relict DOC stocks at 1400-1800 m are instead assumed to be a mixture of LCW and Gulf Stream waters, in which the lower values of DOC represent respiration losses of multiyear inputs from Antarctic source regions; specifically within Antarctic Intermediate Water (AIW of Table 1). Note that the DOC pools of Antarctic Circumpolar Water (ACPW) and of Antarctic Bottom Water (ABW) are estimated to be 1.25 g DOC<sub>pt</sub> m<sup>-3</sup> (0.35 g DOC<sub>uv</sub> m<sup>-3</sup>), somewhat higher than those of the oxygen minimum layer of AIW [Bauer, 1991].

These additional stocks of Southern Ocean origin are assumed to have initial surface values of 1.5 g DOC<sub>pt</sub> m<sup>-3</sup> (0.42 g DOC<sub>uv</sub> m<sup>-3</sup>), half that estimated for Arctic waters, to be consistent with observations of  $k_d$  in the Greenland, Barents, and Bellingshausen Seas [Mitchell, 1992]. Based on 302 bio-optical measurements in these Seas, the diffuse attenuation coefficient due to dissolved substances,  $k_d$ , at 441 nm is 0.036 m<sup>-1</sup> in the Antarctic, compared to 0.063 m<sup>-1</sup> in the Arctic. This situation may result from greater terrestrial loading [Mitchell, 1992], and/or larger marine photosynthetic [Walsh, 1989] release, of DOC in the Arctic.

### 3.3. Basin Waters

To explore the basin (>2000 m) sinking losses of DOC, we estimate how much might be sequestered in the North Atlantic by two convective processes: (1) overturn and lateral induction of NAC waters into the subtropical gyre, south of 50°N [Huang, 1990], and (2) overflow of NADW [Swift, 1984] across the 600-m sill of Denmark Strait at 65°N.

**3.3.1. NAC transfers.** Before transformations of the NAC into the Irminger, Norwegian, and Portugal Currents (Figure 2), seasonal convection occurs en route in the northern North Atlantic, with deepening of the surface mixed layer [Levitus, 1982]. North of 50°N, for example, where the depth of the surface mixed layer in February can exceed 700 m [McClain et al., 1990], convective overturn of part of the NAC may result in lateral induction of an equatorward transport of at least 4.1 Sv, which could reach a depth interval of 600-750 m across 36°25'N (Table 1).

With a NAC stock of 3 g DOC<sub>pt</sub> m<sup>-3</sup>, this transfer would amount to a southward flux of  $12.3 \times 10^3$  kg DOC<sub>pt</sub> s<sup>-1</sup>, or  $0.4 \times 10^{15}$  g DOC<sub>pt</sub> yr<sup>-1</sup> over 12 months. If this shallow portion of the basin export of DOC from the northern North Atlantic does occur year round, it represents twice the estimated annual release of DOC within surface waters between 51°-70°N (Table 2).

A small carbon fixation of 185 g C m<sup>-2</sup> yr<sup>-1</sup> over  $5.4 \times 10^6$  km<sup>2</sup> and a 20% excretion rate yield a release of  $0.2 \times 10^{15}$  g DOC yr<sup>-1</sup> (Table 2). Such low rates of photosynthesis [Thomas, 1971] may lead to larger percentages of DOC excretion by oceanic microflagellates [Wolter, 1982], perhaps even during spring blooms of this region [Kirchman et al., 1991]. A larger excretion rate of 40%, for example, would allow a biotic influx of  $0.4 \times 10^{15}$  g DOC yr<sup>-1</sup>.

An alternative hypothesis is a seasonal decline of photosynthesis and of DOC release during light-limited periods of the year, when initiation of the southward transfer of overturned NAC occurs. The

mean depth of the surface mixed layer at 59°30'N, 20°30'W deepens, for example, from 45.1 m during May-October to 432.2 m during November-April (based on the  $\Delta T/\Delta z$  criterion of 0.5°C [Levitus, 1982]). Finally, a third scenario would be to discard the  $\text{DOC}_{\text{pt}}$  estimate of NAC stocks in favor of an annual southward NAC flux of  $0.11 \times 10^{15} \text{ g DOC}_{\text{uv}} \text{ yr}^{-1}$ .

Since Duursma [1965] suggested that there might be a seasonal influx of surface Arctic DOC stocks to deep waters via sinking NADW as well, we implement the second hypothesis in Table 1. We represent this process by a 50% reduction of the NAC stock to  $1.5 \text{ g DOC}_{\text{pt}} \text{ m}^{-3}$  (Table 1) to reflect lower winter values, yielding an annual export across 36°25'N of  $0.2 \times 10^{15} \text{ g DOC}_{\text{pt}} \text{ yr}^{-1}$ . Validation of this hypothesis of seasonal DOC release is seen in the higher summer values of  $\text{DOC}_{\text{pt}}$  within surface waters between 47°-59°N (Figure 3). A similar logic is invoked for DOC export within sinking NADW.

**3.3.2. NADW transfers.** A continuous tongue of relatively high DOC, about  $0.7 \text{ g DOC m}^{-3}$  with early techniques [Duursma, 1965], could be traced from surface to bottom waters south of Iceland, within NADW during April 1958, but not in the following September. More recent data suggest intermediate values of  $0.8\text{--}1.2 \text{ g DOC}_{\text{uv}} \text{ m}^{-3}$  at the surface of the Lincoln Sea [Gordon and Cranford, 1985], compared to prior observations of  $2\text{--}3 \text{ g DOC m}^{-3}$  in the Canadian Basin [Melnikov and Pavlov, 1978]. Assuming a 3.54 underestimate of  $\text{DOC}_{\text{uv}}$  in these unproductive regions (Table 2) yields a possible mean stock of  $3.5 \text{ g DOC}_{\text{pt}} \text{ m}^{-3}$  within Arctic precursors of NADW in the Greenland and Iceland Seas.

If we further assume that all 5 Sv of the transport of the East Greenland Current (3 Sv of polar origin, 2 Sv of Atlantic origin [Aagaard and Reed, 1987]) are converted to NADW above Denmark

Strait, we obtain the same estimate for NADW formation as Worthington's [1976] calculation: 4 Sv through Denmark Strait and 1 Sv across the Iceland-Scotland ridge. Such a mixture of the NAC and the East Greenland Current end members yields a possible DOC stock for NADW of  $3.3 \text{ g DOC}_{\text{pt}} \text{ m}^{-3}$  ( $0.9 \text{ g DOC}_{\text{uv}} \text{ m}^{-3}$ ). Over 12 months, the NADW export of DOC from the Iceland and Greenland Seas might then be either  $0.15 \times 10^{15} \text{ g DOC}_{\text{uv}} \text{ yr}^{-1}$ , or  $0.52 \times 10^{15} \text{ g DOC}_{\text{pt}} \text{ yr}^{-1}$ , i.e., ignoring seasonality in the release and sequestration of DOC.

Once more, this estimate is an upper bound, because a mean carbon fixation of  $150 \text{ g C m}^{-2} \text{ yr}^{-1}$  [Eilertsen et al., 1989], over both the  $0.7 \times 10^6 \text{ km}^2$  shelf of the Barents Sea [Walsh, 1988] and the  $0.5 \times 10^6 \text{ km}^2$  basin of the Greenland Sea [Carmack and Aagaard, 1973], only sums to  $0.19 \times 10^{15} \text{ g C yr}^{-1}$  (Table 2). An excretion rate of 20% then provides a combined shelf/basin influx of at most  $0.04 \times 10^{15} \text{ g DOC yr}^{-1}$  within local waters. The supply of 2 Sv of NAC from the south, with a stock of  $3 \text{ g DOC}_{\text{pt}} \text{ m}^{-3}$ , may contribute  $0.19 \times 10^{15} \text{ g DOC}_{\text{pt}} \text{ yr}^{-1}$  to NADW (Table 2).

There is presumably no net import of DOM from the Arctic Ocean via Fram Strait, however, since the same  $63 \text{ mg DON m}^{-3}$  is found [Kattner and Becker, 1992] under the ice in the East Greenland Current (Transpolar Drift origin) and in open waters of the West Spitsbergen Current (NAC origin), whose transport is also about 5 Sv [Walsh et al., 1989]. The biogenic and advective sources of DOC within sinking NADW may thus sum to  $0.09 \times 10^{15} \text{ g DOC}_{\text{uv}} \text{ yr}^{-1}$ , or  $0.23 \times 10^{15} \text{ g DOC}_{\text{pt}} \text{ yr}^{-1}$ , i.e., half that of the above DOC exports.

By summing a constant flux over the year, we may have again overestimated the annual sequestration of DOC within sinking waters of the northern North Atlantic. Accordingly, we assume a seasonal supply of DOC within NADW (see Figure 3 for the spatial analogue), like that of NAC, with a winter estimate of  $1.65 \text{ g DOC}_{\text{pt}} \text{ m}^{-3}$  (Table 1), when NADW is presumably formed. As in the case of LCW, we also assume that only 5.4 Sv of NADW transfer, over depths of 3400-4000 m along 36°25'N, represent the annual carbon loading of  $0.28 \times 10^{15} \text{ g DOC}_{\text{pt}} \text{ yr}^{-1}$  (Table 1).

**3.3.3. Southern Ocean transfers.** The additional 6.6 Sv of entrained NADW, over depths of 4000-4300 m, instead represent a multiyear accumulation of both Antarctic and Arctic sources, with an intermediate stock of  $1.35 \text{ g DOC}_{\text{pt}} \text{ m}^{-3}$  (Table 1). Before we turn to the implications of these meridional fluxes over the whole water column at 36°25'N, we first address how realistic our estimates of the DOC stocks might be. An analysis is made of recent data taken during the 1989 and 1991 spring blooms of the North Atlantic.

#### 4. Corroboration

##### 4.1. Vertical Structure

During May 18-19 and June 5-6, 1989, Y. Suzuki measured  $\text{DOC}_{\text{pt}}$  concentrations at several stations [Slagle and Heimerdinger, 1991] near 59°30'N, 20°25'W and 46°30'N, 17°45'W (locations A and B of Figure 1). To provide sufficient depth resolution, we plotted his data from two adjacent stations at each location in Figure 3, which show possible signatures of cabelled slope water and overturned basin water.

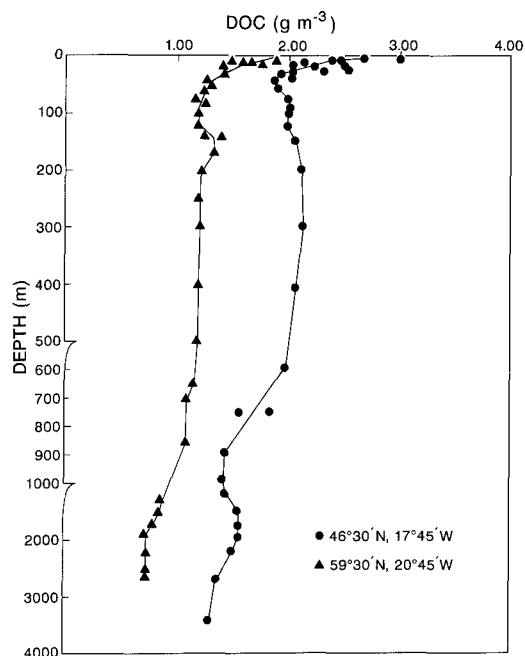


Fig. 3. The vertical structure of  $\text{DOC}_{\text{pt}}$ , as measured by Y. Suzuki, during May-June 1989 in temperate and subarctic regions of the eastern North Atlantic (see Figure 1 for the locations of these regions).

The measured DOC stocks within the upper 25 m of the water column in region A (59°30'N) yield a mean ( $n=11$ ) of  $1.9 \text{ g DOC}_{\text{pt}} \text{ m}^{-3}$ , compared to a mean ( $n=10$ ) of  $2.4 \text{ g DOC}_{\text{pt}} \text{ m}^{-3}$  in region B (46°30'N), where a maximum of  $3.0 \text{ g DOC}_{\text{pt}} \text{ m}^{-3}$  was found. These values at the lower latitude are equivalent to our estimates of  $2.8\text{--}3.0 \text{ g DOC}_{\text{pt}} \text{ m}^{-3}$  for Gulf Stream waters and LCW along 36°25'N (Table 1). Note that the subsurface values of  $\text{DOC}_{\text{pt}}$  at the higher latitude are almost half those of surface waters, reflecting increased excretion during the spring bloom [Kirchman et al., 1991].

Preservation of the vertical structure of DOC partially depends upon latitude, i.e., the extent to which local vertical mixing smears the DOC tracers introduced at the surface. Region A at 59°30'N has a sufficiently deep winter mixed layer [Levitus, 1982] to allow uniform stocks of  $1.2 \text{ g DOC}_{\text{pt}} \text{ m}^{-3}$  over depths of 200 to 500 m (Figure 3). Fall overturn of this part of the summer water column at 59°30'N would indeed lead to a depth-averaged stock of  $1.26 \text{ g DOC}_{\text{pt}} \text{ m}^{-3}$  and a mean density of  $27.37 \sigma$ .

If the overturned basin waters at 59°30'N were to flow south along the  $27.3\text{--}27.5 \sigma$  isopycnals after Ekman pumping [Huang, 1990], these DOC stocks would then occur at deeper depths of 700–900 m near both 46°30'N and 36°25'N, where we assumed a stock of  $1.5 \text{ g DOC}_{\text{pt}} \text{ m}^{-3}$  for NAC (Table 1). The vertical structure of DOC at 46°30'N appears to provide similar validation of our hypothesis of LCW sequestration of excretory products.

The experimental precision of the  $\text{DOC}_{\text{pt}}$  measurements is  $\pm 1\text{--}5\%$ , depending upon sea state [Slagle and Heimerdinger, 1991], such that the 10% subsurface increment of DOC at depths of 1500–2000 m in region B, but not in region A (Figure 3), may reflect cabelling LCW. Since LCW and NADW both travel south mainly in the DWBC of the western Atlantic Ocean, as indicated by tritium dispersal and radiocarbon ages [Broecker et al., 1991], we would expect their signals to be weakest in the northeastern Atlantic along 20°W. Indeed at greater depths of 2700 m in regions A and B, the respective stocks of  $0.8$  and  $1.4 \text{ g DOC}_{\text{pt}} \text{ m}^{-3}$  are equivalent to our assumed  $\text{DOC}_{\text{pt}}$  content of ACPW and AABW (Table 1).

#### 4.2. Horizontal Structure

A transect of nine stations, from site A, south of Iceland, to Nova Scotia during May–June 1991 (Figure 1), provides an assessment of the various values of shelf DOC, assumed to be subducted under the Gulf Stream at depths of 100–350 m (Table 1). The surface values of CDOM absorption at 440 nm show a linear trend with salinity, inshore of the Labrador Current (Figure 4). They are threefold higher in summer waters of the Nova Scotian shelf (Table 4), compared to either site A, or the hibernian Sargasso Sea (Table 3). The shelf observations of  $0.052\text{--}0.078 \text{ m}^{-1}$  are similar to that of  $0.063 \text{ m}^{-1}$  in the Arctic [Mitchell, 1992], but half the absorption values observed [Topliss et al., 1989] in MAB shelf waters (Table 3).

The spectral absorption coefficients of these CDOM data were converted [Carder et al., 1989] to estimates of humic and fulvic acids (Table 4). Equation (2) for a spring bloom situation of less photolysis was then used to convert (H+F) to  $\text{DOC}_{\text{uv}}$ ,

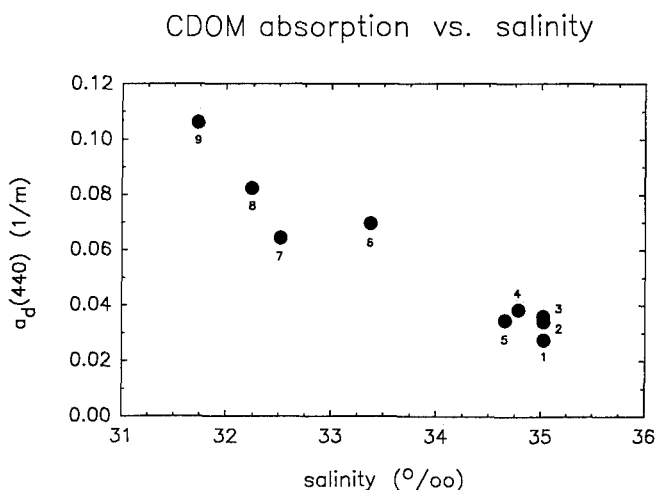


Fig. 4. The relation of Gelbstoff absorption at 440 nm to surface salinity between Iceland and Nova Scotia (see Figure 1 for locations of stations 1–9).

TABLE 4. Absorption Coefficients ( $a_d$  440) due to DOM Within the Upper Meter at Stations of the 1991 Transect From Iceland to Nova Scotia

Station	$a_d$ 440, $\text{m}^{-1}$	$S_\lambda$ , $\text{nm}^{-1}$	H+F, $\text{g m}^{-3}$	$\text{DOC}_{\text{uv}}$ , $\text{g m}^{-3}$	$\text{DOC}_{\text{pt}}$ , $\text{g m}^{-3}$
1	0.0256	-0.0150	1.24	1.26	2.27
2	0.0344	-0.0133	1.12	1.17	2.11
3	0.0333	-0.0146	1.47	1.44	2.59
4	0.0325	-0.0150	2.05	1.89	3.40
5	0.0327	-0.0156	2.23	2.03	3.65
6	0.0603	-0.0141	2.90	2.55	4.59
7	0.0519	-0.0159	4.05	3.44	6.19
8	0.0619	-0.0160	4.84	4.05	7.29
9	0.0775	-0.0165	4.90	4.10	7.37

The samples were filtered with preflushed  $0.2 \mu\text{m}$  pore diameter, Nucleopore pads, and measured in 10 cm cells of a Cary 2200 spectrophotometer. The spectral slope of the semi-log regression between 310 and 490 nm is denoted as  $S_\lambda$ , while the humic (H) and fulvic (F) acid concentrations are estimated from  $a_d$  450,  $S_\lambda$ , and the equations provided by Carder et al. [1989]. Our estimates of  $\text{DOC}_{\text{uv,pt}}$  are then derived from the H+F values, as discussed in the text.

yielding values of 1.16 to 1.51 g DOC<sub>uv</sub> m<sup>-3</sup> for stations 1-3 at site A (Table 4). With our eutrophic DOC<sub>pt</sub>/DOC<sub>uv</sub> ratio of 1.85, the estimated surface DOC stocks at site A in 1991 become 2.15-2.79 g DOC<sub>pt</sub> m<sup>-3</sup> (Table 4), compared to observations of 1.50-1.97 g DOC<sub>pt</sub> m<sup>-3</sup> during 1989 (Figure 3).

While these offshore observations are from different years, they are from the same site in the same season, providing a check on our hypotheses of various gradients of DOC between shelf and basin regions of the North Atlantic. Our bio-optical measurements indicate a rapid increase of DOM on the Grand Banks, with perhaps 3.5-fold greater values of DOC<sub>pt</sub> on the outer Nova Scotian shelf than at site A (Table 4). Recall that the aircraft estimates of Gelbstoff fluorescence also suggested a fourfold winter gradient of DOC between coastal and oceanic waters of the MAB [Topliss et al., 1989]. Furthermore, previous shipboard observations of DOM fluorescence indicate a threefold to sixfold gradient of stocks between basin waters at 60°N, 20°W and either the East Greenland Current, or shelf waters just west of Scotland [Duursma, 1965].

### 5. Conclusions

What then are the consequences of our many assumptions? We begin with the implications of the depth-integrated DOC<sub>pt</sub> transports. The net DOC<sub>pt</sub> transfer of the whole water column sums to a southward export across 36°25'N of  $16.87 \times 10^3$  kg DOC<sub>pt</sub> s<sup>-1</sup>, or  $1.4 \times 10^3$  kmol DOC<sub>pt</sub> s<sup>-1</sup>, in the case of the largest value of shelf DOC<sub>pt</sub> stocks (Table 1). The same flow fields and the observed oxygen concentrations along 36°25'N yield a net southward flux of  $2.9 \times 10^3$  kmol O<sub>2</sub> s<sup>-1</sup> [Rintoul, 1988].

If we assume a molar O<sub>2</sub>/C consumption ratio of 1.3 for bacterial degradation of subsurface carbon substrates [Redfield et al., 1963], the ratio of 2.1 for the above O<sub>2</sub>/DOC<sub>pt</sub> net fluxes suggests that 63% of the AOU demands across 36°25'N would be met by sinking DOC, and 37% by falling POC, if all of the O<sub>2</sub> were consumed. Furthermore, a DOC/DON ratio of 10 from dry combustion [Gordon and Sutcliffe, 1973], which is an intermediate value between that of 5 [Sugimura and Suzuki, 1988] and 15 [Benner et al., 1992] from platinum catalysts, suggests a net equatorward flux of  $1.7 \times 10^3$  kg DON s<sup>-1</sup>. This fortuitously balances the postulated poleward export of  $1.7 \times 10^3$  kg NO<sub>3</sub> s<sup>-1</sup> across 36°25'N [Rintoul, 1988] of unutilized nitrate within the Gulf Stream.

The smaller, fourfold gradient of DOC<sub>pt</sub> between nearshore and offshore regions suggests instead a net southward flux of only  $3.85 \times 10^3$  kg DOC<sub>pt</sub> s<sup>-1</sup> (Table 1), or  $0.32 \times 10^3$  kmol DOC<sub>pt</sub> s<sup>-1</sup> and an O<sub>2</sub>/DOC<sub>pt</sub> ratio of 9.1. With this second scenario and the Redfield ratio, 86% of the oxidizable carbon substrate may be in particulate form, with just 14% as DOC. Using the same DOC/DON ratio,  $0.4 \times 10^3$  kg DON s<sup>-1</sup> may cross 36°25'N towards the equator, offsetting only 24% of the poleward flux of NO<sub>3</sub> in this case.

If we choose a larger C/N ratio, say, 15 [Benner et al., 1992] or 25 [Jackson and Williams, 1985], then just 9-15% of the northward flux of Gulf Stream nitrate would be returned as DON in the second scenario. Larger values of shelf DOM, or greater oceanic rates of photosynthesis and excretion,

would then be required to support Rintoul and Wunsch's [1991] hypothesis. In contrast, a zero seaward gradient of DOC<sub>pt</sub> leads to a net poleward transfer of  $8.88 \times 10^3$  kg DOC<sub>pt</sub> s<sup>-1</sup> in the third case (Table 1), such that no DON would move equatorward.

Even if the DOC<sub>pt</sub> estimates are artifacts, the net DOC<sub>uv</sub> fluxes show a similar pattern (Table 1). Because of the different DOC<sub>pt</sub>/DOC<sub>uv</sub> ratios used for shelf and oceanic waters (1.85 versus 3.54), the second DOC<sub>uv</sub> scenario reflects an eightfold gradient of DOC<sub>uv</sub>, while the third case poses a twofold gradient. In this third scenario, no DOC<sub>uv</sub>, nor DON, are exported south from the northern North Atlantic (Table 1).

In contrast, the second case yields a net southward export of  $5.48 \times 10^3$  kg DOC<sub>uv</sub> s<sup>-1</sup> (Table 1), with an O<sub>2</sub>/DOC<sub>uv</sub> ratio of 6.3. This calculation suggests that 79% of the AOU demands might be met by POC, and 21% by DOC<sub>uv</sub>, similar to Ogura's [1970] conclusions. Only 32% of the proposed northward influx of NO<sub>3</sub> would then be returned south as DON, leaving open the possibility of an equatorward flux of ammonium, if nitrification is slow and N<sub>2</sub> is not lost to the atmosphere north of 36°25'N.

Further quantification of our present estimates are confounded, however, by seasonal and inter-annual variations of the sinking processes, by uncertainties in the amount of primary production and excretion of DOC, and by accurate assessment of spatio-temporal changes of DOM stocks. Reduced subduction beneath the Gulf Stream, increased coastal photosynthesis, reduced CDOC/DOC ratios, and increased release of DOC within coastal habitats from the marine food web and/or anthropogenic loadings would all favor (1) larger stocks of shelf DOC, and (2) a larger role of DOC in oxygen consumption within the deep sea. The opposite trends of these processes would lead to smaller stocks and roles of shelf DOC in global carbon cycles.

We do conclude that some shelf export of DOC, with a positive gradient between coastal and oceanic stocks, as well as falling particles, are required to balance carbon, nitrogen, and oxygen budgets of the North Atlantic, based on one snapshot of hydrographic properties [Roemmich and Wunsch, 1985]. Seasonal subduction, cabelling, and convection of surface waters may initiate annual storage, in sinking waters of the North Atlantic, of perhaps  $0.9-1.2 \times 10^{15}$  g DOC yr<sup>-1</sup> (Table 1). Depending upon the different estimates of primary production and DOC stocks of coastal waters, the amount of DOM supplied by rivers and the shelf food web may constitute 29-43% of the proposed basin-wide sequestration of carbon and nitrogen.

The next generation of biophysical models involving satellite color imagery must improve upon more primitive ones [Walsh et al., 1987; Wroblewski et al., 1988; Wroblewski, 1989; Ishizaka, 1990; Platt et al., 1991; Gregg and Walsh, 1992] by (1) first distinguishing between the dissolved and particulate components of the radiance signal, and (2) by providing resolution of the fates of the terrestrial and marine sources of CDOC. Future bio-optical research must now also focus on coastal waters of high and middle latitudes, as well as open ocean regimes, to provide eventual validation data, from follow-on satellite and aircraft color sensors, for our crude mathematical hypotheses of carbon and nitrogen cycling in the North Atlantic.

**Acknowledgments.** This research was funded by the National Aeronautics and Space Administration, the Department of Energy, and the Office of Naval Research under grants NAGW-678, NAGW-465, DE-FG05-85ER60285, N00014-87-J-1218, and N00014-89-J-1091.

### References

- Aagaard, K., and R. Reed, Fram Strait: Exchange and dynamics, *Eos Trans. AGU*, 68, 124-125, 1987.
- Aldredge, A. L., and C. C. Gotschalk, Direct observations of the mass flocculation of diatom blooms: Characteristics, settling velocities, and formation of diatom aggregates, *Deep Sea Res.*, 36, 159-171, 1989.
- Armstrong, F. A., P. M. Williams, and J. D. Strickland, Photo-oxidation of organic matter in seawater by ultra-violet radiation: Analytical and other applications, *Nature*, 211, 481-483, 1966.
- Atkinson, L. P., and D. Wallace, The source of unusually low surface salinities in the Gulf Stream off Georgia, *Deep Sea Res.*, 22, 913-916, 1975.
- Bacastow, R., and E. Maier-Reimer, Dissolved organic carbon in modeling oceanic new production, *Global Biogeochem. Cycles*, 5, 71-86, 1991.
- Baines, S. B., and M. L. Pace, The production of dissolved organic matter by phytoplankton and its importance to bacteria: Patterns across marine and freshwater systems, *Limnol. Oceanogr.*, 36, 1078-1090, 1991.
- Bauer, J., Dissolved organic carbon in the ocean: Current perspectives from past and recent findings, paper presented at The Oceanographic Society meeting, St. Petersburg, Fla., March 24-28, 1991.
- Benner, R., J. D. Pakulski, M. McCarthy, J. I. Hedges, and P. G. Hatcher, Bulk chemical characteristics of dissolved organic matter in the ocean, *Nature*, 255, 1561-1564, 1992.
- Bradshaw, A. L., and P. G. Brewer, High precision measurements of alkalinity and total carbon dioxide in seawater by potentiometric titration, 1, Presence of unknown protolyte(s)?, *Mar. Chem.*, 23, 69-86, 1988.
- Broecker, W. S., S. Blanton, W. M. Smethie, and G. Ostlund, Radiocarbon decay and oxygen utilization in the deep Atlantic Ocean, *Global Biogeochem. Cycles*, 5, 87-117, 1991.
- Brophy, J. E., and D. J. Carlson, Production of biologically refractory dissolved organic carbon by natural seawater microbial populations, *Deep Sea Res.*, 36, 497-507, 1989.
- Carder, K. L., R. G. Steward, G. R. Harvey, and P. B. Ortner, Marine humic and fulvic acids: Their effects on remote sensing of ocean chlorophyll, *Limnol. Oceanogr.*, 34, 68-81, 1989.
- Carmack, E., and K. Aagaard, On the deep water of the Greenland Sea, *Deep Sea Res.*, 20, 687-716, 1973.
- Chapman, D. C., and R. C. Beardsley, On the origin of shelf water in the Middle Atlantic Bight, *J. Phys. Oceanogr.*, 19, 384-391, 1989.
- Choi, C. I., Primary production and release of dissolved organic carbon from phytoplankton in the western North Atlantic Ocean, *Deep Sea Res.*, 19, 731-736, 1972.
- Druffel, E. R., P. M. Williams, and Y. Suzuki, Concentrations and radiocarbon signatures of dissolved organic matter in the Pacific Ocean, *Geophys. Res. Lett.*, 16, 991-994, 1989.
- Duursma, E. K., The dissolved organic constituents of sea water, in *Chemical Oceanography*, Vol. 1, edited by J. P. Riley and G. Skirrow, pp. 433-477, Academic, San Diego, Calif., 1965.
- Eilertsen, H. C., J. P. Taasen, and J. M. Weslawski, Phytoplankton studies in the fjords of West Spitzbergen: Physical environment and production in spring and summer, *J. Plankton Res.*, 11, 1245-1260, 1989.
- Gordon, D. C., and P. J. Cranford, Detailed distribution of dissolved and particulate organic matter in the Arctic Ocean and comparison with other oceanic regions, *Deep Sea Res.*, 32, 1221-1232, 1985.
- Gordon, D. C., and W. H. Sutcliffe, A new dry combustion method for the simultaneous determination of total organic carbon and nitrogen in seawater, *Mar. Chem.*, 1, 231-244, 1973.
- Gordon, H. R., and A. Y. Morel, *Remote Assessment of Ocean Color for Interpretation of Satellite Visible Imagery*, pp. 1-114, Springer-Verlag, Berlin, 1983.
- Gregg, W. W., and J. J. Walsh, Simulation of the 1979 spring bloom in the Mid-Atlantic Bight: A coupled physical/biological/optical model, *J. Geophys. Res.*, 97, 5723-5743, 1992.
- Harvey, G. R., D. A. Boran, L. A. Chesal, and J. N. Takar, The structure of marine fulvic acid and humic acids, *Mar. Chem.*, 12, 119-133, 1983.
- Hochman, H. T., Interpretation of the Coastal Zone Color Scanner (CZCS) signature of the Orinoco River, M.S. thesis, pp. 1-82, Univ. of South Florida, Tampa, 1992.
- Hoge, F. E., and R. N. Swift, Airborne spectroscopic detection of laser-induced water raman backscatter and fluorescence from chlorophyll a and other naturally occurring pigments, *Appl. Opt.*, 20, 3197-3205, 1981.
- Huang, R. X., On the three-dimensional structure of the wind-driven circulation in the North Atlantic, *Dyn. Atmos. Oceans*, 15, 117-159, 1990.
- Ishizaka, J., Coupling of Coastal Zone Color Scanner data to a physical-biological model of the southeastern U.S. continental shelf ecosystem, 3, Nutrient and phytoplankton fluxes and CZCS data assimilation, *J. Geophys. Res.*, 95, 20,201-20,212, 1990.
- Jackson, G. A., Implications of high dissolved organic matter concentrations for oceanic properties and processes, *Oceanography*, 1, 28-33, 1988.
- Jackson, G. A., and P. M. Williams, Importance of dissolved organic nitrogen and phosphorus to biological nutrient cycling, *Deep Sea Res.*, 32, 223-235, 1985.
- Jenkins, W. J., and J. C. Goldman, Seasonal oxygen cycling and primary production in the Sargasso Sea, *J. Mar. Res.*, 43, 465-491, 1985.
- Johns, E., D. R. Watts, and H. T. Rossby, A test of geostrophy in the Gulf Stream, *J. Geophys. Res.*, 94, 3211-3222, 1989.
- Jumars, P. A., D. L. Penry, J. A. Baross, M. J. Perry, and B. W. Frost, Closing the microbial loop: Dissolved carbon pathway to heterotrophic bacteria form incomplete ingestion, digestion, and absorption in animals, *Deep Sea Res.*, 36, 483-496, 1989.
- Kattner, G., and H. Becker, Nutrients and organic nitrogenous compounds in the marginal ice zone



- of the Fram Strait, *J. Mar. Syst.*, in press, 1992.
- Keiber, R. J., J. A. McDaniel, and K. Mopper, Photochemical source of biological substrates in seawater: Implications for geochemical carbon cycling, *Nature*, 341, 637-639, 1989.
- Keiber, R. J., X. Zhou, and K. Mopper, Formation of carbonyl compounds from UV-induced photodegradation of humic substances in natural waters: Fate of riverine carbon in the sea, *Limnol. Oceanogr.*, 35, 1503-1515, 1990.
- Kirchman, D. L., Y. Suzuki, C. Garside, and H. W. Ducklow, High turnover rates of dissolved organic carbon during a spring phytoplankton bloom, *Nature*, 352, 612-614, 1991.
- Krauss, W., R. H. Kase, and H. H. Hinrichsen, The branching of the Gulf Stream southeast of the Grand Banks, *J. Geophys. Res.*, 95, 13,089-13,103, 1990.
- Leenheer, J., United States Geological Survey data information service, in *Transport of Carbon and Minerals in Major World Rivers, Part 1*, edited by E. T. Degens, pp. 355-366, Mitt. Geol. - Palaont. Inst., Univ. Hamburg, Germany, 1982.
- Legendre, L., and M. Gosselin, New production and export of organic matter to the deep ocean: Consequences of some recent discoveries, *Limnol. Oceanogr.*, 34, 1374-1380, 1989.
- Levitus, S., Climatological atlas of the world ocean, *NOAA Prof. Pap.*, 13, 1-173, 1982.
- Lillibridge, J. L., G. Hitchcock, T. Rossby, E. Lessard, M. Mork, and L. Golmen, Entrainment and mixing of shelf/slope waters in the near-surface Gulf Stream, *J. Geophys. Res.*, 95, 13,065-13,087, 1990.
- Martin, J. H., G. A. Knauer, D. M. Karl, and W. W. Broenkow, VERTEX: Carbon cycling in the northeast Pacific, *Deep Sea Res.*, 34, 267-285, 1987.
- McClain, C. R., W. E. Esaias, G. C. Feldman, J. Elrod, D. Endres, J. Firestone, M. Darzi, R. Evans, and J. Brown, Physical and biological processes in the North Atlantic during the first GARP global experiment, *J. Geophys. Res.*, 95, 18,027-18,048, 1990.
- Melnikov, I. A., and G. L. Pavlov, Characteristics of organic carbon distribution in water and ice of the Arctic Basin, *Oceanology*, 18, 163-167, 1978.
- Menzel, D. H., and J. H. Ryther, The annual cycle of primary production in the Sargasso Sea off Bermuda, *Deep Sea Res.*, 6, 351-367, 1960.
- Menzel, D. W., and R. F. Vaccaro, The measurement of dissolved organic and particulate carbon in seawater, *Limnol. Oceanogr.*, 9, 138-142, 1964.
- Meyers-Schulte, K. J., and J. I. Hedges, Molecular evidence for a terrestrial component of organic matter dissolved in seawater, *Nature*, 321, 61-63, 1986.
- Mitchell, B. G., Predictive bio-optical relationships for polar oceans and marginal ice zones, *J. Mar. Syst.*, in press, 1992.
- Morel, A., and L. Priour, Analysis of variations in ocean color, *Limnol. Oceanogr.*, 22, 708-722, 1977.
- Mueller, J. A., A. A. Anderson, and J. S. Jeris, Contaminants entering the New York Bight: Sources, mass loads, significances, *ASLO Symp.*, 2, 162-170, 1976.
- Najjar, R. G., J. L. Sarmiento, and J. R. Toggweiler, Downward transport and fate of organic matter in the ocean: Simulations with a general circulation model, *Global Biogeochem. Cycles*, 6, 45-76, 1992.
- Ogura, N., The relation between dissolved organic carbon and apparent oxygen utilization in the western North Pacific, *Deep Sea Res.*, 17, 221-231, 1970.
- Pedlosky, J., The dynamics of the oceanic subtropical gyres, *Science*, 248, 316-322, 1990.
- Platt, T., and W. G. Harrison, Reconciliation of carbon and oxygen fluxes in the upper ocean, *Deep Sea Res.*, 33, 273-276, 1986.
- Platt, T., C. Caverhill, and S. Sathyendranath, Basin-scale estimates of oceanic primary production by remote sensing: The North Atlantic, *J. Geophys. Res.*, 96, 15,147-15,159, 1991.
- Plunkett, M. A., and N. W. Rakestraw, Dissolved organic matter in the sea, *Deep Sea Res.*, 3, Suppl., 12-14, 1955.
- Pocklington, R., and F. Tan, Organic carbon transport in the St. Lawrence River, in *Transport of Carbon and Minerals in Major World Rivers, Part 2*, edited by E. T. Degens, S. Kempe, and H. Soliman, pp. 243-252, Mitt. Geol. - Palaont. Inst., Univ. Hamburg, Germany, 1983.
- Putter, A., *Die ernahrung der wassertiere und der stoffhaushalt der gewasser*, pp. 1-168, Gustav Fischer, Jena, 1909.
- Redfield, A. C., B. H. Ketchum, and F. A. Richards, The influence of organisms on the composition of seawater, in *The Sea*, Vol. 2, edited by M. N. Hill, pp. 26-77, Wiley, New York, 1963.
- Richardson, P. L., Average transport and velocity of the Gulf Stream near 55 W, *J. Mar. Res.*, 43, 83-111, 1985.
- Rintoul, S., Mass, heat, and nutrient fluxes in the Atlantic Ocean determined by inverse methods, Ph.D. thesis, pp. 1-287, Mass. Inst. of Technol./Woods Hole Oceanogr. Inst., Woods Hole, Mass, 1988.
- Rintoul, S. R., and C. Wunsch, Mass, heat, oxygen and nutrient fluxes and budgets in the North Atlantic Ocean, *Deep Sea Res.*, 38, S355-S378, 1991.
- Roemmich, D., and C. Wunsch, Two trans-Atlantic sections: Meridional circulation and heat flux in the subtropical North Atlantic Ocean, *Deep Sea Res.*, 32, 619-664, 1985.
- Sarmiento, J. L., C. G. Rooth, and W. Roether, The North Atlantic tritium distribution in 1972, *J. Geophys. Res.*, 87, 8047-8056, 1982.
- Sarmiento, J. L., G. Thiele, R. M. Key, and W. S. Moore, Oxygen and nitrate new production and remineralization in the North Atlantic subtropical gyre, *J. Geophys. Res.*, 95, 18,303-18,315, 1990.
- Segar, D. A., and G. A. Berberian, Oxygen depletion in the New York Bight apex: Causes and consequences, *ASLO Symp.*, 2, 220-239, 1976.
- Sharp, J. H., Excretion of organic matter by marine phytoplankton: Do healthy cells do it?, *Limnol. Oceanogr.*, 22, 381-399, 1977.
- Skopintsev, B. A., S. N. Timofeyeva, and O. H. Vershinina, Organic carbon in the near-equatorial and southern Atlantic and in the Mediterranean, *Oceanology*, 6, 201-210, 1966.
- Slagle, R., and G. Heimerdinger, *North Atlantic Bloom Experiment process study data report P-1 April-July 1989*, pp. 1-315, NODC/U.S. JGOFS Data Management Office, Woods Hole, Mass., 1991.
- Smith, L. T., D. B. Boudra, and R. Bleck, A wind-driven isopycnic coordinate model of the North and Equatorial Atlantic Ocean, 2, *The Atlantic*



- basin experiments, *J. Geophys. Res.*, 95, 13,105-13,128, 1990.
- Spitzzy, A., V. Ittekkot, and J. Leenheer, Dissolved and particulate organic matter in rivers, in *Ocean Margin Processes in Global Change*, edited by R. F. Mantoura, J. M. Martin, and R. Wollast, pp. 6-17, John Wiley, New York, 1991.
- Sugimura, Y., and Y. Suzuki, A high temperature catalytic oxidation method for nonvolatile dissolved organic carbon in seawater by direct injection of liquid samples, *Mar. Chem.*, 42, 105-131, 1988.
- Suzuki, Y., and E. Tanoue, Dissolved organic carbon enigma - implication for ocean margins, in *Ocean Margin Processes in Global Change*, edited by R. F. Mantoura, J. M. Martin, and R. Wollast, pp. 197-210, John Wiley, New York, 1991.
- Suzuki, Y., T. Sugimura, and T. Itoh, A catalytic oxidation method for the determination of total nitrogen dissolved in seawater, *Mar. Chem.*, 16, 83-97, 1985.
- Suzuki, Y., E. Tanoue, and H. Ito, A high-temperature catalytic oxidation method for the determination of dissolved organic carbon in seawater: Analysis and improvement, *Deep Sea Res.*, 39, 185-198, 1992.
- Sverdrup, H. U., M. W. Johnson, and R. H. Fleming, *The Oceans*, pp. 1-439, Prentice-Hall, Englewood Cliffs, N. J., 1942.
- Swift, J. H., The circulation of the Denmark Strait and Iceland-Scotland overflow waters in the North Atlantic, *Deep Sea Res.*, 31, 1339-1356, 1984.
- Tans, P. P., I. Y. Fung, and T. Takahashi, Observational constraints on the global atmospheric CO<sub>2</sub> budget, *Science*, 247, 1431-1438, 1990.
- Thomas, J. P., Release of dissolved organic matter from natural populations of marine phytoplankton, *Mar. Biol.*, 11, 311-323, 1971.
- Thomas, J. P., et al., Biological processes: Productivity and respiration, in *Oxygen Depletion and Associated Benthic Mortalities in the New York Bight, 1976*, NOAA Prof. Pap. 11, edited by C. J. Sindermann and R. L. Swanson, pp. 231-262, 1979.
- Toggweiler, J. R., Is the downward dissolved organic matter (DOM) flux important in carbon transport?, in *Productivity of the Oceans: Present and Past*, edited by W. H. Berger, V. S. Smetacek, and G. Wefer, pp. 65-83, John Wiley, New York, 1989.
- Toggweiler, J. R., Bombs and ocean carbon cycles, *Nature*, 347, 122-123, 1990.
- Topliss, B. J., J. R. Miller, and B. Irwin, Ocean optical measurements, I, Statistical analysis of data from the western North Atlantic, *Cont. Shelf Res.*, 9, 113-131, 1989.
- Walsh, J. J., *On the Nature of Continental Shelves*, 520 pp., Academic Press, San Diego, Calif., 1988.
- Walsh, J. J., Arctic carbon sinks: Present and future, *Global Biogeochem. Cycles*, 3, 393-411, 1989.
- Walsh, J. J., Importance of continental margins in the marine biogeochemical cycling of carbon and nitrogen, *Nature*, 350, 53-55, 1991.
- Walsh, J. J., Particle export at Cape Hatteras, *Cont. Shelf Res.*, in press, 1992.
- Walsh, J. J., D. A. Dieterle, and W. E. Esaias, Satellite detection of phytoplankton export from the Mid-Atlantic Bight during the 1979 spring bloom, *Deep Sea Res.*, 34, 675-703, 1987.
- Walsh, J. J., C. D. Wirick, L. J. Pietrafesa, T. E. Whitley, F. E. Hoge, and R. N. Swift, High frequency sampling of the 1984 spring bloom within the Mid-Atlantic Bight: Synoptic shipboard, aircraft, and in situ perspectives of the SEEP-I experiment, *Cont. Shelf Res.*, 8, 529-563, 1988.
- Walsh, J. J., et al., Carbon and nitrogen cycling within the Bering/Chukchi Seas: Source regions of organic matter effecting AOU demands of the Arctic Ocean, *Progr. Oceanogr.*, 22, 279-361, 1989.
- Wei-Bin, G., C. Hui-Ming, and H. Yun-Fang, Carbon transport by the Yangtze (at Nanjing) and Huanghe (at Jinan) Rivers, People's Republic of China, in *Transport of Carbon and Minerals in Major World Rivers, Part 2*, edited by E. T. Degens, S. Kempe, and H. Soliman, pp. 459-470, Mitt. Geol. - Palaont. Inst., Univ. Hamburg, Germany, 1983.
- Williams, P. M., and E. R. Druffel, Radiocarbon in dissolved organic matter in the central North Pacific Ocean, *Nature*, 330, 246-248, 1987.
- Williams, P. M., and E. R. Druffel, Dissolved organic matter in the ocean: Comments on a controversy, *Oceanography*, 1, 14-17, 1988.
- Wolter, K., Bacterial incorporation of organic substances released by natural phytoplankton populations, *Mar. Ecol. Progr. Ser.*, 7, 287-295, 1982.
- Worthington, L. V., On the North Atlantic circulation, *Johns Hopkins Oceanogr. Stud.*, 6, 1-110, 1976.
- Wright, W. R., Northern sources of energy for the deep Atlantic, *Deep Sea Res.*, 19, 865-877, 1972.
- Wroblewski, J. S., A model of the spring bloom in the North Atlantic and its impact on ocean optics, *Limnol. Oceanogr.*, 34, 1563-1571, 1989.
- Wroblewski, J. S., J. L. Sarmiento, and G. R. Flierl, An ocean basin scale model of plankton dynamics in the North Atlantic, I, Solutions for the climatological oceanographic conditions in May, *Global Biogeochem. Cycles*, 2, 199-218, 1988.
- K. L. Carder, F. E. Müller-Karger, and J. J. Walsh, Department of Marine Science, University of South Florida, St. Petersburg, FL 33701.

(Received May 28, 1991;

revised May 21, 1992;

accepted May 22, 1992.)

# Model for the interpretation of hyperspectral remote-sensing reflectance

Zhongping Lee, Kendall L. Carder, Steve K. Hawes, Robert G. Steward, Thomas G. Peacock, and Curtiss O. Davis

Remote-sensing reflectance is easier to interpret for the open ocean than for coastal regions because the optical signals are highly coupled to the phytoplankton (e.g., chlorophyll) concentrations. For estuarine or coastal waters, variable terrigenous colored dissolved organic matter (CDOM), suspended sediments, and bottom reflectance, all factors that do not covary with the pigment concentration, confound data interpretation. In this research, remote-sensing reflectance models are suggested for coastal waters, to which contributions that are due to bottom reflectance, CDOM fluorescence, and water Raman scattering are included. Through the use of two parameters to model the combination of the backscattering coefficient and the  $Q$  factor, excellent agreement was achieved between the measured and modeled remote-sensing reflectance for waters from the West Florida Shelf to the Mississippi River plume. These waters cover a range of chlorophyll of 0.2–40 mg/m<sup>3</sup> and gelbstoff absorption at 440 nm from 0.02–0.4 m<sup>-1</sup>. Data with a spectral resolution of 10 nm or better, which is consistent with that provided by the airborne visible and infrared imaging spectrometer (AVIRIS) and spacecraft spectrometers, were used in the model evaluation.

## Introduction

The use of the power law of spectral-radiance ratios<sup>1,2</sup> to measure pigment concentrations requires that the water-leaving radiance be largely determined by variations in the pigment concentration, with all other optical constituents covarying with this quantity. The method works quite well for the open ocean, or case 1 waters,<sup>3</sup> in part because the water-leaving radiance of open ocean waters is hardly affected by bottom reflectance, land runoff, or suspended sediments. Although aeolian dust may be carried by winds to the open ocean,<sup>4</sup> the dominant effect of the particulates may still derive from phytoplankton.<sup>5</sup>

The power-law approach can be much less accurate for estuarine and coastal areas,<sup>6</sup> however, because many of the optical constituents are independent of phytoplankton concentrations. In these areas, the water-leaving radiance includes not only parts that

are due to elastic scattering by water molecules, phytoplankton detritus, suspended particulates, and bottom reflectance, but also parts that are due to inelastic scattering of colored dissolved organic matter (CDOM) fluorescence and water Raman scattering. Thus, changes in ocean color resulting from suspended sediments or dissolved organic matter may be falsely interpreted as changes in pigment concentration.<sup>6,7</sup>

An approach to address these problems is to measure the light field and analytically separate the different spectral contributors. Optical models have been developed for the subsurface irradiance reflectance,<sup>7,8</sup> but satellites measure the radiance leaving the water surface. The water-leaving radiance is governed by two distinct parts: the solar input and in-water properties. When the remote-sensing reflectance ( $R_{rs}$ ) is defined as the ratio of the water-leaving radiance  $L_w(\lambda)$  to the above-surface downwelling irradiance  $E_d(0^+, \lambda)$ ,  $R_{rs}$  will be independent of the intensity of the solar input. Models have been suggested by Carder and Steward,<sup>9</sup> Gordon *et al.*,<sup>10</sup> and Peacock *et al.*<sup>11</sup> to explain the measured  $R_{rs}$ , but in these works no contributions from CDOM fluorescence, water Raman reflectance, or bottom reflectance were included. Also, in these works<sup>9,11</sup> an arbitrary  $Q$  factor<sup>12</sup> was used.

For water-depth measurements<sup>13,14</sup> or bottom-

C. O. Davis is with the Jet Propulsion Laboratory, California Institute of Technology, 4800 Oak Grove Boulevard, Pasadena, California 91109; the other authors are with the Department of Marine Science, University of South Florida, 140 Seventh Avenue South, St. Petersburg, Florida 33701.

Received 29 December 1992; revised manuscript received 31 January 1994

0003-6935/94/245721-12\$06.00/0.

© 1994 Optical Society of America.

feature mapping,<sup>15</sup> the diffuse attenuation coefficient<sup>14</sup> or an unclear effective attenuation coefficient<sup>15</sup> is usually used. For improvement of the interpretation of such measurements, an explicit expression is necessary for attenuation of the reflectance term that represents bottom reflectance. In this study, hyperspectral remote-sensing reflectance for waters from the West Florida Shelf to the Mississippi River plume was measured and modeled with a derived  $Q$  factor and the addition of bottom reflectance, CDOM fluorescence, and water Raman scattering.

## Theory

The upwelling radiance leaving the ocean is a complicated mix of signals caused by many components. The major contributions arise from the following: absorption by molecules and particulates, elastic scattering by molecules and particulates, and bottom reflectance in shallow waters. Inelastic scattering processes (e.g., water Raman scattering and fluorescence of CDOM, chlorophyll, and phycoerythrin) are also contributors. Works by Carder and Steward<sup>9</sup> and Gordon<sup>16</sup> dealing with chlorophyll  $a$  (chl  $a$ ) fluorescence have been reported, but, because the fluorescence efficiency varies by an order of magnitude,<sup>9</sup> this term is not considered in the present model. As peak chlorophyll fluorescence occurs in a narrow band centered around 685 nm,<sup>17</sup> its absence from the model is clearly seen when one compares values of measured and modeled  $R_{rs}$  (685) at higher chlorophyll concentrations. Perturbations between modeled and measured curves at  $\sim 580$  nm and  $\sim 685$  nm will be considered in the discussion relative to fluorescence that results from phycoerythrin and chl  $a$ , respectively.

It is assumed that the water-leaving radiance  $L_w(\lambda)$  is dominated by the following four components: elastic scattering from molecules and particles  $L_w^w(\lambda)$ , bottom reflectance  $L_w^b(\lambda)$ , CDOM fluorescence  $L_w^f(\lambda)$ , and water Raman scattering  $L_w^R(\lambda)$ . It is also assumed that to the first order (single scattering and quasi-single scattering<sup>18</sup>) the water-leaving radiance can be expressed as

$$L_w(\lambda) = L_w^w(\lambda) + L_w^b(\lambda) + L_w^f(\lambda) + L_w^R(\lambda). \quad (1)$$

The symbols and definitions used in this paper are summarized in Table 1. Wavelength dependence is included here, but for convenience it is not included in the following discussions except when necessary for clarity.

Remote-sensing reflectance is defined as

$$R_{rs} = \frac{L_w}{E_d(0^+)}. \quad (2)$$

Breaking this equation into contributions from the various mechanisms listed in Eq. (1), we have

$$R_{rs} = R_{rs}^w + R_{rs}^b + R_{rs}^f + R_{rs}^R. \quad (3)$$

In the interpretation of the measured  $R_{rs}$  on the left side of Eq. (3), each component on the right side of Eq. (3) is expressed by the optical properties of the water.

### A. Remote-Sensing Reflectance of the Water Column $R_{rs}^w$

For a homogeneous water body consider a wavelength-independent factor  $I$  as the influence of the air-sea interface on water-leaving radiance. Then the  $R_{rs}^w$ , which is due to elastic scattering in the water column, can be described in terms of values just below the interface as

$$R_{rs}^w = I \frac{L_u^w(0^-)}{E_d(0^-)}, \quad (4)$$

where  $I = t_+ t_- / n^2$ . For a zenith Sun, a nadir-viewing instrument, and a calm surface,  $t \approx 0.98$  and  $I \approx 0.533$  (Ref. 12) because  $n$  (1.341) varies only slightly when the salinity changes.<sup>19</sup> For larger solar zenith angles and foam-covered seas,  $t$  will be lower.<sup>12</sup> In our work, we specifically avoid foam-covered seas.

The subsurface-irradiance reflectance from the water column  $R^w$  is defined as the ratio of the subsurface upwelling irradiance  $E_u^w(0^-)$  to the subsurface downwelling irradiance  $E_d(0^-)$  by

$$R^w = \frac{E_u^w(0^-)}{E_d(0^-)}, \quad (5)$$

and Austin<sup>12</sup> has related  $E_u^w(0^-)$  and  $L_u^w(0^-)$  through the  $Q$  factor by

$$Q = \frac{E_u^w(0^-)}{L_u^w(0^-)}, \quad (6)$$

so  $R_{rs}^w$  can be expressed as

$$R_{rs}^w = \frac{I}{Q} R^w. \quad (7)$$

For irradiance reflectance  $R^w$ , Gordon *et al.*<sup>20</sup> developed a series relation with the Monte-Carlo method by

$$R^w = \sum_{m=0}^3 r_m \left( \frac{b_b}{a + b_b} \right)^m. \quad (8)$$

This equation was simplified<sup>21,22</sup> to

$$R^w \approx 0.33 \frac{b_b}{a}, \quad (9)$$

for values of  $b_b/a$  up to  $\sim 0.25$ . The constant 0.33 actually varies slightly with the solar zenith angle.<sup>23,24</sup> Because this paper deals with remote-sensing reflectance, which is less influenced by the fraction of forward scatter that upwells at solar zenith angle  $> 0^\circ$ ,  $R_{rs}$  is not as sensitive to the Sun angle, as is irradiance reflectance. Thus, we retain 0.33 as a

Table 1. Definitions and Units of Variables<sup>a</sup>

Variable	Units <sup>a</sup>	Definition
$a$	$\text{m}^{-1}$	Total absorption coefficient: $a_w + a_g + a_p$
$a_g$	$\text{m}^{-1}$	Gelbstoff-absorption coefficient
$a_p$	$\text{m}^{-1}$	Particle-absorption coefficient
$a_w$	$\text{m}^{-1}$	Pure water absorption coefficient
$b$	$\text{m}^{-1}$	Scattering coefficient
$b_b$	$\text{m}^{-1}$	Backscattering coefficient
$b_{bm}$	$\text{m}^{-1}$	Backscattering coefficient of molecules
$b_{bp}$	$\text{m}^{-1}$	Backscattering coefficient of particles
$b_R$	$\text{m}^{-1}$	Water Raman scattering coefficient
$c$	$\text{m}^{-1}$	Beam attenuation coefficient: $a + b$
$D_d(0)$		Downwelling distribution function just below the surface
$\{D_d\}$		Vertically averaged downwelling distribution function
$E_d$	$\text{W m}^{-2}$	Downwelling irradiance
$E_o$	$\text{W m}^{-2}$	Total scalar irradiance
$E_{od}$	$\text{W m}^{-2}$	Downwelling scalar irradiance
$E_{ou}$	$\text{W m}^{-2}$	Upwelling scalar irradiance
$E_u^w$	$\text{W m}^{-2}$	Upwelling irradiance from water column only
$H$	$\text{m}$	Water depth
$k$	$\text{m}^{-1}$	Radiance attenuation coefficient
$j$	$\text{rad}$	Subsurface solar zenith angle
$K_d$	$\text{m}^{-1}$	Downwelling diffuse attenuation coefficient
$K_u$	$\text{m}^{-1}$	Upwelling diffuse attenuation coefficient
$L_u^w$	$\text{W m}^{-2} \text{sr}^{-1}$	Upwelling radiance from water column (elastic only)
$L_w$	$\text{W m}^{-2} \text{sr}^{-1}$	Total water-leaving radiance
$L_w^b$	$\text{W m}^{-2} \text{sr}^{-1}$	Water-leaving radiance from bottom reflectance
$L_w^f$	$\text{W m}^{-2} \text{sr}^{-1}$	Water-leaving radiance from CDOM fluorescence
$L_w^R$	$\text{W m}^{-2} \text{sr}^{-1}$	Water-leaving radiance from water Raman scattering
$L_w^w$	$\text{W m}^{-2} \text{sr}^{-1}$	Water leaving radiance from water column (elastic only)
$n$		Refractive index of water
$Q$	$\text{sr}$	Ratio of irradiance to radiance
$R$		Irradiance reflectance
$R_{rs}$	$\text{sr}^{-1}$	Remote-sensing reflectance
$R_{rs}^b$	$\text{sr}^{-1}$	Remote-sensing reflectance from bottom reflectance
$R_{rs}^f$	$\text{sr}^{-1}$	Remote-sensing reflectance from CDOM fluorescence
$R_{rs}^{fR}$	$\text{sr}^{-1}$	Sum of $R_{rs}^f$ and $R_{rs}^R$
$R_{rs}^R$	$\text{sr}^{-1}$	Remote-sensing reflectance from water Raman
$R_{rs}^w$	$\text{sr}^{-1}$	Remote-sensing reflectance from water column (elastic only)
$R^w$		Irradiance reflectance from water column (elastic only)
$t_+$		Air-sea surface transmittance for upwelling radiant flux
$t_-$		Air-sea surface transmittance for downwelling radiant flux
$T_{ie}$	$\text{W sr}^{-1}$	Intensity of the inelastically scattered light
$y_b$		Exponent for particle backscattering coefficient
$y_Q$		Exponent for particle $Q$ factor
$\alpha$	$\text{rad}$	Scattering angle
$\beta$	$\text{m}^{-1} \text{sr}^{-1}$	Volume scattering function
$\phi$	$\text{rad}$	Azimuth angle
$\gamma$		Irradiance ratio of skylight to sunlight
$\kappa$	$\text{m}^{-1}$	Quasi-diffuse attenuation coefficient: $a + b_b$
$\lambda_x$	$\text{nm}$	Excitation wavelength for inelastic scattering
$\eta$		Quantum efficiency of CDOM fluorescence
$\psi$	$\text{m}^{-1} \text{nm}^{-1}$	Inelastic scattering coefficient
$\rho$		Bottom albedo
$\Theta$	$\text{rad}$	Zenith angle

<sup>a</sup>Blank entries denote dimensionless quantities.

constant and embed any sun-angle influence within the  $Q$  factor expression (see Appendix A).

The total backscattering coefficient  $b_b$  includes two components: backscattering by molecules  $b_{bm}$  and particulates  $b_{bp}$ . The total absorption coefficient  $a$  includes contributions that are due to pure seawater absorption  $a_w$ , gelbstoff or CDOM absorption  $a_g$ , and particulate absorption  $a_p$ . Inserting these into Eq.

(9) and taking  $I \approx 0.533$ , we can write  $R_{rs}^w$  as

$$R_{rs}^w \approx \frac{0.176}{a_w + a_g + a_p} \frac{b_{bm} + b_{bp}}{Q}. \quad (10)$$

Eq. (10) pertains to optically deep water. When optically shallow water is encountered, scattering media and backscattered signals are reduced because

of the short water column. We consider that the subsurface  $E_u^w$  consists of two parts coming from two layers: one from the layer above the bottom and one from the layer below the bottom. Then the subsurface  $E_u^w$  coming only from the upper layer can be obtained by a reduction of the optically deep expression by an amount equivalent to the contribution of the missing water column below depth  $H$ . Thus for shallow waters with depth  $H$  and a totally absorbing bottom,  $R_{rs}^w$  is approximated by

$$R_{rs}^w \approx \frac{0.176}{a} \frac{b_b}{Q} \left\{ 1 - \exp \left[ - \int_0^H (K_d + K_u) dz \right] \right\}, \quad (11)$$

where  $z$  is positive downward from the surface.

If we define the quasi-diffuse attenuation coefficient as  $\kappa = a + b_b$ , then  $K_d \approx D_d \kappa$  and  $K_u \approx D_u \kappa$ .<sup>20</sup>  $D_d$  and  $D_u$  are the distribution functions for the downwelling and upwelling light fields, and  $D_u/D_d \approx 2$  according to Gordon *et al.*<sup>20</sup> Thus

$$R_{rs}^w \approx \frac{0.176}{a} \frac{b_b}{Q} [1 - \exp[-3\{D_d\}\kappa H]], \quad (12)$$

where  $\{D_d\}$  is the vertically averaged downwelling distribution function and  $\{D_d\} \approx 1.08D_d(0)$ .<sup>25</sup>  $D_d(0)$  is the downwelling distribution function just beneath the surface, and  $D_d(0) \approx 1/\cos(j)$ , with an error of less than 3%.<sup>25</sup>

#### B. Remote-Sensing Reflectance Resulting from Bottom Reflectance $R_{rs}^b$

Assume that the bottom is a Lambertian reflector with bottom albedo  $\rho$ , then  $R_{rs}^b$  can be approximated as

$$R_{rs}^b \approx \frac{0.533}{\pi} \rho \exp[-(\{D_d\}\kappa + k)H], \quad (13)$$

where  $k$  is the effective attenuation coefficient for the radiance from an extended Lambertian source. How  $k$  relates to the quasi-diffuse attenuation coefficient  $\kappa$  is not well understood. Heuristically, it should be a value between the beam attenuation coefficient  $c$  and the quasi-diffuse attenuation coefficient  $\kappa$ . Taken from the Monte-Carlo simulations for a totally diffuse light source,<sup>25</sup>  $k$  is approximately  $1.4\kappa$  to  $1.7\kappa$  for  $\kappa H$  in the range of 0.5–4.0. As an average in this work,  $k = 1.5\kappa$ , as is used by Marshall and Smith.<sup>26</sup> Then Eq. (13) becomes

$$R_{rs}^b \approx 0.17\rho \exp[-(1.5 + \{D_d\})\kappa H]. \quad (14)$$

#### C. Remote-Sensing Reflectance Resulting from CDOM Fluorescence and Water Raman Scattering $R_{rs}^f$ and $R_{rs}^R$

In general, these terms are due to inelastic scattering (indicated by the subscript ie) by CDOM molecules and water molecules. We define the volume scatter-

ing function for inelastic scattering as

$$\beta_{ie}(\alpha, \lambda_x, \lambda) = \frac{T_{ie}(\alpha, \lambda)}{E(\lambda_x)dV}, \quad (15)$$

where  $T_{ie}(\alpha, \lambda)$  is the intensity of the inelastically scattered light at scattering angle  $\alpha$ ,  $dV$  is the scattering volume,  $E(\lambda_x)$  is the irradiance of the excitation beam, and  $\alpha$  is the angle between the excitation beam and the output photon directions.

If  $\beta_{ie}$  is considered to be isotropic, then remote-sensing reflectance resulting from CDOM fluorescence and water Raman can be expressed (see Appendix B for details) as

$$R_{rs}^f \approx 0.072 \int_{\lambda_x} \eta(\lambda_x) \frac{\lambda_x}{\lambda} \frac{a_g(\lambda_x)E_d(0^-, \lambda_x)}{[2a(\lambda) + a(\lambda_x)]E_d(0^-, \lambda)} \exp \left[ -s \left( \ln \frac{\lambda - \lambda_0}{\sigma} \right)^2 \right] \frac{1}{A} d\lambda_x, \quad (16)$$

$$R_{rs}^R \approx 0.072 \frac{b_R(\lambda_x)E_d(0^-, \lambda_x)}{[2a(\lambda) + a(\lambda_x)]E_d(0^-, \lambda)}. \quad (17)$$

#### Field Measurements

From 1990 to 1993, measurements of optical properties for case 1 and case 2 waters, which include waters from the West Florida Shelf to the mouth of Mississippi River, were taken. Case 2 waters are those that contain optical materials that are not derived from phytoplankton, in addition to phytoplankton and phytoplankton-derived materials.<sup>3</sup> Table 2 summarizes the field data for selected stations. Figure 1 shows the station locations in the Gulf of Mexico. For each station, remote-sensing reflectance  $R_{rs}$  and surface-water particulate absorption  $a_p$  were measured. For the 1993 stations, a long-path (50 or 100 cm) spectrophotometer was used to measure  $a_g$ .

For  $R_{rs}$  we directly measured the upwelling radiance above the sea surface and downwelling sky radiance using a Spectron Engineering spectral radiometer (Model SE-590) following the method of Carder *et al.*<sup>27</sup> We measured downwelling irradiance above the sea surface with the SE-590 by viewing a Spectralon diffuse-reflection calibration panel. Remote-sensing reflectance values were determined by removal of the reflected skylight from the upwelling-radiance values<sup>9,27</sup> and division of the result by the downwelling-irradiance values. For each station, three sets of measurements were taken, and an averaged  $R_{rs}$  spectrum was derived, with coefficients of variation much less than 5%.

For  $a_p$ , we measured a surface-water sample immediately after its collection following the method developed by Mitchell and Kiefer.<sup>28</sup> Briefly, for each water sample, ~1000 mL (with variations according to the clarity of the water sample) were filtered through Whatman-type GF/F glass-fiber filters. Hyperspectral optical densities of the sample pad and

Table 2. Station Locations and Water Depth

Station	Latitude	Longitude	Time	Date	Bottom Depth	Mod. Bottom Depth
ST01	27°27' N	82°55' W	10.5 <sup>a</sup>	4 Mar 1990	~ 14 m	13.7 m
ST02	27°20' N	83°03' W	13.0 <sup>a</sup>	4 Mar 1990	~ 25 m	25 m
ST03	27°12' N	83°11' W	14.9 <sup>a</sup>	4 Mar 1990	~ 35 m	36 m
ST08	28°48' N	91°30' W	08.5 <sup>b</sup>	12 Apr 1993	OD <sup>d</sup>	OD
ST10	28°15' N	91°30' W	14.0 <sup>b</sup>	12 Apr 1993	OD	OD
ST27	29°32' N	85°47' W	09.2 <sup>b</sup>	19 Apr 1993	OD	OD
ST12	28°52' N	89°33' W	10.8 <sup>c</sup>	5 Jun 1993	OD	OD
ST14	28°48' N	90°02' W	16.1 <sup>c</sup>	5 Jun 1993	OD	OD
ST19	27°34' N	83°20' W	09.5 <sup>c</sup>	8 Jun 1993	~ 33 m	35 m

<sup>a</sup>Eastern standard time.<sup>b</sup>Central daylight time.<sup>c</sup>Eastern daylight time.<sup>d</sup>Water is optically deep (OD).

a wet blank pad were measured with the Spectron. The optical-path-elongation factor  $\beta$  was calculated with Eq. (2) in Bricaud and Stramski.<sup>29</sup> The optical density measurements were repeated three times with no significant variation noted among them.

At the 1990 stations, gelbstoff absorption  $a_g$  was derived from surface-layer  $K_d$  values determined with a Biospherical Instruments MER-1048, through the use of the expression  $a_g = K_d \cos(j) - a_w - a_p$ . At the 1993 stations,  $a_g$  was measured with 50-cm or 100-cm path-length instruments, respectively, after the sample was filtered through 0.2- $\mu$ m pore-diameter Gelman Supor-200 filters.

### Model

For the modeling of measured  $R_{rs}$  spectra, values for  $a_w$  and  $b_{bm}$  were already known,<sup>30</sup>  $a_p$  was measured, and  $a_g$  was measured or derived from  $K_d$  spectra. What needs to be considered is how  $Q$ ,  $b_{bp}$ ,  $\rho$ ,  $H$ ,  $\eta$ ,  $s$ ,  $\lambda_0$ , and  $\sigma$  change for different environments.

### $R_{rs}^R$

Because Raman is a type of molecular scattering,  $b_R(\lambda_x)$  is considered to have a wavelength dependence similar to that of the water-molecule scattering coefficient,<sup>31</sup> i.e., a function of  $\lambda^{-4}$ . Because  $b_R(488) = 2.6 \times 10^{-4} \text{ m}^{-1}$  (Marshall and Smith<sup>26</sup>), thus  $b_R(\lambda_x) = 2.6 \times 10^{-4} (488/\lambda_x)^4$ , and the frequency shift for water Raman scattering was fixed at  $3350 \text{ cm}^{-1}$  as an average from Collins *et al.*<sup>32</sup> The incoming, total downwelling-irradiance spectrum was measured with a Licor 1800 spectral irradiance meter<sup>27</sup> from 300–850 nm. Then it is straightforward to calculate  $R_{rs}^R$  with Eq. (17) when the total absorption spectrum is known.

### $R_{rs}^I$

As can be seen from Eq. (16), there are at least four variables [ $\eta(\lambda_x)$ ,  $s$ ,  $\lambda_0$ , and  $\sigma$ ] needed to calculate the remote-sensing reflectance that results from CDOM

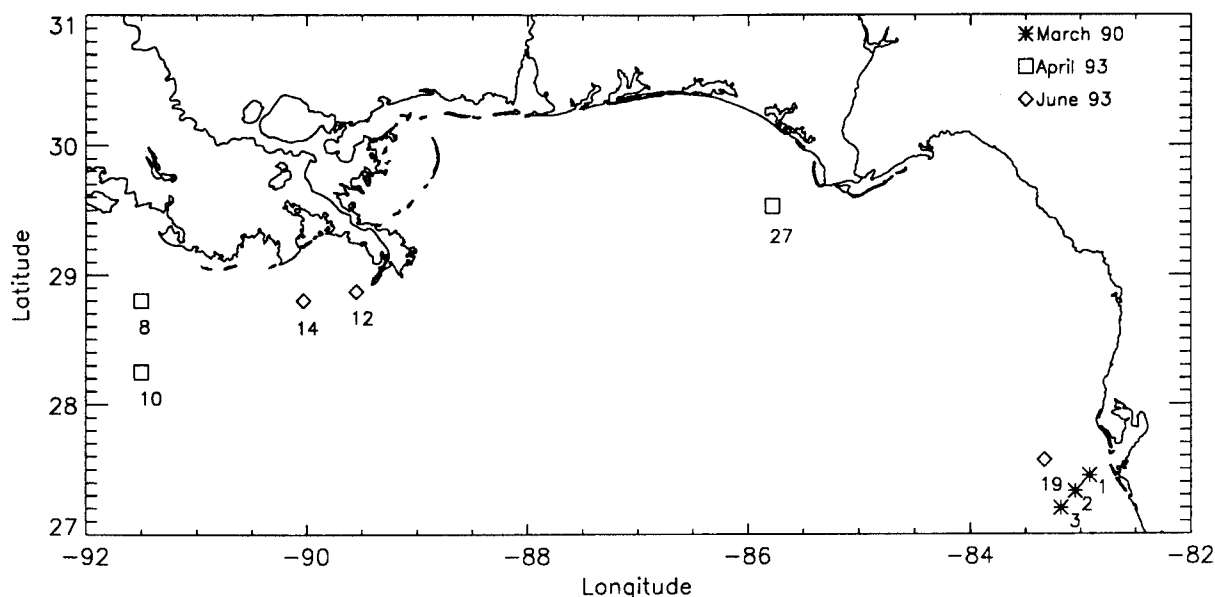


Fig. 1. Station locations in the Gulf of Mexico.

fluorescence when the total absorption coefficient is known. From lab measurements of CDOM fluorescence for the West Florida Shelf experiments,<sup>33</sup> the quantum efficiency  $\eta(\lambda_x)$  was between  $\sim 0.5\%$  and  $\sim 1.5\%$ , and it was generally rather constant for different excitation wavelengths. For the log-normal expression in  $R_{rs}^f$ , the shape factor  $s$  was 10,  $\lambda_0 \sim (.95\lambda_x - 45)$ , and  $\sigma \sim (195 - \lambda_x/5)$ , all of which were quite constant for the different stations.<sup>33</sup> Based on these measurements,  $\eta = 1.0\%$  was used for all the stations except ST03, where  $\eta = 1.5\%$  was measured. At ST12, ST14, and ST01 where significant terrigenous CDOM was present,  $\eta = 0.5\%$  was used.

#### $R_{rs}^b$

This value depends not only on the optical properties of the water body, but also on the water depth and the bottom albedo. In the modeling work, the water depth was based on the Provisional Chart No. 1003<sup>34</sup> for the Gulf Coast, and the bottom albedo was based on earlier measurements of bottom samples from the region that had near-shore values of 0.1–0.2 (used for ST01) and offshore values from 0.4–0.5 (used for ST02 and ST03). Figure 7 (below) shows examples of those albedo spectra. The quasi-diffuse attenuation coefficient  $\kappa$  is assumed to be equal to the absorption  $a$ . For ST19, an albedo value of 0.1 is required, which suggests that the bottom might contain more heavy minerals or grass at that site. Direct bottom-albedo measurements are lacking at individual stations and are needed for a wide variety of bottom types.

#### $R_{rs}^w$

When using Eq. (10) to model the measured  $R_{rs}^w$ , we need to know  $a_w$ ,  $a_g$ ,  $a_p$ ,  $b_{bm}$ ,  $b_{bp}$ , and  $Q$ . Values of  $a_w$  and  $b_{bm}$  are already known.<sup>30</sup> When  $a_g$  and  $a_p$  are measured, only  $b_{bp}$  and  $Q$  for different water bodies and solar zenith angles are required. The particulate backscattering coefficient  $b_{bp}$  has been considered to be a spectral function of  $\lambda^{-1}$  for offshore waters or to be spectrally constant for near-shore waters.<sup>11,35</sup>

For the factor  $Q$ , however, only a few measurements exist, and its values have been reported from 3.2 to 12.<sup>9</sup>  $Q$  has been taken to be approximately 4.7 and spectrally constant from 440–550 nm,<sup>36</sup> although Kirk<sup>37</sup> gives  $Q$  as  $\sim 4.9$ , and Gordon *et al.*<sup>10,20</sup> suggest a value of  $\sim 3.4$ . For many studies,  $Q$  is often arbitrarily chosen as a spectral constant.<sup>9,11,13</sup> From measurements by Davis,<sup>38</sup> however, Carder *et al.*<sup>6</sup> found that  $Q$  is not spectrally constant for the 1990 stations, and there was a trend for  $Q$  to increase with wavelength (an inverse trend compared with  $b_{bp}$ ). Recently, Morel and Gentili<sup>39</sup> published Monte-Carlo simulations of  $Q$  for a variety of water types, but they provide no explicit expression for  $Q$  as a function of  $a$  and  $b_b$  or  $\beta$ . So, for modeling  $R_{rs}^w$  for a region where spectral  $b_{bp}$  and  $Q$  need to be considered, at least four parameters are needed based on Eq. (10): two for  $b_{bp}(\lambda)$  and two for  $Q(\lambda)$ .

If we consider the upwelling radiance of the water column  $L_u^w$  as consisting of two parts—one  $L_u^m$  that is due to scattering by molecules and one  $L_u^p$  that is due to scattering by particles—with the assumption that to the first order (for single scattering and quasi-single scattering<sup>18</sup>) the sum of  $L_u^m$  and  $L_u^p$  gives  $L_u^w$ , then Eq. (10) can be written as

$$R_{rs}^w \approx \frac{0.176}{a_w + a_g + a_p} \left( \frac{b_{bm}}{Q_m} + \frac{b_{bp}}{Q_p} \right), \quad (18)$$

in which  $Q_m$  and  $Q_p$  are the  $Q$  factors for molecules and particles, respectively, and are defined as

$$Q_m = \frac{E_u^m(0^-)}{L_u^m(0^-)}, \quad Q_p = \frac{E_u^p(0^-)}{L_u^p(0^-)}. \quad (19)$$

For  $Q_m$  to the first order an estimate can be made based on the phase function and illumination geometry. For a given illumination geometry, the shape of the radiance distribution within the water is determined primarily by the volume scattering function through single scattering. For example, Gordon<sup>25</sup> suggested that a single-scattering approximation can be used to specify the variation of  $R$  with the solar zenith angle, and Kirk<sup>22</sup> used single scattering to describe the average cosine. We combined the approach used by Jerlov<sup>40</sup> to provide an estimation of radiance and irradiance with Sun angle and depth, Austin's definition of the  $Q$  factor,<sup>12</sup> and the volume scattering function of water molecules given by Morel<sup>41</sup> to calculate the  $Q_m$  for sunlight (see Appendix A for details). The results can be approximated with the following simple function:

$$Q_m^{\text{sun}}(j) \approx 5.92 - 3.05 \cos(j). \quad (20)$$

With the assumption that the  $Q_m$  attributable to skylight is approximately 3.14, the effective  $Q_m$  for a mixture of sunlight and skylight is given by (Appendix A)

$$Q_m = \frac{1 + \gamma(\lambda)}{1 + \gamma(\lambda) \frac{Q_m^{\text{sun}}(j)}{3.14}} Q_m^{\text{sun}}(j), \quad (21)$$

if we define  $\gamma(\lambda) = E_d^{\text{sky}}/E_d^{\text{sun}}$ , and calculate  $\gamma(\lambda)$  using the model developed by Gregg and Carder.<sup>42</sup> Model results of  $Q_m^{\text{sun}}(j)$  centered around 3.3 for environments studied in this contribution and are shown in Table 3, and the calculated  $Q_m^{\text{sun}}$  is consistent with Morel and Gentili's Monte-Carlo results.<sup>39</sup>

Because we know the volume scattering function for neither the total water sample nor the particles,  $b_{bp}$  and  $Q_p$  cannot be independently estimated. However, because  $b_{bp}$  has been considered a function of  $b_{bp}(400)(400/\lambda)^{y_b}$  as in Smith and Baker,<sup>30</sup> we may also consider  $Q_p$  to be a function of  $Q_p(400)(\lambda/400)^{y_Q}$ .

Table 3. Parameters for Each Station<sup>a</sup>

Station	$j$	$Q_{m\text{sun}}$	$X$	$Y$	$a_g(440)$	$a_p(440)$	$a_p^{\text{mea}}(440)$	[chl $a$ ] (mg/m <sup>3</sup> )
ST01	35°	3.3	0.0090	1.5	0.082	0.040	0.045	1.05
ST02	26°	3.2	0.0020	2.4	0.042	0.036	0.035	0.61
ST03	27°	3.2	0.0010	2.4	0.034	0.028	0.026	0.70
ST08	43°	3.7	0.0062	0.3	0.31	0.28	0.295	
ST10	17°	3.0	0.0009	1.8	0.059	0.023	0.021	
ST27	36°	3.5	0.0011	1.7	0.078	0.029	0.034	
ST12	30°	3.3	0.0029	0	0.42	1.40	1.12	38.58
ST14	21°	3.1	0.0066	0	0.38	1.21	1.16	20.26
ST19	37°	3.5	0.00061	1.9	0.023	0.022	0.013	0.22

<sup>a</sup>Blank entries indicate that no data are available.

Then  $b_{bp}/Q_p$  can be combined and modeled as

$$\frac{b_{bp}}{Q_p} = \frac{b_{bp}(400)}{Q_p(400)} \left( \frac{400}{\lambda} \right)^{(yb+yQ)}$$

$$= X \left( \frac{400}{\lambda} \right)^Y, \quad (22)$$

where  $X$  and  $Y$  are two unknowns determined for specific particulate suites and solar illumination situations if Eq. (18) is inverted.

After calculating  $R_{rs}^R$ ,  $R_{rs}^f$ , and  $R_{rs}^b$ , only  $X$  and  $Y$  remain unknown. The modeled  $R_{rs}^w$  and the residual of  $R_{rs} - R_{rs}^R - R_{rs}^f - R_{rs}^b$  were matched to derive  $X$  and  $Y$  with a predictor-corrector approach to modeling, as in Carder and Steward.<sup>9</sup>

## Results and Discussion

Using the methodology described above (see Model) we modeled  $R_{rs}$  for case 1 and case 2 waters, which include (1) the West Florida Shelf waters, with shallow, gelbstoff-rich coastal waters, and (2) Gulf of Mexico waters, with phytoplankton blooms in the Mississippi River plume ( $S > 17\%$ ). As examples, Figs. 2–5 show the detailed model components for  $R_{rs}$ , and Fig. 6 shows the results of all the listed stations. Table 2 provides the station locations as well as the measured and modeled water depths of the shallow stations. Table 3 lists the model parameters  $j$ ,  $Q_{m\text{sun}}$ ,

$X$ ,  $Y$ ,  $a_g(440)$  and  $a_p(440)$  along with the measured values of  $a_p(440)$  and the chl  $a$  concentration values for each station. Table 4 details the fractional contributions that  $R_{rs}^w$ ,  $R_{rs}^R$ ,  $R_{rs}^f$ , and  $R_{rs}^b$  make to the measured  $R_{rs}$  at 440 and 550 nm.

It can be seen from Figs. 2–6 that excellent fittings were achieved between the measured and modeled  $R_{rs}$  for all the stations except the spectral region near 685 nm, where chl  $a$  fluorescence is present in the field data. The overall averaged difference between the measured and modeled  $R_{rs}$  is 2%, which is well within the measurement accuracy. The  $a_p$  that is required by the model is within 15% of the measured  $a_p$  except near the Mississippi River at ST12 (25%), with the highest chl  $a$  concentration (38.6 mg/m<sup>3</sup>). The average difference between the measured and required  $a_p$  is 8.9% (6.9% when ST12 is excluded). The maximum 15% or 25% difference can perhaps be explained by the accuracy involved in the method of  $a_p$  measurement because of the  $\beta$  factor, which varies significantly among species.<sup>29</sup> This may be especially important for ST12, which was near the Mississippi River mouth where the heavy load of sediments and minerals might cause additional uncertainty. Also, the influence of the horizontal and vertical structures of the waters increases for mesotrophic-eutrophic waters, so patchiness can affect accuracies in the more hypertrophic waters. Finally, the low signal obtained for the upwelling radiance measurements at

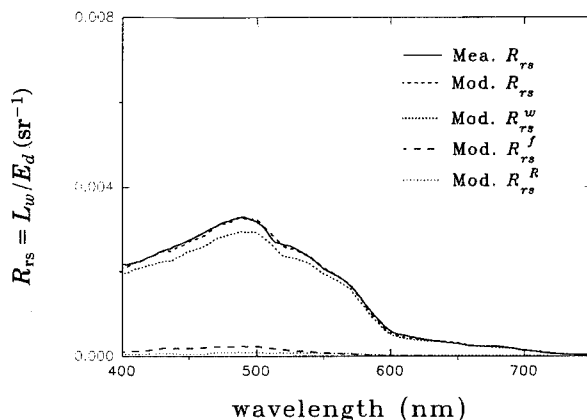


Fig. 2. Measured versus modeled  $R_{rs}$  for ST27.

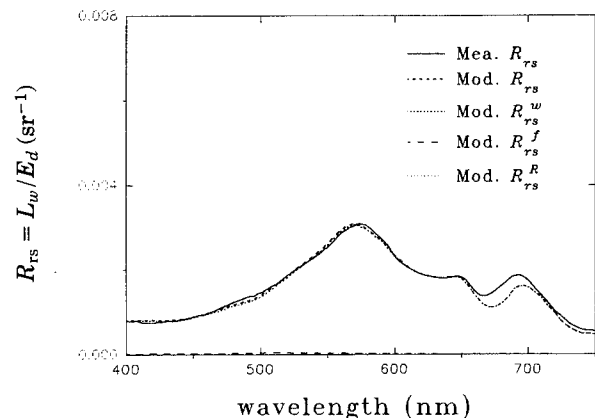


Fig. 3. Measured versus modeled  $R_{rs}$  for ST14.



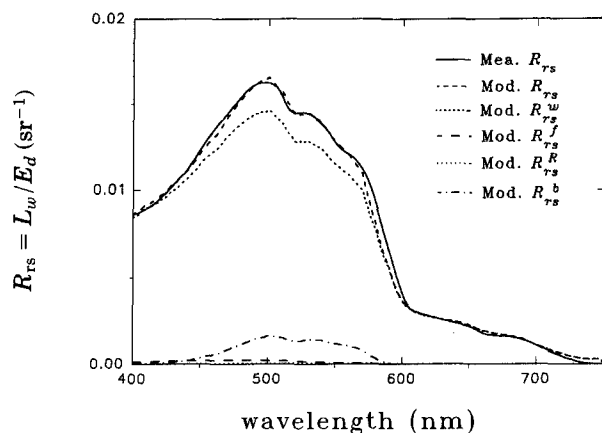


Fig. 4. Measured versus modeled  $R_{rs}$  for ST01.

ST12 made the  $R_{rs}$  calculation sensitive to corrections for reflected skylight.

From Table 3, the ratio of  $a_g(440)$  to  $a_p(440)$  is highly variable, with a range from  $\sim 0.3$  to  $\sim 3.0$ , and the  $X$  value does not covary with the pigment concentration of chl  $a$  for the waters studied. This illustrates that the model works well over a wide range of conditions and also suggests why the power-law algorithm does not work well for coastal waters. The highest  $X$  value,  $0.0090 \text{ m}^{-1} \text{ sr}^{-1}$ , was at the shallow, mesotrophic waters at ST01, which suggests a high influence of detritus and suspended sediments. Brisk northwesterly winds suspended sediments in the shoal regions to the east and north of the station, and sediment and detritus likely were transported by the ebb tidal currents from Tampa Bay to the study site.<sup>27</sup>

The  $Y$  values were generally within the range of 0–2.4 for the waters reported here. This range might be interpreted to be partially due to  $b_{bp}$  and partially due to  $Q_p$ . For the particle backscattering coefficient  $b_{bp}$  the wavelength exponent is in the range 0–3.0 for a range of particle sizes (e.g., bacteria,<sup>43</sup> phytoplankton cells,<sup>44</sup> and coccoliths<sup>10</sup>). From Eq. (22), if  $Y = 2.4$  and  $y_Q = 1.0$ , then  $y_b = 1.4$ , which is within the 0–3.0 range reported elsewhere.

Model results at ST03 suggest relatively higher CDOM fluorescence and water Raman influences,

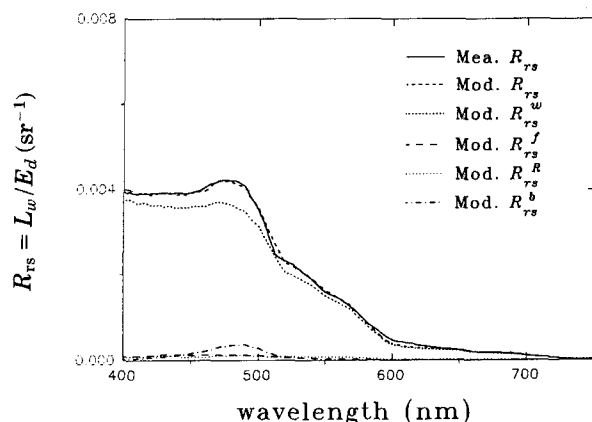


Fig. 5. Measured versus modeled  $R_{rs}$  for ST19.

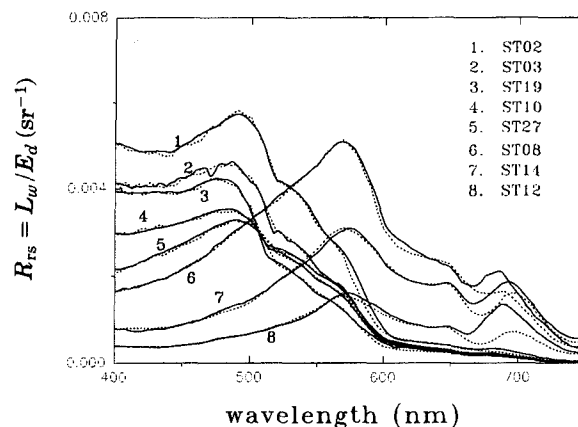


Fig. 6. Measured (solid curve) versus modeled (dashed curve)  $R_{rs}$  for all the stations except ST01.

because a higher  $\eta$  (1.5%) was encountered.<sup>33</sup> This value is  $\sim 3$  times greater than the value suggested by Spitzer and Dirks<sup>45</sup> for terrigenous CDOM. If we exclude this station, more than 90% of the water-leaving radiance is accounted for by the sum of the elastic scattering from molecules, particles, and the bottom. This is consistent with the reports of Marshall and Smith<sup>26</sup> and Stavn,<sup>46</sup> because the waters studied in their reports were clearer. Water Raman scattering makes more of a contribution when the water is clear, and  $R_{rs}^w/R_{rs}$  will typically have a higher value at 550 nm than at 440 nm.

It is interesting that the ratio  $R_{rs}(440)/R_{rs}(550)$  did not vary widely (within 15%) because of inelastic scattering (see Table 4). Among stations without bottom influence, differences in the ratio were within  $\sim 10\%$ , which suggests the spectral-radiance ratio is effective for most deep waters without consideration of CDOM fluorescence and water Raman scattering. But it is obvious that as the bottom influence increases the usefulness of the power-law algorithm decreases. Also, the power-law algorithm cannot distinguish between the absorption of CDOM and that of pigments. Note also that  $R_{rs}^w(490)/R_{rs}(490)$  values as low as 0.77 were determined (not explicitly shown), which suggests that great care must be taken when one is interpreting remote-sensing curves for the intermediate wavelength at shallow coastal stations.

At the optically shallow stations (ST01, ST02, ST03, and ST19), the model-derived depths were within approximately 10% of the chart depths without consideration of any tidal influence (typically  $< 0.5 \text{ m}$ ). This demonstrates a potential to use this model to survey, e.g., by aircraft overflights, dramatic changes in shelf bathymetry that can occur as a result of major storm.

For ST01, ST02, ST03, ST08, ST12, and ST14, the general agreement between the modeled and measured  $R_{rs}$  values are very good, with small differences near 580 nm, where the measured  $R_{rs} >$  modeled  $R_{rs}$ . Other than the modeling error, there are at least three possible reasons for this: (1) bottom-albedo uncertainty, (2) phycoerythrin fluorescence,<sup>47</sup> and (3)

Table 4. Optical Component Contributions<sup>a</sup> to  $R_{rs}$ 

Station	$R_{rs}^w/R_{rs}$		$R_{rs}^R/R_{rs}$		$R_{rs}^b/R_{rs}$		$R_{rs}(440)/R_{rs}(550)$	
	440 nm	550 nm	440 nm	550 nm	440 nm	550 nm	Measured $R_{rs}$	Corrected $R_{rs}$
ST01	0.95	0.89	0.02	0.01	0.02	0.10	0.87	0.92
ST02	0.91	0.80	0.05	0.06	0.04	0.12	1.48	1.73
ST03	0.86	0.81	0.10	0.12	0.02	0.04	1.87	2.00
ST08	0.98	0.99	0.03	0.02			0.49	0.48
ST10	0.92	0.93	0.08	0.07			1.64	1.60
ST27	0.90	0.94	0.08	0.07			1.34	1.29
ST12	0.90	0.97	0.09	0.03			0.31	0.27
ST14	0.97	0.99	0.03	0.01			0.32	0.30
ST19	0.92	0.92	0.06	0.07	0.03	0.01	2.46	2.36

<sup>a</sup> $R_{rs}^R = R_{rs}^f + R_{rs}^R$  and corrected  $R_{rs} = \text{measured } R_{rs} - R_{rs}^R - R_{rs}^b$ . Blank entries indicate that no data are available.

water-absorption coefficient uncertainty.<sup>11</sup> A spectrally constant bottom albedo was used for the shallow stations. Earlier measurements of bottom albedo (Fig. 7) did display some spectral dependence, but these types of changes could not provide the sharp increase and then decrease with wavelength in  $R_{rs}$  required for the measured and modeled  $R_{rs}$  curves to converge. Also, there was no bottom contribution to  $R_{rs}$  at ST08, ST12, or ST14. More realistic explanations include the lack of a term for phycoerythrin fluorescence or the differences between the water-absorption coefficients in this spectral region reported by Smith and Baker<sup>30</sup> and Tam and Patel.<sup>48</sup> Further study is required to resolve this issue. The differences between the measured and modeled  $R_{rs}$  curves near 685 nm are expected because no term is included in the model to describe the chl *a* fluorescence.

### Summary

Contributions to the water-leaving radiance spectra for a variety of waters were attributed to elastic scattering by water molecules, suspended particles, and bottom reflectance, and to inelastic scattering by water Raman and CDOM (or gelbstoff) fluorescence. Inelastic scattering by pigments was not considered. For optically deep water, remote-sensing reflectance

of the water-column part (elastic scattering only)  $R_{rs}^w$  was simulated as follows:

$$R_{rs}^w \approx \frac{0.176}{a_w + a_g + a_p} \left[ \frac{b_{bm}}{Q_m} + X \left( \frac{400}{\lambda} \right)^Y \right], \quad (23)$$

where  $b_{bm}$  is known,  $Q_m$  can be estimated, and  $X$  and  $Y$  are spectral constants.  $Q_m^{\text{sun}}$  averaged approximately 3.3, and  $Y$  was less than 2.4 for the waters considered. For optically shallow waters, the expression for bottom reflectance

$$R_{rs}^b \approx 0.17\rho \exp[-(1.5 + [D_d])aH], \quad (24)$$

works well for the shallow waters that we considered. Together, the water-column term and the bottom-reflectance term accounted for more than 90% of the total remote-sensing reflectance.

Close agreement between modeled and measured  $R_{rs}$  was achieved for all stations when all scattering mechanisms mentioned above (both elastic and inelastic) were included. The ratio  $a_g(440)/a_p(440)$  covered a range from ~0.3 to ~3.0, which indicates the wide usefulness of the model. For contributions other than those from the water column, as much as 23% of  $R_{rs}(490)$  is attributable to water Raman, CDOM fluorescence, and bottom reflectance for an optically shallow (25 m) station. For the power law of spectral radiance ratio, most error comes from reflected bottom radiance for coastal waters. For most deep waters, the power-law algorithm can be used without the correction of CDOM fluorescence and water Raman with little error if the optical properties covary with chlorophyll, because the inelastic effects cover the whole range from 400–600 nm with generally less than 10% contributions to the water-leaving radiance.

The  $a_p$  required by the model is generally within 15% of the measured  $a_p$ , with an average difference of 8.9% (6.9% when ST12 is excluded). This suggests a method to remotely measure the pigment- and gelbstoff-absorption coefficients, although derivation of chl *a* concentration will depend on knowledge of the specific absorption coefficient for a region. Also the model-derived bottom depths for optically shallow waters are within 10% of the chart depths, which

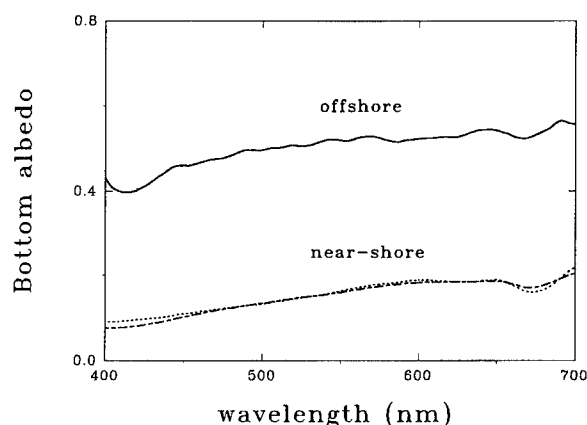


Fig. 7. Bottom-albedo spectra for near-shore (dashed curve) and offshore (solid curve) sediments, measured for samples on earlier cruises and retrieved from a grab sampler or by divers.

suggests its possible use to remotely measure bottom depth for the shelf waters.

#### Appendix A: Simple Estimation of $Q_m(j, \lambda)$

If we follow the method described by Jerlov,<sup>40</sup> the subsurface upwelling irradiance  $E_u^{\text{sun}}(0^-, \lambda)$  caused by subsurface sunlight  $E_d^{\text{sun}}(0^-, \lambda)$  can be obtained for single scattering and quasi-single scattering<sup>18</sup> by

$$E_u^{\text{sun}}(0^-, \lambda) = E_d^{\text{sun}}(0^-, \lambda) \frac{\sec(j) \exp[-cz \sec(j)]}{c} \times \int_0^{2\pi} \int_{\pi/2}^{\pi} \frac{\beta(\alpha, \lambda) \sin(\theta)}{\sec(\theta) + \sec(j)} d\theta d\phi, \quad (\text{A1})$$

where  $\alpha$  is the scattering angle,  $\theta$  is the zenith angle,  $\phi$  is the azimuth angle, and

$$\cos(\alpha) = -\cos(\theta)\cos(j) + \sin(\theta)\sin(j)\cos(\phi).$$

The upwelling radiance from the nadir resulting from this situation is

$$L_u^{\text{sun}}(0^-, \lambda) = E_d^{\text{sun}}(0^-, \lambda) \frac{\beta(\pi - j, \lambda)}{c[\cos(j) + 1]} \times \exp[-cz \sec(j)]. \quad (\text{A2})$$

Recalling Austin's definition<sup>12</sup> for the  $Q$  factor  $E_u/L_u$ , we get

$$Q_m^{\text{sun}}(j, \lambda) = \frac{\int_0^{2\pi} \int_{\pi/2}^{\pi} \frac{\beta(\alpha, \lambda)}{\cos(j) + \cos(\theta)} \cos(\theta) \sin(\theta) d\theta d\phi}{\frac{\beta(\pi - j, \lambda)}{\cos(j) + 1}}. \quad (\text{A3})$$

Because  $\beta(\alpha, \lambda)$  for water molecules is given by Morel<sup>41</sup> and its angular distribution is considered to be wavelength independent for the visible region, the above equation can be simplified to

$$Q_m^{\text{sun}}(j) \approx 5.92 - 3.05 \cos(j). \quad (\text{A4})$$

As backscattered skylight also contributes to the upwelling-radiance field, its influence on the actual  $Q_m(j, \lambda)$  needs to be considered. Defining the ratio between the subsurface, downwelling sky irradiance and solar irradiance to be  $\gamma(\lambda)$  and assuming that the  $Q$  factor that is due to skylight is  $\sim 3.14$ , we have

$$Q_m(j, \lambda) = \frac{1 + \gamma(\lambda)}{1 + \gamma(\lambda) \frac{Q_m^{\text{sun}}(j)}{3.14}} Q_m^{\text{sun}}(j). \quad (\text{A5})$$

So, for molecular scattering and when  $j$  and  $\gamma(\lambda)$  are known for any station,  $Q_m(j, \lambda)$  can be estimated.

#### Appendix B: Remote-Sensing Reflectance for CDOM Fluorescence and Water Raman

For  $z$  positive downward from the surface,  $\theta$  the zenith angle, and  $\phi$  the azimuthal angle, with the consideration of isotropic  $\beta_{ie}$ , to the first order, the inelastic radiance  $L_{u,ie}$  in the direction  $\theta$  and the upwelling irradiance  $E_{u,ie}$  at depth  $z$  resulting from the depth interval  $dz$  are simplified to

$$dL_{u,ie}(z, \theta, \lambda) = \int_{\lambda_x} \beta_{ie}(\lambda_x, \lambda) E_o(z, \lambda_x) d\lambda_x \frac{dz}{\cos(\theta)}, \quad (\text{B1})$$

and

$$dE_{u,ie}(z, \lambda) = 2\pi \int_{\pi/2}^{\pi} dL_{u,ie}(z, \theta, \lambda) \cos(\theta) \sin(\theta) d\theta = 2\pi \int_{\lambda_x} \beta_{ie}(\lambda_x, \lambda) E_o(z, \lambda_x) d\lambda_x dz, \quad (\text{B2})$$

where  $E_o(z, \lambda_x)$  is the scalar irradiance at depth  $z$ , and  $E_o(z, \lambda_x) = E_{od}(z, \lambda_x) + E_{ou}(z, \lambda_x) \approx D_d(1 + 2R(\lambda_x)) E_d(z, \lambda_x)$ . Consider that  $R(\lambda_x)$  is small ( $< 0.05$ ) and  $D_u/D_d (\approx 2)^{20}$  is independent of depth, the subsurface irradiance resulting from the inelastic scattering for a deep water column is

$$E_{u,ie}(0^-, \lambda) \approx 2\pi \int_{\lambda_x} \frac{\beta_{ie}(\lambda_x, \lambda) E_d(0^-, \lambda_x)}{2\kappa(\lambda) + \kappa(\lambda_x)} d\lambda_x. \quad (\text{B3})$$

If one defines  $Q_{ie}$  as the  $Q$  factor for the inelastic-scattering field, then the subsurface upwelling radiance caused by inelastic scattering is

$$L_{u,ie}(0^-, \lambda) \approx \frac{2\pi}{Q_{ie}} \int_{\lambda_x} \frac{\beta_{ie}(\lambda_x, \lambda) E_d(0^-, \lambda_x)}{2\kappa(\lambda) + \kappa(\lambda_x)} d\lambda_x. \quad (\text{B4})$$

The inelastic total scattering coefficient  $\psi(\lambda_x, \lambda)$  ( $\text{m}^{-1}/\text{nm}$ ) is defined as

$$\psi(\lambda_x, \lambda) = \int_{4\pi} \beta_{ie}(\alpha, \lambda_x, \lambda) d\omega. \quad (\text{B5})$$

Because  $\beta_{ie}(\alpha, \lambda_x, \lambda)$  is considered isotropic, then

$$\psi(\lambda_x, \lambda) = 4\pi\beta_{ie}(\lambda_x, \lambda). \quad (\text{B6})$$

According to the definition of remote-sensing reflectance and with Eqs. (B4) and (B6), we have

$$R_{rs,ie}(\lambda) \approx \frac{I}{2Q_{ie}} \int_{\lambda_x} \frac{\psi(\lambda_x, \lambda) E_d(0^-, \lambda_x)}{[2\kappa(\lambda) + \kappa(\lambda_x)] E_d(0^-, \lambda)} d\lambda_x. \quad (\text{B7})$$

For CDOM fluorescence, if  $\eta(\lambda_x)$  is defined as the quantum efficiency for the emission band excited by

$\lambda_x$ , then<sup>9,16</sup>

$$\eta(\lambda_x) = \int_{\lambda} \frac{\lambda}{\lambda_x} \frac{\psi(\lambda_x, \lambda)}{a_g(\lambda_x)} d\lambda. \quad (\text{B8})$$

$\psi(\lambda_x, \lambda)$  can be characterized by a log-normal curve,<sup>33</sup> so

$$\psi(\lambda_x, \lambda) = \frac{\eta(\lambda_x) \lambda_x a_g(\lambda_x)}{\lambda A} \exp \left[ -s \left( \ln \frac{\lambda - \lambda_0}{\sigma} \right)^2 \right] \quad (\text{B9})$$

in which

$$A = \int_{\lambda} \exp \left[ -s \left( \ln \frac{\lambda - \lambda_0}{\sigma} \right)^2 \right] d\lambda, \quad (\text{B10})$$

where  $\eta(\lambda_x)$ ,  $\lambda_0$ ,  $s$ , and  $\sigma$  may vary with the type of CDOM and  $\lambda_x$ .

In general,  $b_b \ll a$  for most oceanic waters,<sup>21</sup> so  $\kappa$  is close to  $a$ , and based on the calculation for chl  $a$  fluorescence made by Gordon<sup>16</sup> the  $Q_{ie}$  factor for inelastic scattering is  $\sim 3.7$ . Then combining Eqs. (B7) and (B9), the remote-sensing reflectance caused by CDOM fluorescence can be reduced to

$$R_{rs}^f(\lambda) \approx 0.072 \int_{\lambda_x} \eta(\lambda_x) \frac{\lambda_x}{\lambda} \frac{a_g(\lambda_x) E_d(0^-, \lambda_x)}{[2a(\lambda) + a(\lambda_x)] E_d(0^-, \lambda)} \exp \left[ -s \left( \ln \frac{\lambda - \lambda_0}{\sigma} \right)^2 \right] \frac{d\lambda_x}{A} \quad (\text{B11})$$

Unlike broadband ( $\sim 100$  nm) CDOM fluorescence, the water Raman emission has a half bandwidth of approximately 20 nm.<sup>32</sup> If this bandwidth, is omitted, i.e., a narrow Raman emission is assumed, the inelastic-scattering coefficient  $\psi(\lambda_x, \lambda)$  for water Raman can be related to the Raman scattering coefficient as

$$\psi(\lambda_x, \lambda) d\lambda_x = b_R(\lambda_x),$$

and from Eq. (B7), with  $\kappa \approx a$ , the remote-sensing reflectance for water Raman is

$$R_{rs}^R(\lambda) \approx 0.072 \frac{b_R(\lambda_x) E_d(0^-, \lambda_x)}{[2a(\lambda) + a(\lambda_x)] E_d(0^-, \lambda)}. \quad (\text{B12})$$

Financial support was provided by NASA through grant NAGW-465 and Goddard Space Flight Center contract NAS5-30779, and by the Office of Naval Research through grant N00014-89-J-1091. Some ship support was provided by the State of Florida through the Florida Institute of Oceanography. The authors thank B. Chen and J. Hesler for administrative assistance.

## References

1. H. R. Gordon, D. K. Clark, J. L. Mueller, and W. A. Hovis, "Phytoplankton pigments from the Nimbus-7 Coastal Zone

- Color Scanner: comparisons with surface measurements," *Science* **210**, 63-66 (1980).
2. K. L. Carder, R. G. Steward, J. H. Paul, and G. A. Vargo, "Relationships between chlorophyll and ocean color constituents as they affect remote-sensing reflectance models," *Limnol. Oceanogr.* **31**, 403-413 (1986).
3. A. Morel, "Optical modeling of the upper ocean in relation to its biogenous matter content (case 1 waters)," *J. Geophys. Res.* **93**, 10,749-10,768 (1988).
4. K. L. Carder, W. W. Gregg, D. K. Costello, K. Haddad, and J. M. Prospero, "Determination of Saharan dust radiance and chlorophyll from CZCS imagery," *J. Geophys. Res.* **96**, 5369-5378 (1991).
5. A. Morel and J. M. Andre, "Pigment distribution and primary production in the western Mediterranean as derived and modeled from Coastal Zone Color Scanner observations," *J. Geophys. Res.* **96**, 12,685-12,698 (1991).
6. K. L. Carder, S. K. Hawes, K. A. Baker, R. C. Smith, R. G. Steward, and B. G. Mitchell, "Reflectance model for quantifying chlorophyll  $a$  in the presence of productivity degradation products," *J. Geophys. Res.* **96**, 20,599-20,611 (1991).
7. T. Platt, C. Caverhill, and S. Sathyendranath, "Basic-scale estimates of oceanic primary production by remote sensing: the North Atlantic," *J. Geophys. Res.* **96**, 15,147-15,159 (1991).
8. S. Sathyendranath, L. Prieur, and A. Morel, "A three-component model of ocean colour and its application to remote sensing of phytoplankton pigments in coastal waters," *Int. J. Remote Sensing* **10**, 1373-1394 (1989).
9. K. L. Carder and R. G. Steward, "A remote-sensing reflectance model of a red tide dinoflagellate off West Florida," *Limnol. Oceanogr.* **30**, 286-298 (1985).
10. H. R. Gordon, O. B. Brown, R. H. Evans, J. W. Brown, R. C. Smith, K. S. Baker, and D. K. Clark, "A semianalytic radiance model of ocean color," *J. Geophys. Res.* **93**, 10,909-10,924 (1988).
11. T. G. Peacock, K. L. Carder, C. O. Davis, and R. G. Seward, "Effects of fluorescence and water Raman scattering on models of remote-sensing reflectance," in *Ocean Optics X*, R. W. Spinrad, ed., Proc. Soc. Photo-Opt. Instrum. Eng. **1302**, 303-319 (1990).
12. R. W. Austin, "Inherent spectral radiance signatures of the ocean surface," in *Ocean Color Analysis (Final Technical Report)*, S. Q. Duntley, ed., SIO ref. 74-10 (Scripps Institution of Oceanography, La Jolla, Calif., 1974), pp. 2.1-2.20.
13. F. C. Polcyn, W. L. Brown, and I. J. Sattinger, "The measurement of water depth by remote-sensing techniques," Rep. 8973-26-F (Willow Run Laboratories, University of Michigan, Ann Arbor, Mich., 1970).
14. R. K. Clark, T. H. Fay, and C. L. Walker, "Bathymetry calculations with Landsat 4 TM imagery under a generalized ratio assumption," *Appl. Opt.* **26**, 4036-4038 (1987).
15. D. R. Lyzenga, "Passive remote-sensing techniques for mapping water depth and bottom features," *Appl. Opt.* **17**, 379-383 (1978).
16. H. R. Gordon, "Diffuse reflectance of the ocean: the theory of its augmentation by chl  $a$  fluorescence at 685 nm," *Appl. Opt.* **18**, 1161-1166 (1979).
17. C. S. Yentsch and D. A. Phinney, "Spectral fluorescence: an ataxonomic tool for studying the structure of phytoplankton populations," *J. Plankton Res.* **7**, 617-632 (1985).
18. H. R. Gordon, "Modeling and simulating radiative transfer in the ocean," in *Ocean Optics*, R. W. Spinrad, K. L. Crader, and M. J. Perry, eds., Oxford Monogr. Geol. Geophys. No. 25 (Oxford U. Press, New York, 1994), pp. 3-39.
19. J. P. Riley and R. Chester, *Introduction to Marine Chemistry*, (Academic, London, 1971), Chap. 2, p. 17.

20. H. R. Gordon, O. B. Brown, and M. M. Jacobs, "Computed relationship between the inherent and apparent optical properties of a flat homogeneous ocean," *Appl. Opt.* **14**, 417-427 (1975).
21. A. Morel and L. Prieur, "Analysis of variations in ocean color," *Limnol. Oceanogr.* **22**, 709-722 (1977).
22. J. T. O. Kirk, "Volume scattering function, average cosines, and the underwater light field," *Limnol. Oceanogr.* **36**, 455-467 (1991).
23. J. T. O. Kirk, "Dependence of relationship between inherent and apparent optical properties of water on solar altitude," *Limnol. Oceanogr.* **29**, 350-356 (1984).
24. A. Morel and B. Gentili, "Diffuse reflectance of oceanic waters: its dependence on sun angle as influenced by the molecular scattering contribution," *Appl. Opt.* **30**, 4427-4438 (1991).
25. H. R. Gordon, "Dependence of the diffuse reflectance of natural waters on the sun angle," *Limnol. Oceanogr.* **34**, 1484-1489 (1989).
26. B. R. Marshall and R. C. Smith, "Raman scattering and in-water ocean properties," *Appl. Opt.* **29**, 71-84 (1990).
27. K. L. Crader, P. Reinersman, R. F. Chen, F. Muller-Karger, C. O. Davis, and M. Hamilton, "AVIRIS calibration and application in coastal oceanic environments," *Remote Sens. Environ.* **44**, 205-216 (1993).
28. B. G. Mitchell and D. A. Kiefer, "Chl *a* specific absorption and fluorescence excitation spectra for light limited phytoplankton," *Deep-Sea Res.* **35**, 635-663 (1988).
29. A. Bricaud and D. Stramski, "Spectral absorption coefficients of living phytoplankton and nonalgal biogenous matter: A comparison between the Peru upwelling area and the Sargasso Sea," *Limnol. Oceanogr.* **35**, 562-582 (1990).
30. R. C. Smith and K. S. Baker, "Optical properties of the clearest natural waters," *Appl. Opt.* **20**, 177-184 (1992).
31. R. H. Stavn and A. D. Weidemann, "Optical modeling of clear ocean light fields: Raman scattering effects," *Appl. Opt.* **27**, 4002-4011 (1988).
32. D. J. Collins, J. A. Bell, R. Zanoni, I. S. McDermid, J. B. Breckinridge, and C. A. Sepulveda, "Recent progress in the measurement of temperature and salinity by optical scattering," in *Ocean Optics VII (Monterey)*, M. A. Blizard, ed., *Proc. Soc. Photo-Opt. Instrum. Eng.* **489**, 247-269 (1984).
33. S. K. Hawes, K. L. Carder, and G. R. Harvey, "Quantum fluorescence efficiencies of marine humic and fulvic acids: effects on ocean color and fluorometric detection," *Ocean Optics XI*, G. D. Gilbert, ed., *Proc. Soc. Photo-Opt. Instrum. Eng.* **1750**, 212-223 (1992).
34. National Oceanic and Atmospheric Administration, Provisional Chart No. 1003, United States: Gulf Coast and Key West to the Mississippi River (National Oceanic and Atmospheric Administration, Washington, D.C., 1972).
35. H. R. Gordon and A. Morel, *Remote Assessment of Ocean Color for Interpretation of Satellite Visible Imagery: A Review* (Springer-Verlag, New York, 1983), p. 44.
36. R. W. Austin, "Coastal zone color scanner radiometry," *Ocean Optics VI (Monterey)*, S. Q. Duntley, ed., *Proc. Soc. Photo-Opt. Instrum. Eng.* **208**, (1979), 170-177.
37. J. T. O. Kirk, *Light and Photosynthesis in Aquatic Ecosystems*. (Cambridge U. Press, London, 1986), Chap. 6, p. 117.
38. C. O. Davis, Jet Propulsion Laboratory, Pasadena, Calif. 91109 (personal communication, August 1992).
39. A. Morel and B. Gentili, "Diffuse reflectance of oceanic waters (2): Bi-directional aspects," *Appl. Opt.* **32**, 6864-6879 (1993).
40. N. G. Jerlov, *Optical Oceanography*, Vol. 5 of Elsevier Oceanography Series (Elsevier, New York, 1968), pp. 81-84.
41. A. Morel, "Optical properties of pure water and pure sea water," in *Optical Aspects of Oceanography*, N. G. Jerlov and E. S. Nielsen, eds. (Academic, New York, 1974), pp. 1-24.
42. W. W. Gregg and K. L. Crader, "A simple spectral solar irradiance model for cloudless maritime atmospheres," *Limnol. Oceanogr.* **35**, 1657-1675 (1990).
43. A. Morel and Y. H. Ahn, "Optical efficiency factors of free-living marine bacteria: influence of bacterioplankton upon the optical properties and particulate organic carbon in oceanic waters," *J. Mar. Res.* **48**, 145-175 (1990).
44. A. Bricaud and A. Morel, "Light attenuation and scattering by phytoplanktonic cells: a theoretical modeling," *Appl. Opt.* **25**, 571-580 (1986).
45. D. Spitzer and R. W. J. Dirks, "Contamination of the reflectance of natural waters by solar-induced fluorescence of dissolved organic matter," *Appl. Opt.* **24**, 444-445 (1985).
46. R. H. Stavn, "Raman scattering effects at the shorter visible wavelengths in clear ocean waters," in *Ocean Optics X*, R. W. Spinrad, ed., *Proc. Soc. Photo-Opt. Instrum. Eng.* **1302**, 94-100 (1990).
47. C. S. Yentsch and C. M. Yentsch, "Fluorescence spectral signatures: the characterization of phytoplankton populations by the use of excitation and emission spectra," *J. Mar. Res.* **37**, 471-483 (1979).
48. A. C. Tam and C. K. N. Patel, "Optical absorptions of light and heavy water by laser optoacoustic spectroscopy," *Appl. Opt.* **18**, 3348-3358 (1979).